PhD dissertation

From the: *Comprehensive Pneumology Center/Institute of Lung Biology and Disease, Helmholtz Center Munich*

Dissertation

zum Erwerb des Doctor of Philosophy (Ph.D.)
an der Medizinischen Fakultät der

Ludwig-Maximilians-Universität zu München

Ontological and anatomical origin of cutaneous scar-forming cells

vorgelegt von:

Donovan, Correa-Gallegos

.....

aus:

Mexico City, Mexico

.....

Jahr:

2021

.....

First supervisor:	*Prof. Dr. Jürgen Behr*
Second supervisor*:*	*Prof. Dr. Silke Meiners*
Third supervisor:	*Dr. Yuval Rinkevich*

Dean: **Prof. Dr. med. dent. Reinhard Hickel**

Datum der Verteidigung:

_____24.02.2021_____

LMU LUDWIG-MAXIMILIANS-UNIVERSITÄT MÜNCHEN

Dean's Office
Medical Faculty

MMRS MUNICH MEDICAL RESEARCH SCHOOL

Affidavit

Donovan, Correa-Gallegos

Surname, first name

Max-Lebsche-Platz 31

Street

81377 Munich

Zip code, town

Germany

Country

I hereby declare, that the submitted thesis entitled

Ontological and anatomical origin of cutaneous scar-forming cells

is my own work. I have only used the sources indicated and have not made unauthorised use of services of a third party. Where the work of others has been quoted or reproduced, the source is always given.

I further declare that the submitted thesis or parts thereof have not been presented as part of an examination degree to any other university.

Munich, 10.03.2021

Place, date

Correa-Gallegos, Donovan

Signature doctoral candidate

Contents

Abbreviations

- PDGF, platelet-derived growth factor.
- TGF-β, transforming growth factor-beta.
- αSMA, alpha-smooth muscle actin
- ECM, extracellular matrix.
- DPP4/CD26, dipeptidyl peptidase-4.
- ITGB1/CD29, integrin beta-1.
- ROS, reactive oxygen species.
- CTGF, connective tissue growth factor.
- FAP, prolyl endopeptidase/fibroblast activation protein.
- CRABP1, cellular retinoic acid-binding protein 1.
- COL11A1, collagen alpha-1(XI) chain.
- LSP1, lymphocyte-specific protein 1.
- SFRP2, secreted frizzled-related protein 2.
- WIF1, Wnt inhibitory factor 1.
- APOE, apolipoprotein E.
- MFAP5, microfibrillar associated protein 5.
- MEST, mesoderm-specific transcript.
- ELN, elastin.
- RGS5, regulator of G-protein signaling 5.
- TAGLN, transgelin

Introductory summary

Mammalian wound repair and scarring

Tissue repair ensures restoration of form and function after acute or chronic injury. Repair encompass a kaleidoscope of different outcomes in the animal kingdom, ranging from tissue regeneration to fibrotic scars. Tissue regeneration represents the optimal outcome where, in response to injury, full restoration of form and function occurs. For example, whole body regeneration in planaria or colonial ascidians (1; 2) and limb regeneration of salamanders/newts (3). Repair could also involve restoring of the main function of the damaged tissue in absence of morphologic regeneration. Examples of such a repair process is lung and liver compensatory growth. Here, after a lobectomy or a partial hepatectomy the remaining organ capacity is increased to compensate for the missing tissue without recovering the original form (4; 5). Interestingly, higher vertebrates such as mammals generally favor functional over morphologic regeneration. The ability of some species to regenerate whole tissues/organs, and its absence in humans, has inspired scientists for over a century to understand and improve the reparative processes in humans (6).

Another clear example of a reparative process in mammals is skin wound healing, in which the main function as an external barrier is quickly restored without regaining the original architecture. Indeed, skin wounds usually do not regenerate secondary appendages such as hair follicles and sebaceous glands. Instead, skin wounds repair by depositing a dense plug of fibrous tissue that seals the injury site with a scar (7).

The extensive accretion and deposition of extracellular connective tissue (termed fibrotic scar), severely affects the normal physiology of numerous organs, and it often leads to a decreased life expectancy (8). Besides esthetical and psychological concerns, pathological skin scars such as keloids, hypertrophic scars, and skin contractures severely impair normal movement and lifestyle of an individual (9). On the other side of the spectrum, when the wound healing and scarring process are compromised, and the external barrier function of the skin is not quickly restored, life-threatening non-healing chronic wounds expose patients to persistent infections, poor thermoregulation, and fluid loss (10). Considering both pathological skin fibrosis and non-healing chronic wounds, estimates indicate an economical burden for wound care between $28.1 billion to $96.8 billion in the U.S. alone (11). Thus, is imperative to increase our understanding on the basic biological mechanisms of skin wound repair, which in turn would lead to innovative approaches to restore a healthy repair process in patients with either excessive scarring or non-healing wounds.

The current wound-healing model is divided in three consecutive and overlapping stages (12). In the initial *inflammatory stage*, platelets released from adjacent damaged blood vessels aggregate during the coagulation process leading to the formation of a fibrin clot that works as a provisional matrix, this in turn allows cell infiltration into the site of injury. Concurrently, influx of initially neutrophils and later monocytes, contribute to tissue clearance and pathogen removal. In the following *proliferative stage,* the barrier function of the damaged area is restored. Contraction of the provisional matrix mediated by myofibroblasts, a transient fibroblast state linked to scar formation (13), gradually decreases the repair area and closes the wound. Simultaneously, neo-angiogenesis in the provisional matrix ensures normoxia of the new tissue. Finally, re-epithelialization onto the new tissue via keratinocyte migration establishes a new skin barrier. In the last *remodeling stage*, the scar formation is accreted, local apoptosis in the wound bed decreases the cellular density in the scar tissue and the matrix composition becomes enriched in collagen type I in a dense and regular conformation of parallel thick fibers.

Not all wounds scar

Wound repair in the skin is highly contextual. It depends on the injury type, anatomic location, age, and the species. All these parameters dictate the severity of scarring or scarless regeneration. The current basic and clinical thinking is that this diversity of responses in the skin is mediated by different environments. However, as you will see bellow, this conclusion seems incorrect. Instead, a new picture is emerging where mixtures of heterogeneous populations of fibroblast dictate the responses of skin tissues to either scar or regenerate. This, in fact, represents a paradigm shift in our understanding of wound repair.

Ontological discrepancies

More than six decades ago and inspired by the regenerative capacity of salamanders, Arthur Hess questioned whether the regenerative capabilities of these lower forms was also present in a "more primitive" mammalian form, the fetus (14). Hess inflicted injuries *in utero* on the back of guinea pig embryos and, although he failed to detect a regenerative response similar to amphibians, he noticed a "greater growth (healing) potential than those of postnatal animals". In the following decades, these observations were replicated in opossum (15), rat (16; 17), rabbit (18; 19), lamb (20), primates (21; 22), and observed in human as well (23). The common theme across several species was a lack of a robust immune response and minimal or absence of scar tissue (termed scarless repair).

Initially, it was believed that the fetal environment could promote scarless repair due to the inherent sterile nature, low oxygen levels, and high growth factors present in the amniotic fluid; all of which are variables known to directly affect the scar repair in adults (24). A series of heterochronic (young-to-old) grafting experiments later showed that embryonic skin repair scarlessly in the adult environment (25), and conversely, adult skin generates scars in the fetal setting (26). These results demonstrated the minimal influence of the environment for the repair outcome and, furthermore indicated that inherent changes in the embryonic and adult skin are responsible for the respectively scarless regeneration and scarring repair responses.

Interestingly, it was observed that the scarless regeneration potential decreases at later gestational stages. Injuries on mouse and rat E16.5 embryos (16.5 days post coitum, 76% of full term) regenerate scarlessly while injuries in E18.5 embryos (86% of full term) resembled adult wounds with scars (27; 28). Similar transitions from regeneration-to-scarring were observed in fetal lambs between 69-83% of full term (29), in 51-60% of full term rhesus monkeys (22), and in 55-64% of full term or beginning of third trimester in human (25). These observations lead to the hypothesis of a regeneration-to-scar transition during late development as conserved in all mammals, where the intrinsic mechanisms that regulate the scarring repair response in the skin are established.

An inverse scar-to-regeneration transition appears to occur much later in life. Wound healing studies performed during World War I indicated an inverse relation between the closure rate of wounds and age (30). Several animal models have corroborated that aged mammals repair wounds slower than younger ones (31). This slow closure has been assumed to occur because of cell intrinsic changes such as impaired cell migration, cellular senescence, delayed cytokine secretion; and systemic changes such as hormone levels decline, and a weakened immune system and inflammatory response (24). The delayed repair in aged organisms often leads to an improved tissue repair with diminished scar tissue formation (32; 33; 34). Nonetheless, co-morbidities in aged individuals, such as diabetes, completely worsen the repair response and result in non-healing chronic wounds (35) making the wound healing outcomes in aged individuals highly variable. Altogether, the scar-forming aptitude of the skin seems particularly augmented throughout the early postnatal life to mid-adulthood as a possible evolutionary mechanism to ensure survival of the organism during the most vulnerable and later reproductive stages. Then, injuries preluding the

establishment of this mechanism or after their decline would allow other scarless reparative processes to take place.

Phylogenetic and anatomical discrepancies

Scar-mediated repair has been observed in several mammalian species such as horses (36; 37), rodents (38; 39), dogs (40), sheep (26), and primates (41). These observations suggest that scar-mediated repair is a common 'mono-phyletic' trait that has emerged once in mammals. Nonetheless, extraordinary instances of full regeneration were documented in few mammals. For example, male deer undergo annual rounds of antler shedding and regrowth as part of their reproductive cycle. The fast-growing appendages include not only bone but blood vessels and a specialized velvet skin, thus represents a full organ regeneration without the formation of scar-like tissue (42; 43). A second example of skin regeneration has been observed in hibernating black bears after inducing full-thickness excisional wounds and fully restoring the native architecture of the skin including hair follicles (44).

The most deeply studied case of full skin regeneration in a mammal belong to the African spiny mouse from the genus *Acomys*. Members of this genus have adapted a skin autotomy strategy, or self-shedding, to prevent predation. The skin shedding generates open wounds that can cover up to 60% of the dorsal surface. These wounds quickly heal, and all cell types and appendages of the skin in the injury area are fully regenerated without scar tissue formation (45; 46; 47). This incredible feat has been directly compared to the wound healing process in the common laboratory mouse *Mus musculus* to reveal important mechanisms that could be responsible or facilitate skin regeneration. These differences include a low presence of pro-inflammatory leukocytes such as neutrophils and macrophages in *Acomys*, and poor cytokine release with an anti-inflammatory profile in the spiny mouse wounds (48; 49). *Acomys* wounds also present low collagen deposition and high protease expression, and low conversion rates of fibroblasts into scar-producing myofibroblasts (50; 51; 52). All these observations lead to the hypothesis that skin regeneration in *Acomys* resembles the fetal wound healing response and suggests that retaining these characteristics into adulthood is feasible and if extended to humans-would enable natural scarless regeneration in the skin.

Variances in the scarring outcome exist at different anatomical locations, even within a single organism. In contrast to the scar-forming repair in cutaneous skin such as the back-skin, injuries in the oral mucosa resolve without scar formation, even in adults (53; 54). Furthermore, within the oral cavity there are striking differences in the wound healing rate between hard and soft palate tissues, with soft palate tissue repairing wounds much faster (55). Just like *Acomys* skin, the oral mucosa repair has been compared to fetal healing. Oral mucosa wound healing displays limited immune responses and a particularly faster re-epithelialization (56; 57; 58). These observations suggest that the scarless repair mechanisms are not restricted to the embryonic environment or differentiation status and thus could potentially be induced in adulthood and extended to different human organs.

Injury severity

Another factor that directly determines the occurrence of scars is the area and depth of the insult. For example, larger and deeper wounds are more susceptible to develop larger scars.

As example of diverse scarring responses across anatomic depths occurs in the cornea. Injury-induced corneal scarring is a major determinant of corneal blindness, which is second only to cataract as the leading cause of blindness (59). The prevalence of corneal scarring induced after repair depends on the severity and depth of injury (60). Similar to skin (discussed below), the anatomy of the cornea is composed of a stratified external epidermal wall sustained underneath by a stromal layer (59). Penetrating injuries that pierce through

both layers present the highest prevalence of corneal scarring, while more superficial injuries by blunt-force ruptures show lower incidence of scars (61).

Pathological scars, such as hypertrophic scars and keloids, are frequent sequels of severe skin burns and thus a huge effort has been done to prevent and manage these fibrotic pathologies (62). Burn severity parameters, such as percentage of total body surface area affected and injury depth (partial or full-thickness injury), directly correlate with a more severe scarring outcome; independently of other factors such as burn type (scald or flame), age, or sex (63; 64; 65). Scar contractures, a complication of large hypertrophic scars that harshly limits the body movement (66), also prevail in burn victims with a higher burn severity (67).

The correlation between injury depth/extent and scar severity occurs not only in burn injuries but also in incisional/excisional wounds. The human skin includes three functionally discreate layers: epidermis, dermis, and hypodermis (68; 69). The *epidermis* is composed of a stratified epithelium. It hosts several keratinocyte subpopulations that range in depths from 0.075 - 0.15 mm up to 0.6 mm in hairless thick skin such as the skin on the palms and soles. This layer is considered highly regenerative and injuries are quickly repaired via keratinocyte proliferation and migration (70). The *dermis* lays bellow the epidermis. It is a connective tissue layer that extends in humans between 1 to 4 mm in thickness, depending on the anatomical region. This compartment has been classically subdivided into two main anatomical layers: papillary and reticular dermis. The most superficial papillary dermis, adjacent to the epidermis, is a thin layer (0.3 - 0.4 mm thick in humans) that contains thin collagen fibers densely packed that connects the deeper reticular dermis encompassed by thicker fibers organized in interwoven bundles. The complex extracellular matrix lattice of the dermis is produced and maintained by resident fibroblasts and supports extensive neurovascular and lymphatic networks, and secondary skin appendices such as hair follicles and sebaceous glands. Scars usually develop when injuries traverse this deeper reticular layer. Indeed, measurements in humans indicate a critical injury depth of at least 33% of the total epidermis-dermis thickness is required to generate visible scars (71). This indicates that injuries penetrating only the epidermis, papillary dermis, and partially the reticular dermis can repair scarlessly. The innermost layer that connects dermis to the musculoskeletal system bellow the skin, is the *hypodermis*. It is comprised of loose collagen fibers, resident fibroblasts, macrophages, and fat tissue. Although severely understudied as compared to papillary and reticular dermis, the main functions of the hypodermis relate to interstitial fluid control and thermoregulation. Even though some fibrotic pathologies in this layer have been described, such as in localized scleroderma (72) or Dupuytren's contractures (73), the role of this layer in the typical cutaneous scar process remains highly unexplored.

The above direct correlation between injury depth and scar tissue severity suggests that the intrinsic scar-free reparative mechanisms in mammals are restricted to skin layers. It is only when an injury surpasses the capacity of the regenerative processes that the scarring repair takes place, possibly, because scarring occurs much faster than regeneration. Approaches that enhance the scar-free healing, or that prevent the scarring mechanisms from ensuing could in principle improve the regenerative capacity of mammalian tissues and organs.

(Myo)fibroblasts as cellular inducers of scars

These contradictory findings can be understood considering the complex cellular activities that occur in wounds, especially of myofibroblasts, the scar producing cells in wounds and the main determinants of scar vs. scarless repair. The “myofibroblast” term was coined by Giulio Gabbiani in his seminal works where he detailed a fibroblast population with cytoskeletal attributes resembling smooth muscle cells. Gabbiani noticed that these unique fibroblasts locally emerge in wounds and then disappear during the cutaneous wound healing process, suggesting a pivotal role on wound contraction (74; 75). Ever since,

myofibroblasts have been detected in virtually every fibrotic pathology of any organ and their sustained or augmented presence directly correlates with a more severe fibrosis (76). The cellular source of these myofibroblasts have been a controversial field for the last decades. Depending on the organ and injury model, more than one possible source has been reported (77; 78; 79; 80; 81; 82; 83; 84). Nonetheless, the more consistent and prominent source of myofibroblasts are resident fibroblasts (85; 86; 87; 88; 89; 90; 91; 92).

Myofibroblast conversion in response to injury starts with the activation of resident fibroblasts. Fibroblasts are the primary cells that synthesize, secrete and remodel the extracellular matrix in all tissues and organs of the body (93). Damage-induced stress signals such as platelet-derived growth factor (PDGF) and changes in tissue stiffness activate fibroblasts. These activated fibroblasts or proto-myofibroblasts migrate into the damaged tissue and secrete new ECM components. Further local signals like the transforming growth factor-beta (TGF-β) prompts their maturation into mature myofibroblasts, characterized by their contractile apparatus and expression of alpha-smooth muscle actin (αSMA). At later stages of the wound closure, myofibroblasts recede via a non-completely understood process (76).

Altogether, myofibroblast derived from resident fibroblasts directly affect the repair outcome making them attractive to understand the discrepancies of the mammalian repair responses.

Not all fibroblasts scar, fibroblast heterogeneity to understand repair discrepancies

Classically, fibroblasts have been phenotypically described as dedicated extracellular matrix (ECM) producers but with the advent of new technologies, such as marker screening methods, genetic lineage tracing, multi-omics tools, and more recently single-cell transcriptomics, an unexpected functional heterogeneity in this cell type has surged in the last decades (93). This new appreciation on the multifaceted nature of these cells have not only boosted our understanding on their role during the wound healing process but give us a new direction to explain the different repair outcomes in mammals.

Ontological fibroblast heterogeneity: Scarless fetal/aged dermis versus scarring adult dermis

Fibroblasts isolated from embryos at scarless stages express higher levels of TGF-β, and particularly TGF-β3, compared to adult or neonatal fibroblasts that heal wounds with scars (94; 95; 96). TGF-β isoforms are multifunctional growth factors that regulate cell proliferation, migration, differentiation, extracellular matrix (ECM) production, and the immune response. TGF-β3 has been linked to scarless repair, whereas TGF-β1 is known to promote fibrosis (97). Despite fetal fibroblasts expressing higher levels of TGF-β isoforms than adult fibroblasts, they proliferate slower in response to TGF-β stimulation (98). Interestingly, old fibroblasts have a lower expression of growth factors than adult fibroblasts, including TGF-β (99; 100). Furthermore, damage accumulation during aging leads to a buildup of senescent fibroblasts in the dermis (101; 102; 103; 104; 105), indicating that diminished proliferation, due to a low responsiveness to or lower expression of growth factors, is a shared characteristic in scarless repair-related fibroblasts. ECM production in fetal and aged fibroblasts is also different than adult fibroblasts. Fetal fibroblasts express higher levels of collagen III while late-gestational, neonatal, and adult fibroblasts express mainly collagen I (106; 96; 107). Similarly, old fibroblasts have reduced collagen expression compared to adult fibroblasts (108; 34; 109). Altogether, a poor growth factor production/responsiveness, low proliferation, and diminished ECM production might account for the heterogeneity of fibroblasts and license scarless skin repair.

Fetal fibroblasts migrate faster than their adult counterparts (110) and are not inhibited by cell density (111) while aged fibroblast migration is highly variable depending on the donor (112; 113). More recently, a report showed that wound closure rate in aged mice is highly variable and fast healers possess dermal fibroblasts with signatures of proto-myofibroblasts

(migratory and proliferative) compared to slow healers (34). This suggest that fibroblast heterogeneity in aging might be vastly influenced by extrinsic factors such as lifestyle, nutrition, and environmental influences (101). Indeed, it was shown that caloric restriction in old mice can maintain fibroblasts with a transcriptomic profile more similar to young fibroblasts (108). Fetal fibroblasts and *in vitro* aged fibroblasts possess poor contractility (114; 115; 116; 117; 118) but no differences were detected in primary fibroblasts from old and adult donors (119). Nonetheless, poor migratory fibroblasts from old donors showed a reduced contractility compared to robust migratory aged fibroblasts (113) indicating that contractility might be also influenced by extrinsic factors during aging. Thus, in the case of migration and contractility, although important for the wound healing process, are not consistent traits in fibroblasts from scarless stages.

In summary, several intrinsic differences in fibroblasts from different ontological stages uncovered clues regarding cell processes that might influence the scarless repair outcome, yet little attention has been given to what mechanisms drive these changes in the fibroblasts. Furthermore, most work in both fetal and aged fibroblasts derive from *in vitro* studies that might just partially recapitulate the *in vivo* process. In the case of aged fibroblasts, general age-related effects such as chronological senescence, accumulated DNA alterations and protein modifications might induce these observed changes (101). On the other hand, it was assumed that the transition from scarless- to scar-producing fibroblasts in late embryonic development may well be a matter of maturation of the same fibroblast population, yet an alternative hypothesis could be the existence of non-overlapping populations with different scarring abilities. In the present **Publication I**, we explored this question and provided *in vivo* evidence supporting the latter option in the back-skin. We showed that fibroblasts from scarless-repairing embryonic stages get transiently replaced by a mature population of scar-forming fibroblasts (120). Interestingly, a similar replacement mechanism was reported to occur in aged fibroblasts where the amount of dipeptidyl peptidase-4 (DPP4/CD26) positive fibroblasts, linked to scar formation in adult mice, get replaced in old mice by integrin beta-1 (ITGB1/CD29) expressing fibroblasts (121). Thus, the repair outcome discrepancies along ontology seemed to be caused by the exchange of intrinsic different fibroblasts populations, rather than a change in their physiology.

Phylogenetic and anatomical fibroblast heterogeneity: Acomys versus Mus and gingiva versus dermis

Reports comparing *Acomys* to *Mus musculus* fibroblasts, indicate that fibroblasts from *Acomys* proliferate more in culture than mouse fibroblasts and have an enhanced resistance to reactive oxygen species (ROS)-induced senescence. This resistance was linked to an intrinsic mitochondrial protection and an improved intracellular detoxification against ROS (122). A carefully regulated ROS production modulates the mammalian wound healing process (123) and an excessive production or impaired detoxification results in non-healing chronic wounds (124). Counterintuitively, *in vivo* ROS production in wounds is higher in *Acomys* than mice (49), suggesting that the intrinsic ROS resistance in *Acomys* fibroblasts might be an evolutionary adaptation to the high ROS production in these animals. ROS-mediated redox signaling mediate fibroblast conversion into myofibroblast, including αSMA expression (125). Still, *Acomys* fibroblasts showed lower αSMA expression in *in vivo* (45) and in cultures (126), thus, it is plausible that the enhanced ROS clearing in *Acomys* fibroblasts prevent their conversion into myofibroblasts and, as a result, avoid scar tissue formation.

Unlike the mesoderm origin of dermal fibroblasts, gingival fibroblasts originate from the neural crest (127) and their neuroectodermal origin endows them with an intrinsic regenerative potential (128). Indeed, reciprocal transplantations of gingival fibroblasts into the skin further showed their intrinsic propensity to scarless repair, even when placed into a scarring environment such as the back-skin (91). Analogous to *Acomys* fibroblasts, gingival fibroblasts are resistant to ROS detrimental effects (129) and express higher levels of ROS-related genes compared to dermal fibroblasts (130) indicating that higher ROS production

and an intrinsic cellular adaptation to prevent ROS-induced toxicity are common traits in scarless scenarios. ROS also mediate αSMA expression in both human gingival and dermal fibroblasts (131). Yet, unlike the *Acomys* equivalents, gingival fibroblasts have a constant expression of αSMA *in vitro*, compared to the transient expression in dermal fibroblasts, and they also express higher levels of ECM-remodeling enzymes (132), suggesting that a more efficient matrix remodeling prevents scar formation in the oral mucosa. Analogously, models of lung fibrosis in mice often restore the original organ architecture and ECM-remodeling is believed to be a crucial step on this endeavor (133). These comparative studies imply for high ROS levels as drivers of scarless repair by preventing fibroblast-to-myofibroblast conversion (as in Acomys) and by improving ECM remodeling (as in the oral mucosa).

Injury depth-related fibroblast heterogeneity: papillary versus reticular versus hypodermal fibroblasts

Fibroblast heterogeneity within the skin further helps to understand the repair discrepancies occurring in response to different injury depth. Papillary fibroblasts from the superficial papillary dermis proliferate more than reticular fibroblasts, migrate faster, and are more resistant to apoptosis but are less contractile and express lower levels of ECM components (134; 135; 136; 137; 138; 139; 140; 141; 142). Papillary fibroblasts sustain basement membrane production and epidermal morphogenesis *in vitro* (143; 141; 144), indicating that this population might be specialized in epidermal homeostasis. Papillary fibroblasts are more sensitive to deleterious effects of aging and *in vitro* prolonged culture acquiring phenotypes similar to reticular counterparts regarding low proliferation, contractility, and epidermal morphogenesis sustenance (145; 146; 147).

Human deep skin fibroblasts (2-3 mm in depth, most likely reticular and or hypodermal fibroblasts) proliferate less than superficial fibroblasts (< 1.5 mm in depth, reticular and papillary-likely populations) and express higher levels of collagens, αSMA, and profibrotic growth factors like TGF-β1 and connective tissue growth factor (CTGF); these characteristics makes deeper fibroblasts more comparable to fibroblasts extracted from hypertrophic scars (148; 149). Similarly, pig fibroblasts from the “deep dermis” (reticular/hypodermal) express higher amounts of αSMA *in vivo* upon injury and produce thicker scars than superficial (papillary/reticular) fibroblasts (150; 151). In comparison, human hypodermal fibroblasts proliferate less than both reticular and papillary fibroblasts, are less contractile and poorly sustain epidermal morphogenesis. Nonetheless, from the three subpopulations hypodermal fibroblasts have the highest *in vitro* differentiation potential to other mesenchymal cell types such as adipocytes, osteocytes, and chondrocytes (152). Altogether, the traits of deeper fibroblasts resemble characteristic of myofibroblasts and implies these subpopulations predominantly contributes to cutaneous scar formation.

Papillary and reticular fibroblasts possess distinct molecular signatures (153; 154) and higher expression of common fibroblast markers such as prolyl endopeptidase/fibroblast activation protein (FAP) and CD90/THY1 have been used to discriminate between papillary and reticular fibroblasts respectively (155).

With the advent of single-cell transcriptomics, a more complex fibroblast heterogeneity and new molecular identifiers have recently emerged. Studies using human skin report inconsistent numbers of fibroblast subpopulations. Tabib and colleagues reported two major subpopulations in the forearm dermis (156; 157), while He *et al.* and Solé-Boldo *et al*. reported four subpopulations in arm and inguinoiliac skin respectively (158; 109). A fourth study by Vorstandlechner and colleagues further expanded the kaleidoscope of fibroblastic types by identifying six subpopulations in the ventral skin (abdomen) (159).

However, many of these populations may include other mesenchymal residents of the skin besides interfollicular fibroblasts. Tabib *et al*. detected a population expressing both cellular retinoic acid-binding protein 1 (CRABP1) and collagen alpha-1(XI) chain (COL11A1) while

He *et al*. and Solé-Boldo *et al*. also detected a subpopulation marked by COL11A1 expression. CRABP1 is highly expressed in the dermal papilla and COL11A1 in the dermal sheath, two closely related mesenchymal cell types dedicated to hair follicle sustenance (160; 161), while lymphocyte-specific protein 1 (LSP1) marks for the other major subpopulation in Tabib *et al*. study which is also a marker of fibrocytes (162). These findings argue against CRABP1/COL11A1- and LSP1-positive clusters being true interfollicular fibroblast subpopulations.

Previously detected interfollicular fibroblast markers such as secreted frizzled-related protein 2 (SFRP2), DPP4/CD26, and Wnt inhibitory factor 1 (WIF1) were detected in half of the subpopulations of Tabib *et al*. and Vorstandlechner *et al*. reports while Solé-Boldo *et al*. reported one WIF1 positive cluster. All these markers have been reported to be highly expressed in fibroblasts in diverse skin fibrotic conditions (163; 164; 165; 166; 167; 91; 168; 169; 170; 90), suggesting their likely involvement in scar formation.

Novel potential fibroblasts subpopulations were also detected. Apolipoprotein E (APOE) marked a single population in He *et al*. and Solé-Boldo *et al*., and two subpopulations in Vorstandlechner *et al*., while a microfibrillar associated protein 5 (MFAP5) expressing subpopulation was detected in all three reports. Functional characterization of cells expressing these population-restricted markers is still missing and would allow definitive assignments as true fibroblast subpopulations.

From these four studies, only Solé-Boldo and colleagues could assign each subpopulation with a distinct skin compartment. Using RNA-fluorescence *in situ* hibridization they traced the COL11A1 population into hair follicles, supporting the idea of this population representing both dermal papilla and dermal sheath cells. The WIF1 population allocated in the papillary dermis while MFAP5 expressing cells populated the reticular dermis. The pro-inflammatory APOE population was strongly associated with blood vessels suggesting it might represent a perivascular fibroblast population.

Single-cell transcriptomics from healthy mouse skin added further complexity to the classical papillary and reticular division. Two superficial subpopulations, that reside in the papillary and superficial reticular dermis, showed dynamic changes linked to the hair cycle, while two deeper static subpopulations reside in the deep reticular layer and hypodermis (171).

Studies from mouse wounds reported the existences of three to five different fibroblast subpopulations (172; 173). Guerrero-Juarez *et al*. showed that a subpopulation expressing CRABP1 reside in the upper section of the wound (thus devoid of hair follicles and mature dermal papilla) while the deeper layers were populated by a subpopulation expressing mesoderm-specific transcript (MEST) and elastin (ELN). Gay *et al*. also showed a subpopulation of fibroblasts expressing ELN, suggesting that this deep subpopulation remains static during later stages of wound healing. Nonetheless, these studies neglected other mesenchymal residents during the analysis making the real number of fibroblasts subpopulations likely lower. Guerrero-Juarez *et al*. described a population marked by the expression of regulator of G-protein signaling 5 (RGS5), which has been previously described to be a pericyte marker (174) and Gay *et al*. reported a transgelin (TAGLN) and αSMA expressing population, yet these two markers are co-expressed by the dermal sheath cells (171).

In summary, deeper fibroblast populations and particularly reticular fibroblasts have been linked to fibrosis (90). This would explain why critical injury depths are needed to induce scar formation. Although the cellular characteristics of hypodermal fibroblasts make them more similar to reticular fibroblasts, there has been limited number of studies that test whether this population could play a role in scar formation *in vivo*. In the accompanying **Publication II** we tested this hypothesis and proved that fibroblasts from the hypodermal connective tissue, termed fascia, populate wounds of deep injuries and they intrinsically generate large

scars whereas superficial wounds resolved in smaller scars by fibroblasts from the dermis (175).

Aims

To understand the influence of fibroblast heterogeneity and their relation to different repair outcomes, we aimed to characterize the origin of scar-forming fibroblasts in cutaneous wounds. First, we proved during development, that scar-forming fibroblasts outcompete native regenerative populations of dermal fibroblasts. Furthermore, we showed that this transition from regenerative-predominance in fetal tissues to scarring-predominance in adult tissues results from a transition between 2 distinct fibroblast communities, which shape dermis maturation and progressively transitions the response of skin wound, from regeneration-to scarring. This novel cellular replacement mechanism explains the regeneration-to-scarring transition on the premise that regenerative-prone fibroblasts get replaced by a scar-preferring population late in development.

In the second publication, we delve deep into the diversity of wound responses across skin depths. We show that on one hand, when injuries are superficial, the classical *de novo* matrix deposition is orchestrated by the dermal fibroblasts, culminating in smaller scars. On the other hand, when injures are deep, a novel mechanism driven by fibroblasts in the deep areas of the hypodermis initiates, in which plugs of mobile tissue patch the open wound and serve as a provisional matrix that generates larger scars.

These observations provide a better understanding of the basic biology of the scar-forming fibroblasts and wound repair. The generated knowledge would provide innovative approaches to tackle pathological scarring conditions such as hypertrophic scars, scar contractures, and keloids, to restore the reparative prowess in non-healing chronic wounds, or to improve the scarless regenerative potential of the skin after injury.

Publication I

Jiang D, Correa-Gallegos D, Christ S, Stefanska A, Liu J, Ramesh P, Rajendran V, De Santis MM, Wagner DE, Rinkevich Y. Two succeeding fibroblastic lineages drive dermal development and the transition from regeneration to scarring. Nat Cell Biol. 2018;20(4):422-431.

Publisher's version is available online in: doi: 10.1038/s41556-018-0073-8.

In the presenting work my contribution included:

Histological preparations and image analysis, *ex vivo* experiments, and manuscript and figure preparation.

In particular:

a) Fig.1 d-f: histological analysis to describe the role of cell proliferation and apoptosis in the increase and decrease of the EPF and ENF populations respectively during development.
b) Supp Fig.2: immunodetection of classical fibroblast markers to depict EPF and ENF heterogeneity.
c) Supp Fig.3: histological analysis showing the direct correlation between EPF invasion and Collagen I deposition in the developing dermis.
d) Fig.4 and Supp Fig.5: Implementation of fractal analysis to describe collective cytomorphological changes during dermis development.
e) Supp Fig.6: histological analysis showing the EPF influence on the fibronectin matrix stiffness during development.
f) Fig.5 g-i: *Ex vivo* explant culture to functionally prove the anterior-to-posterior scar-prowess acquisition of the dermis associated with the anterior-to-posterior EPF invasion.
g) Fig.5 f,i, Fig.6 f, and Fig.7 d: Implementation of fractal analysis to describe ECM changes related to fibrosis.
h) Supp Fig.7: Preparation of summary scheme depicting the major findings of the research.

Two succeeding fibroblastic lineages drive dermal development and the transition from regeneration to scarring
(Final manuscript)

Dongsheng Jiang[1,ξ], Donovan Correa-Gallegos[1,ξ], Simon Christ[1,ξ], Ania Stefanska[1], Juan Liu[1], Pushkar Ramesh[1], Vijayanand Rajendran[1], Martina M. De Santis[1,2,3], Darcy E. Wagner[1,2,3,4], Yuval Rinkevich[1,4,*]

[1] Comprehensive Pneumology Centre / Institute of Lung Biology and Disease, Helmholtz Zentrum München, Munich, Germany
[2] Department of Experimental Medical Sciences, Lund University, Lund, Sweden
[3] Wallenberg Centre for Molecular Medicine, Lund University, Lund, Sweden
[4] Member of the German Centre for Lung Research (DZL), Munich, Germany

[ξ] These authors have contributed equally

* Correspondence should be addressed to:
Yuval Rinkevich
Phone: +49 (89) 3187 4685
Fax: +49 (89) 3187 4661
yuval.rinkevich@helmholtz-muenchen.de

Abstract
During fetal development mammalian back-skin undergoes a natural transition in response to injury, from scarless regeneration to skin scarring. Here we characterize dermal morphogenesis and follow two distinct embryonic fibroblast lineages, based on their history of expression of the Engrailed1 gene. We use single cell fate-mapping, live 3D confocal imaging and *in silico* analysis coupled with immuno-labelling to reveal unanticipated structural and regional complexity and dynamics within the dermis. We show that dermal development and regeneration are driven by Engrailed1-history-naive fibroblasts, whose numbers subsequently decline. Conversely, Engrailed1-history-positive fibroblasts possess scarring abilities at this early stage and their expansion later on drives scar emergence. The transition can be reversed, locally, by transplanting Engrailed1-naive cells. Fibroblastic lineage replacement thus couples the decline of regeneration with the emergence of scarring, and creates potential clinical avenues to reduce scarring.

Introduction

Skin develops in fetus when dermal fibroblasts establish a porous, 'basket-weave' scaffold, providing the tensile strength and extensibility needed for the structural integrity and for protective and sensing functions. Injuries to the skin commonly lead to loss of these frameworks and replacement by scar tissues, which have greatly limited functions. Scar tissue is rarely observed in lower vertebrates, where the normal response to injury is a complete regeneration of the original dermal structure. Mammals however have evolved to heal with scar tissue and undergo a regeneration-to-scar phenotypic transition during fetal life[1-2]. This transition has been documented in the back-skin of all mammalian embryos studied to date including human[3-7].

Previous studies into the fetal commencement of scarring have focused on a multitude of environmental differences between early and late fetal stages, including inflammatory responses to injury, expressions of morphogenetic proteins, growth factors and extracellular matrix (ECM) components such as hyaluronic acid[8]. In the early 90s, Longaker and colleagues addressed the influence of the environment on the commencement of scarring by performing fetal/adult heterochronic transplantations of back-skin tissues in sheep. They found that donor back-skin tissues respond to injury (scar/regenerate) independent of host microenvironment or developmental stage. They thus concluded that the determining factor/s of the commencement of scarring are likely intrinsic to the transplanted back-skin graft, most likely its fibroblasts, the tissue's primary secretors of ECM[9-10].

More recently, we have discovered that functionally diverse lineages of fibroblasts coexist in the mouse back-skin and oral cavity[11]. Embryonic cells that have expressed Engrailed-1 (En1), termed EPFs (En1-lineage-Past fibroblasts) are the primary contributors to scarring in various models of pathologic scars. Conversely, En1-lineage-Naive fibroblasts (ENFs) do not participate in scar production. By transplanting adult ENFs or EPFs in different anatomical locations, we determined that the difference in the capacity of EPFs & ENFs to form a scar *in vivo* is cell-intrinsic and permanent[11].

Here, we followed the fates of EPF & ENF progenitors. We used genetic fate-mapping approaches at single cell and lineage levels, live 3D confocal imaging of lineage-specific cellular migrations and immuno-labelling coupled with *in silico* approaches to determine how the dermal structure in the back-skin develops. We find that ENFs form the sculptures of the dermal lattice and that their cell lineage declines during development, concurrent with a surge in EPF numbers that predisposes back-skin to scarring.

Results

ENFs are replaced by EPFs during back-skin development

The En1 gene is expressed in a small subset of early embryonic cells and switched off permanently later in embryogenesis[11]. To distinguish En1-expressing cells and follow their fibroblastic descendants in the developing back-skin, we used a transgenic mouse system where En1 expression drives genetic rearrangements (*En1*^{Cre}). Crossing *En1*^{Cre} with a reporter mouse system (*R26*^{mTmG}), generated offspring where the genetic rearrangement replaced membrane bound tomato red protein (RFP) expression with membrane bound green fluorescence protein (GFP) expression[12] (Fig. 1a). The permanent replacement of RFP with GFP in all descendant cells allowed purification schemes of EPFs and ENFs based on GFP^{+}RFP^{-}Lin^{-} and GFP^{-}RFP^{+}Lin^{-}, respectively.

We thus performed flow cytometric analysis of EPFs and ENFs from the total fibroblast population (Lin^{-}, see Methods) in early fetal back-skin. Dermal fibroblasts were mostly ENFs early on, and they declined slowly during subsequent development, followed by a steep decline between E14.5-E18.5 (~90% down to ~20%, Fig. 1b-c). The drop in ENFs was proportional to total dermal cells (including hematopoietic, endothelial, lymphatic) and to dermal fibroblasts alone (Lin-), indicating a clonal disadvantage to ENFs as compared to all other dermal progenitors. Conversely, EPFs increased from ~2% of dermal cells at E14.5

(EPF:ENF = 1:33) to ~72% at P0 (EPF:ENF = 4:1) (Fig. 1b-c) and in proportion to all other dermal progenitors (Fig. 1c). We then placed ENF and EPF lineages in relation to previously described adult mesenchymal cell populations based on the expression of surface markers (Supplementary Fig. 1). About 3% of Lin^- cells expressed fibro-adipogenic progenitor (FAP) markers[13-15] (Lin^-integrin □7$^-$$Sca1^+$PDGFR□$^+$) that were enriched in EPFs (Supplementary Fig. 1c,f,g); while pericyte markers[16] (Lin^-CD146^+) comprised 5% of total Lin^- cells and were enriched in ENFs (Supplementary Fig. 1d,f,g). Mesenchymal stem cell markers[17] ($Lin^-CD29^+CD105^+$) were abundant in both ENFs and EPFs (Supplementary Fig. 1e-g). Immuno-labelling on *En1*^{Cre};*R26*$^{VT2/GK3}$ (see Methods) neonates sections showed adipocytes (FABP4) or pre-adipocytes[18] (Dlk1 and Sca1) were more abundant in EPFs (Supplementary Fig 2a-c). Similarly, the smooth muscle marker □SMA was enriched in EPFs compared to ENFs (Supplementary Fig 2d). Immunostaining of reticular and papillary dermis markers (Dlk1, TNC, CD26) showed that their expression was not exclusive to either lineage (Supplementary Fig 2b,e,f), indicating that EPFs and ENFs do not preferentially allocate to either anatomic location.

To determine if the decline in ENFs numbers is due to programed cell death or a decrease in proliferation, we performed TUNEL staining and immuno-labelling of cleaved Caspase 3 (Cas3) and the proliferation marker Ki67 on sections of E14.5, E16.5 and E18.5 *En1*^{Cre};*R26*^{mTmG} embryos. ENFs underwent significantly more apoptosis than EPFs at E14.5 and E16.5 (Fig 1e-f). Conversely, the number of proliferating EPFs steadily increased from E14.5 to E18.5 while ENF proliferation significantly decreased (Fig 1d, f). Together, our results show that the decay in ENF population is primarily due to a clonal disadvantage.

To study the clonal dynamics of ENF-to-EPF replacements *in situ* at single cell levels, we used a transgenic ‘Rainbow’ reporter system (*En1*^{Cre};*R26*$^{VT2/GK3}$)[19]. From the moment of En1 expression, individual EPF progenitors were genetically marked with one out of three alternate fluorescent colours (YFP, RFP, CFP), while ENFs express GFP. EPF progenitors were absent in dermis at E9.5 and first appeared at E10.5 (Fig 2a-d). Coronal sections at E10.5 showed that single EPFs and mono-clones developed in close association with ectoderm and then extend from the most anterior regions (neck level) down to half of the trunk (Fig 2b-c). EPFs remained absent in most posterior regions (including hindlimbs) at this stage. At E11.5 EPFs formed two parallel mid-lateral lines that cover the entire back (Fig 2e). 3D reconstruction of E12.5 embryos showed that EPFs arrange themselves in an arc across the back-skin, with migration ‘protrusions’ at anterior sites (Fig 2f and Video 1).

We next performed immuno-labelling of ECM proteins on histological sections of *En1*^{Cre};*R26*$^{VT2/GK3}$ early developing dermis. Unexpectedly, we found that ENFs deposited Fibronectin fibres, but not Collagen I & Collagen III (Fig 2g), indicating that ENFs generate a provisional matrix. At anterior sites, Collagen I & Collagen III fibres were visible within the dermal matrix in association with EPF clones, indicating EPFs form a ‘mature’ dermis (Fig 2h-i). Indeed, at later stages, Collagen I expression was associated with EPFs (Supplementary Fig 3). To view the dynamics of ENF-to-EPF replacement, we performed live 3D confocal imaging, of the developing back-skin of *En1*^{Cre};*R26*^{mTmG} embryos (E12.5), at the anterior margin of the EPF arc (Supplementary Fig 4). We found that the ENF cytological structure is displaced to create open gaps into which EPFs migrated (Fig 2j, Supplementary Fig 4, and Video 2). EPFs colonized the provisional dermis, through both dorsal and lateral trajectories (Fig 2j arrows). This local dynamic displacement of ENF-to-EPF cytological structures was completed within 24 hours.

We then analysed the migration behaviours of single cells in three-dimension by automatically tracking the migration paths of EPFs at 15min intervals. We obtained 144 high-quality tracks of fibroblasts across an area of ~170 μm^2 and ~100 μm deep (Fig 3a). From a coronal plane of view, we observed characteristic reticular patterns wherein EPFs follow seemingly collective behaviours (Fig 3b). The EPFs migrated in vertical columns along the dorsal-ventral axis (Fig 3c-d). Anterior tracks had more dispersed points along the dorsal-

ventral axis than posterior tracks, indicating that anterior EPFs migrated faster than posterior EPFs (Fig 3e-f).

Unexpectedly, EPFs migrated ununiformly, and in three distinctive ways: (1) "converging" migration to a fixed space (Fig 3b), (2) "localized" migration where EPFs move in a limited space without directly contacting each other (Fig 3g), or (3) "diverging" migration of several EPFs from a space unit (Fig 3h). These three migration types occurred in clusters of 3-6 fibroblasts that shared common behaviours. Sequences of several units with varied migration behaviours could be detected even along a relative short distance of 170 μm, indicating that EPF movements *in situ* are directed locally, by micro-environmental cues. These observations are in contrast to observations from fibroblast migration assays in two-dimension, and demonstrate that EPFs exhibit intricate migration repertoires *in vivo*.

Dermal lattice development follows Engrailed-1 lineage replacement

Having documented the cellular conversion from ENFs to EPFs, we went on to describe dermal lattice development. Since dermal structure is too complex to be analysed with simple Euclidean geometry parameters, we turned to fractal analysis to measure the complexity of cellular and ECM fiber arrangements. In this analysis, the fractal dimensions (FD) and lacunarity (L) values quantitatively assess the complexity and porosity of 2D shapes (Supplementary Fig. 5a). The complex arrangements (e.g. blood vessels and tumors[20-22]) score higher FD values than simpler arrangements (e.g. geometrical shapes). Porous structures (e.g. sponges) score higher L values than smooth surfaces (eg. scales).

We first resolved the cellular organization during dermal morphogenesis using histological sections of *En1*^{Cre};*R26*$^{VT2/GK3}$ embryos. Early (E11.5-12.5) ENF regions were smoother and more complex, while later stages (E14.5-E16.5) became simpler and more porous (Supplementary Fig 5b-c). This indicates a drift from a compact mesenchymal arrangement to a more interspaced cellular organization of a mature dermis. Anterior ENF arrangements at E12.5 were more complex and smoother than posterior cells (Supplementary Fig. 5c), indicating that, at E12.5, anterior and posterior regions have different cellular organizations. Conversely, EPFs underwent two major cellular rearrangements during development: 1) Early EPFs (E10.5-11.5) cluster tightly in complex patterns with individual cells having smooth shapes, 2). After E12.5 these clusters split into individual cells with increasing complex arrangements (Fig. 4a-b). At E12.5 anterior EPFs decreased in FD value, while posterior EPFs retained similar complexity to their earlier stage. 3D rendered pictures of single EPFs revealed that posterior EPFs were morphologically simpler than anterior EPFs (Fig. 4c). A sudden increase in complexity of anterior EPFs in E12.5 embryos correlated in time with the migration of EPFs (Fig. 2f, j, Fig. 3, Supplementary Fig. 4, and Video 1-2), suggesting that changes in EPF morphology cause or are caused by migrations. Together, our fractal analysis characterizes dynamic spatiotemporal changes in dermal lattice development, and link dermal maturation steps to distinct embryonic fibroblastic lineages.

To determine if dermal lattice organization is changed following EPF's expansion, we analysed matrix fibre alignment at different stages in dermal regions that do or do not contain EPFs. Since Collagen precludes the earlier stages of development where EPFs initially seed the back-skin, we used Fibronectin to study the patterns of dermal lattice development. The distance between fibres increased progressively from E11.5 to E16.5 (Fig. 4d and Supplementary Fig. 6), concurrent with EPF development. At the same time there was a progressive decrease in complexity and an increase in porosity (Fig. 4e-f). This demonstrates that a gradual transformation of the dermal Fibronectin matrix occurs, from a relaxed and disorganized framework towards a more stretched conformation (Fig. 4g). Our fractal analysis of EPF's cellular arrangements stresses that E12.5 is a pivotal time-point when anterior regions are actively changing while posterior regions are still dormant. The co-occurrence of Fibronectin framework transformation and EPF morphological changes links ECM arrangements with distinct cell migration behaviours during development. To

directly prove this link, we used an inducible-Cre labelling system to follow single fibroblastic cells (either ENFs or EPFs) and their sibling cells during back-skin development, and compared behaviours between anterior and posterior sites. Fibroblastic clone size increased and clone expansion extended across the dorsal-ventral axis in the most anterior locations; while singly labelled cells and small clones remained close to the ectoderm in posterior regions (Fig. 4h-i). These experiments show that the dynamics of structure changes across the anterior-posterior dermal axis influence both the cell division rate of fibroblastic precursors and the migration trajectories of their clonal colonies.

Next we aimed to detect in more detail discrete cellular arrangements at later stages, when fibroblast clones are too widespread and intermixed. We generated a tissue-level description of dermal cellular organization by calculating local FD and L values from E16.5 *En1*^{Cre};*R26*$^{VT2/GK3}$ embryos. Low-power images showed that more compact tissues such as epidermis, hypodermis, muscle and cartilage had higher FD values than dermis (Supplementary Fig. 5d-e), indicating the validity of the fractal analysis. From the high-power images, we could identify five distinct dermal layers (DL-1-5) organized in parallel sheets across the back-skin (Fig. 4j-n). DL-1 and DL-5 were in direct contact with the epidermis and hypodermis respectively, were more complex and smoother, and were composed of densely packed EPFs (~85% and ~75%). DL-2 and DL-4 were simpler and porous, were composed predominantly of EPFs (~75% and ~90%). DL-3 was complex and porous and was composed primarily of elongated ENFs (~75%). The cellular organization of the dermis at E16.5 therefore has a mirrored pattern with outer flanking dense dermal layers in direct contact with the epidermis and hypodermis, and two intermediate porous layers, separated by a middle layer devoid of EPFs. Critically, within each internal layer there are micro-domains with distinct complexity values across the anterior-posterior axes. Tissue structure complexity and porosity does not vary linearly across these micro-domains. In fact, in several places the deep dermis is abruptly interspersed with distinct cellular arrangements (Fig. 4j right panels), which might result from local migration patterns at earlier stages of development.

Scarring transition follows an anterior-to-posterior sequence

We showed above that EPFs increase within the back-skin from an anterior to posterior sequence. We previously showed that adult EPFs produce scars[11]. We therefore speculated that the fetal regeneration-to-scar transition is linked to engrailed lineage replacement and could be due to the gradual increase in EPF abundance during dermal development. If this is correct, we would expect that wounds inflicted at early fetal stages would regenerate from ENFs, and that the transition from regeneration-to-scarring would take on an anterior to posterior sequence.

To test our 1st hypothesis, we generated wounds in the back-skin of *En1*^{Cre};*R26*^{mTmG} E12.5 embryos and analysed both lineage compositions and ECM depositions (Fig. 5a). At 48 hours post-wounding, ENFs had migrated into wound beds, where a provisional Fibronectin-rich matrix had been generated, virtually absent of EPFs or Collagen I fibres (Fig. 5b-c). Fractal analysis of fetal wounds indicated that lattice arrangement at the injury site was not different from that of the adjacent fetal skin (Fig. 5d-f). Thus, during fetal skin regeneration, ENFs sculpt the wound bed matrix without the intervention of EPFs.

To test our 2nd hypothesis, we cultured skin biopsies from different anterior-posterior regions of E19.5 WT embryos (Fig. 5g). Anterior biopsies deposited significantly more Collagen-rich scars (Fig. 5h right panel) than posterior biopsies (Fig. 5h left panel). Fractal analysis revealed that posterior matrix was significantly simpler than anterior one (Fig. 5i), suggesting that at this stage anterior fibroblasts are more fitted to create a scar than posterior fibroblasts. Collectively, these experiments demonstrate that the fetal regeneration-to-scar transition follows the increase in EPF abundance during dermal development.

Engrailed-1 lineage replacement drives regeneration-to-scar transition

We next asked whether EPFs from early stages possess scarring capacities or if, alternatively, they undergo a developmental maturation, whereby they acquire scar-producing abilities, over time. To test this idea, we purified EPFs from the back-skin of *En1*^{Cre};*R26*^{mTmG} embryos/neonates at regenerating (E16.5) or scarring (P1) stages and intradermally transplanted them in equal number ($2x10^5$) around the edges of fresh splinted wounds on the back-skin of adult immuno-deficient (Rag2$^{-/-}$) mice. We then assessed the contribution of EPFs from different ages to scar formation 14 days after transplantation/wounding (Fig. 6a). Transplanted EPFs from P1 that migrated into the wounds, deposited Collagen I extensively within host wound beds (Fig. 6b). Some EPFs deposited ectopic Collagen I at their original transplanted location (Fig. 6c). Strikingly, transplanted EPFs from E16.5 embryos had the same scarring capacities as P1 EPFs, depositing Collagen I both within wounds and at ectopic uninjured sites (Fig. 6d-e). EPFs from both E16.5 and P1 had pathologically active cell morphologies, with membrane protrusions that span across and intermingle with the Collagen I fibres (Fig. 6e'). Fractal analysis showed that Collagen I arrangements were more complex and smoother in EPF-transplanted regions (day 14 post-wounding) and in adult scars (day 21 post-wounding), while simpler and more porous in non-injured adult and fetal dermis (Fig 6f). Our results demonstrate that fetal EPFs are capable of producing and organizing a scar tissue, just as well as newborn EPFs, and that the absence of scar-formation in early fetal skin is due to scarcity of EPFs, rather than their developmental immaturity. Together, the mechanism behind the dynamic transition from regeneration to scarring in fetus is En1 lineage replacement during back-skin development.

ENFs or native lattice reduce scarring in adult wounds

Since we found that ENF abundance in dermis was associated with regenerative outcomes at early stages, and since we also showed that ENFs sculpted a provisional lattice during development, we asked whether transplantation of ENFs alone would regenerate adult dermal wounds. To test this hypothesis, we transplanted fetal (E16.5) ENFs into back-skin wounds of adult Rag2$^{-/-}$ mice and allowed wounds to heal for 14 days (Fig. 7a). As expected, sites of ENF transplantations had a more reticular lattice arrangement, compared to fibrotic lattice arrangements at sites of EPF transplantations (Fig. 7b-c). Fractal analysis indicated that ENF transplantation sites were significantly simpler and more porous in lattice arrangements, compared to EPF-transplanted sites or to mock-transplanted control wounds (Fig. 7d). In line with the reduction of scarring severity, immune-labelling of an endothelial marker CD31 showed a significantly higher infiltration of blood vessels into the wound beds at sites of ENF transplantations, as compared to EPF- or mock-transplanted wounds (Fig. 7e-i). Many of the transplanted ENFs were closely associated with blood vessels, which were interlaced with one another to generate vascular networks within the transplanted sites (Fig. 7g).

To test if the ENF-generated lattice itself promotes a regenerative outcome, we transplanted de-cellularized back-skin from P5 WT mice into back-skin wounds of Rag2$^{-/-}$ mice (Fig. 7j). 10 days later, we found that fibroblasts in the control wounds and in the borders between the wound and the transplanted matrix had a typical active morphology with membrane protrusions (Fig. 7k-l). Conversely, resident cells within the transplanted matrix had an inactive morphology with round cytoplasm (Fig. 7m). Immuno-labelling of □SMA revealed the activated fibroblasts were present in the control wound beds and in the matrix-wound border (Fig. 7n-o), and mostly devoid from transplanted matrix (Fig. 7p). These experiments show that a 'healthy' dermal lattice can be imposed, locally, in two ways. First, transplanting ENFs expands the existing pool of resident ENFs, and allows ENFs to sculpt a provisional matrix. Alternatively, transplantations of de-cellularized dermal lattice, in essence, mimic dermal development, and in the presence of which EPFs do not promote a

pathologic scar. Both approaches, if they could be made industrially, provide therapeutic possibilities for a range of dermal pathologies, including patients suffering from large skin burns or wounds.

Discussion

We have previously shown[11] that EPFs are the primary cells responsible for fibrotic outcomes in adult settings of wound healing, irradiation fibrosis and melanoma cancer growth. Here, we find that ENFs, not EPFs, are the primary sculptors that drive dermal lattice development and its regeneration in fetal wound healing settings. We show that transplanted fetal ENFs/EPFs into adult wounds impose regenerative vs. scarring outcomes, respectively, and that the phenotypic shift in dermal response to injury (from regeneration to scarring) is driven by Engrailed-1 lineage replacement (Supplementary Figure 7).

Using *in vivo* live imaging, we disclose 3 distinct migration patterns of dermal fibroblasts during back-skin development: localized, diverging or converging migrations. To our knowledge, these migration patterns have never been described in 2D or 3D assays to date. We hypothesize that each of the three migration patterns establishes distinct dermal architectures that collectively drive the remarkable architectural complexity that we observe during dermal development. Diverging migration patterns could indicate fibroblastic cell invasiveness, while converging migrations indicates collective and interconnected behaviours as opposed to individualistic. Since fibroblastic migrations impinge on collagen bundle alignments, we expect these individual migration patterns, through their distinct molecular programs, to influence scar tissue severity, as well as fibroblastic invasiveness into tumours.

Our findings have additional developmental, evolutionary and clinical implications outlined below.

Other groups have recently implicated separate fibroblastic lineages in the differentiation of the back-skin epidermis[18,23-24]. Fetal processes of epidermal development, hair follicle and sebaceous gland differentiation, may require specialized stromal signals and cells. The priority for adults is a quick fix of breached skin, which likely requires different stromal signals and cells to produce a scar. These two diverged requirements at different stages of fetal life are maintained through dynamic cellular shuffling of fibroblastic populations, allowing specialized types of fibroblasts to accommodate specific fetal and adult requirements.

We demonstrate here that the ENF-to-EPF switch in dermis imposes the phenotypic transition from regeneration to scarring in response to injury. In evolutionary terms this switch provides a model to explain how dermal regeneration was retained in some adult rodent species such as African spiny mice[25]. We speculate that such species have retained the fibroblastic cell compositions of fetal stage dermis (ENFs>EPFs), and have resisted the ENF-to-EPF lineage successions.

We describe, and map in detail, here a mechanism for the general acquisition of scarring ability in the skin. We believe both the temporal- and spatial-dynamics of EPFs, the determinants of scarring, will be widely clinically applicable. Consideration of lineages with engrailed history will outline a favourable time window for surgeons to work in, when scarring outcomes will be predicted to be at a bare minimum, such as during corrective surgery for *Spina bifida*, or equally, it could be applicable to the removal of paediatric malignancies.

Our findings also carry implications for adult scarring. There are no definitive strategies to prevent scar formation, and current clinical practice is focused on scar acceptance rather than its amelioration. We have demonstrated two separate strategies that reduce scar outcomes in adult injured skin. Both ENF transplantation and de-cellularized dermis transplantation assays provide a proof-of-concept for a therapeutic option that could be used to treat large wounds, scolds or burns.

Our findings also create opportunities for the intense field of bio-engineered autologous dermo-epidermal human skin grafts that are currently being tested in Phase I and II clinical

studies. Skin grafts include all fibroblastic lineages within dermis and are therefore likely to produce scars upon transplantation. We predict it would be advantageous to graft pure human ENFs or ENFs combined with dermo-epidermal skin. In essence, this dermal milieu would override the ENF-to-EPF population shift and favour regeneration over scarring.

In sum, we use single cell clonal analysis, 3D imaging, computational cell tracking and in silico analysis, to follow the behaviours of fibroblast lineages *in vivo*. We document fibroblast lineage specific proliferations, migrations and secretions, and demonstrate how such a fundamental process as dermal morphogenesis actually occurs. Our finding of Engrailed-1 lineage replacement links dermal morphogenesis with the phenotypic shift in response to dermal injury. We believe our findings open up previously unrecognised opportunities for clinical approaches to ameliorate scar tissues in injured adult skin.

Data availability

Statistical reports for Fig. 1, 4, 5, and 7 and Supplementary Fig. 3 and 5, have been provided as Supplementary Table 1. All other data supporting the findings of this study are available from the corresponding author on reasonable request.

Acknowledgements

Y.R. was supported by the Human Frontier Science Program Career Development Award (CDA00017/2016), the German Research Foundation (RI 2787 / 1-1 AOBJ: 628819), and the Fritz-Thyssen-Stiftung (2016-01277). J.L. was supported by the China Scholarship Council. D.C.G. was supported by the Consejo Nacional de Ciencia y Tecnología (CONACYT) and the Deutscher Akademischer Austauschdienst (DAAD).

Author Contributions

Y.R. outlined and supervised the research narrative, and designed all experiments. D.J. performed the wound healing studies, performed flow cytometric analysis and sorting of EPFs and ENFs, performed cell transplantations and de-cellularized skin transplantations. D.C.G. and A.S. performed and analysed the clonal analysis studies and generated the confocal images. D.C.G. performed the fractal analysis. S.C. and P.R. performed live imaging and cell tracking analysis. J.L. and V.R. assisted with clonal analysis, confocal imaging and histological sectioning. M.S. and D.E.W. generated the de-cellularized dermis. Y.R. wrote the manuscript.

Competing interests

The authors declare no competing financial interests.

References

1. Gurtner, G. C., Werner, S., Barrandon, Y., Longaker, M. T. Wound repair and regeneration. *Nature* **453**, 314-321 (2008).
2. Ud-Din, S., Volk, S. W., Bayat, A. Regenerative healing, scar-free healing and scar formation across the species: current concepts and future perspectives. *Exp. Dermatol.* **23**, 615-619 (2014).
3. Armstrong, J. R., Ferguson, M. W. Ontogeny of the skin and the transition from scar-free to scarring phenotype during wound healing in the pouch young of a marsupial, Monodelphis domestica. *Dev. Biol.* **169**, 242-260 (1995).
4. Ihara, S., Motobayashi, Y., Nagao, E., Kistler, A. Ontogenetic transition of wound healing pattern in rat skin occurring at the fetal stage. *Development*. **110**, 671-680 (1990).
5. Lorenz, H. P., Whitby, D. J., Longaker, M. T., Adzick, N. S. Fetal wound healing. The ontogeny of scar formation in the non-human primate. *Ann. Surg.* **217**, 391-396 (1993).
6. Longaker, M. T., Dodson T. B., Kaban L. B. A rabbit model for fetal cleft lip repair. *J. Oral Maxillofac. Surg.* **48**, 714-719 (1990).
7. Kishi, K., Okabe, K., Shimizu, R., Kubota, Y. Fetal skin possesses the ability to regenerate completely: complete regeneration of skin. *Keio J. Med.* **61**, 101-108 (2012).
8. Ferguson, M. W., O'Kane, S. Scar-free healing: from embryonic mechanisms to adult therapeutic intervention. *Philos. Trans. R. Soc. Lond. B. Biol. Sci.* **359**, 839-50 (2004).
9. Longaker, M. T,, *et al.* Adult skin wounds in the fetal environment heal with scar formation. *Ann. Surg.* **219**, 65-72 (1994).
10. Cass, D. L., *et al*. Wound size and gestational age modulate scar formation in fetal wound repair. *J. Pediatr. Surg*. **32**, 411-415 (1997).
11. Rinkevich, Y., *et al.* Identification and isolation of a dermal lineage with intrinsic fibrogenic potential. *Science*. **348**, aaa2151 (2015).
12. Muzumdar, M. D., Tasic, B., Miyamichi, K., Li, L., Luo, L. A global double-fluorescent Cre reporter mouse. *Genesis*. **45**, 593-605 (2007).
13. Joe AW, *et al.* Muscle injury activates resident fibro/adipogenic progenitors that facilitate myogenesis. *Nat Cell Biol.* **12**, 153-163 (2010).
14. Uezumi A, Fukada S, Yamamoto N, Takeda S, Tsuchida K. Mesenchymal progenitors distinct from satellite cells contribute to ectopic fat cell formation in skeletal muscle. *Nat Cell Biol.* **12**, 143-152 (2010).
15. Cordani N, Pisa V, Pozzi L, Sciorati C, Clementi E. Nitric oxide controls fat deposition in dystrophic skeletal muscle by regulating fibro-adipogenic precursor differentiation. *Stem Cells.* **32**, 874-885 (2014).
16. Crisan M, Yap S, Casteilla L, Chen CW, et al. A perivascular origin for mesenchymal stem cells in multiple human organs. *Cell Stem Cell.* **3**, 301-313 (2008).
17. Dominici, M., *et al*. Minimal criteria for defining multipotent mesenchymal stromal cells. The International Society for Cellular Therapy position statement. *Cytotherapy* 8, 315 – 317 (2006).
18. Driskell, R. R., *et al*. Distinct fibroblast lineages determine dermal architecture in skin development and repair. *Nature*. **504**, 277-281 (2013).
19. Rinkevich, Y., Lindau, P., Ueno, H., Longaker, M. T., Weissman, I. L. Germ-layer and lineage-restricted stem/progenitors regenerate the mouse digit tip. *Nature*. **476**, 409-413 (2011).
20. Khorasani, H. et al. A quantitative approach to scar analysis. *Am. J. Pathol*. **178**, 621-628 (2011).

21. Gould, D. J., Vadakkan, T. J., Poché, R. A., Dickinson, M. E. Multifractal and lacunarity analysis of microvascular morphology and remodeling. *Microcirculation*. **18**, 136-151 (2011).
22. Di leva, A., Esteban, F. J., Grizzi, F., Klonowski, W., Martín-Landrove, M. Fractals in the neurosciences, Part II: clinical applications and future perspectives. *Neuroscientist*. **21**, 30-43 (2015).
23. Rognoni, E., *et al*. Inhibition of β-catenin signalling in dermal fibroblasts enhances hair follicle regeneration during wound healing. *Development*. **143**, 2522-2535 (2016).
24. Sennett, R., *et al*. An integrated transcriptome atlas of embryonic hair follicle progenitors, their niche, and the developing skin. *Dev. Cell*. **34**, 577-591 (2015).
25. Seifert, A. W., *et al*. Skin shedding and tissue regeneration in African spiny mice (Acomys). *Nature*. **489**, 561-565 (2012).

Figures

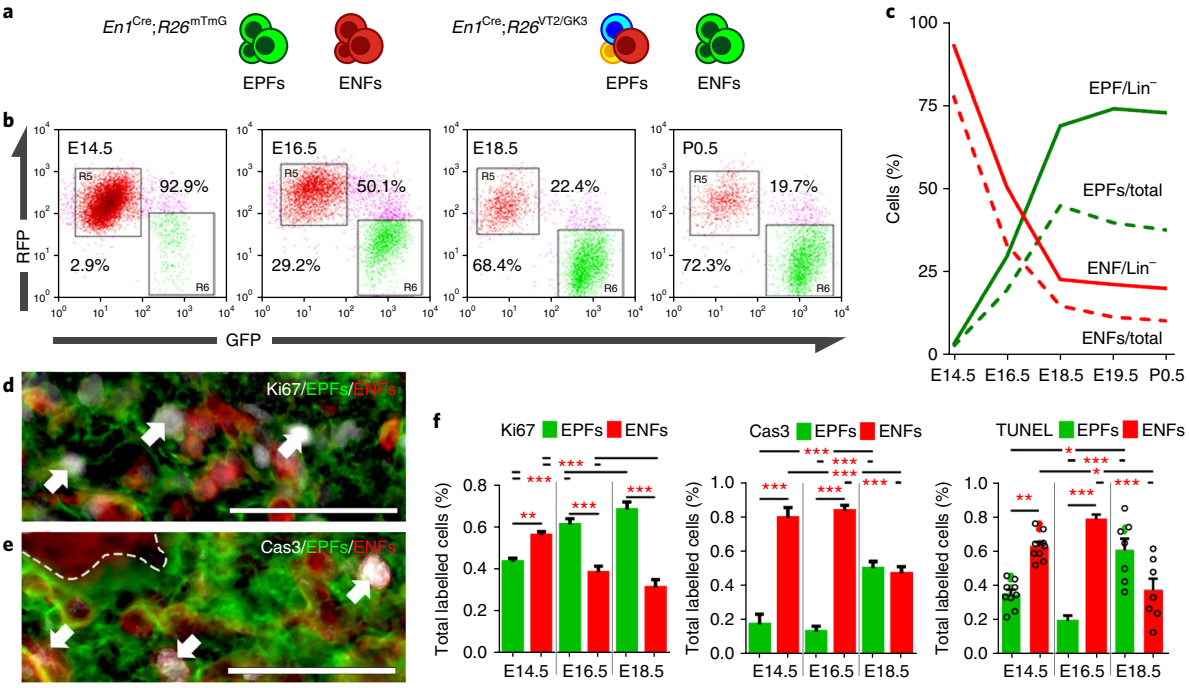

Figure 1 EPFs replace ENFs during mouse back-skin development. a, Genetic labeling systems used 'color-code' cells. **b**, Representative flow cytometry plots of ENFs/EPFs from *En1*^{Cre};*R26*^{mTmG} embryos at different developmental stages. All Cre^{+} embryos (ranging from 3-6 embryos) from an entire litter were pooled together for a single analysis. GFP intensity (X-axis) is plotted against RFP intensity (Y-axis). **c**, EPFs/ENFs percentages of Lin^{-} (lines), or total live cells (dashed lines). **d**,**e**, Representative immunofluorescence images of Ki67 (**d**) or Cas3 (**e**) in E18.5 *En1*^{Cre};*R26*^{mTmG} embryos, arrows indicate Ki67 or Cas3 positive cells, Scales: 50 µm. **f**, EPFs/ENFs positive for Ki67, Cas3, or TUNEL. n = optical fields analysed from sections of three E14.5 embryos, two E16.5 embryos and one E18.5 embryo stained for Ki67 (n = 24, 28 and 16, respectively), Cas3 (n = 20, 15 and 14, respectively), TUNEL (n = 9, 28 and 7, respectively). Mean ± SEM. ANOVA, Tukey test, *p<0.05, **p<0.01, ***p<0.001. Additional adjusted p values are listed in Supplementary Table 1.

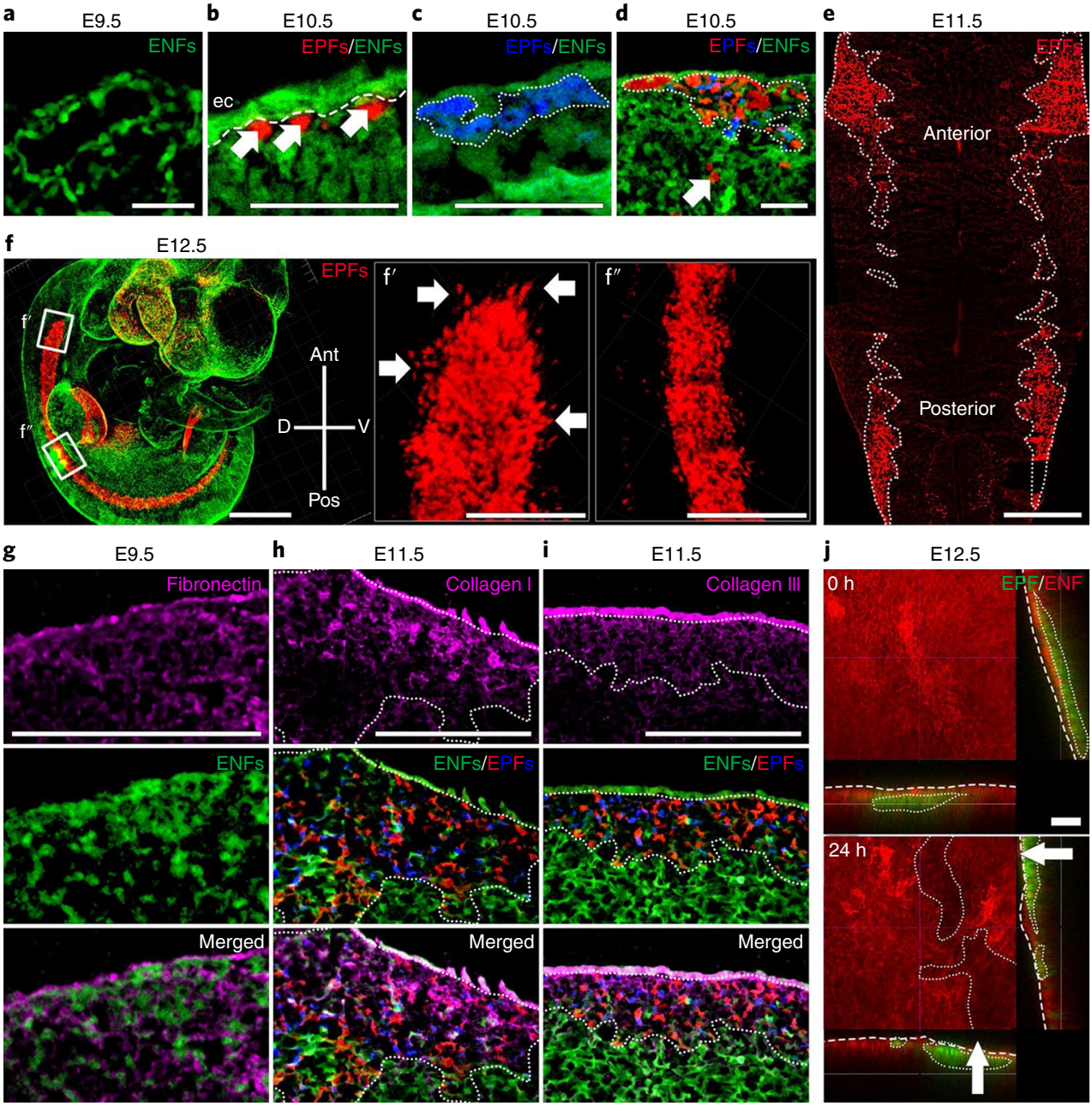

Figure 2 EPFs direct dermis development. a-e, Coronal sections of E9.5-E11.5 *En1*^{Cre};*R26*$^{VT2/GK3}$ embryos. Arrows indicate single EPFs (**b**, **d**). Dashed line indicates ectoderm border (**b**). Dotted lines delimitate EPFs clones (**c-e**). **f**, E12.5 *En1*^{Cre};*R26*$^{VT2/GK3}$ embryo showing EPFs arc across the back skin. **f'**,**f''**, high magnification from boxes in **f**. Arrows indicate migrating EPFs. Cross indicate embryonic axes. **g-i**, Immunofluorescences for Fibronectin (**g**), Collagen I (**h**), or Collagen III (**i**) in coronal section of E9.5 or E11.5 *En1*^{Cre};*R26*$^{VT2/GK3}$ embryos. Doted lines delimitate EPFs. **j**, Orthogonal view from time-lapse images (0 h and 24 h) from the anterior region of E12.5 *En1*^{Cre};*R26*^{mTmG} embryo. Dotted lines in X-Y frame delimitate the EPF-induced ENF gap. Green channel (EPFs) was omitted in X-Y frames for clarity. Dotted lines from X-Z and Y-Z delimitate EPFs. Dashed lines mark the dorsal surface. Arrows indicate EPFs movement direction. Scales: a-d = 50 µm, e-f = 500 µm, f'-f''-g-i = 200 µm, j = 100 µm. ec = ectoderm, Ant = anterior, Pos = posterior, D = dorsal, V = ventral. Images in a-j are representative of three experiments.

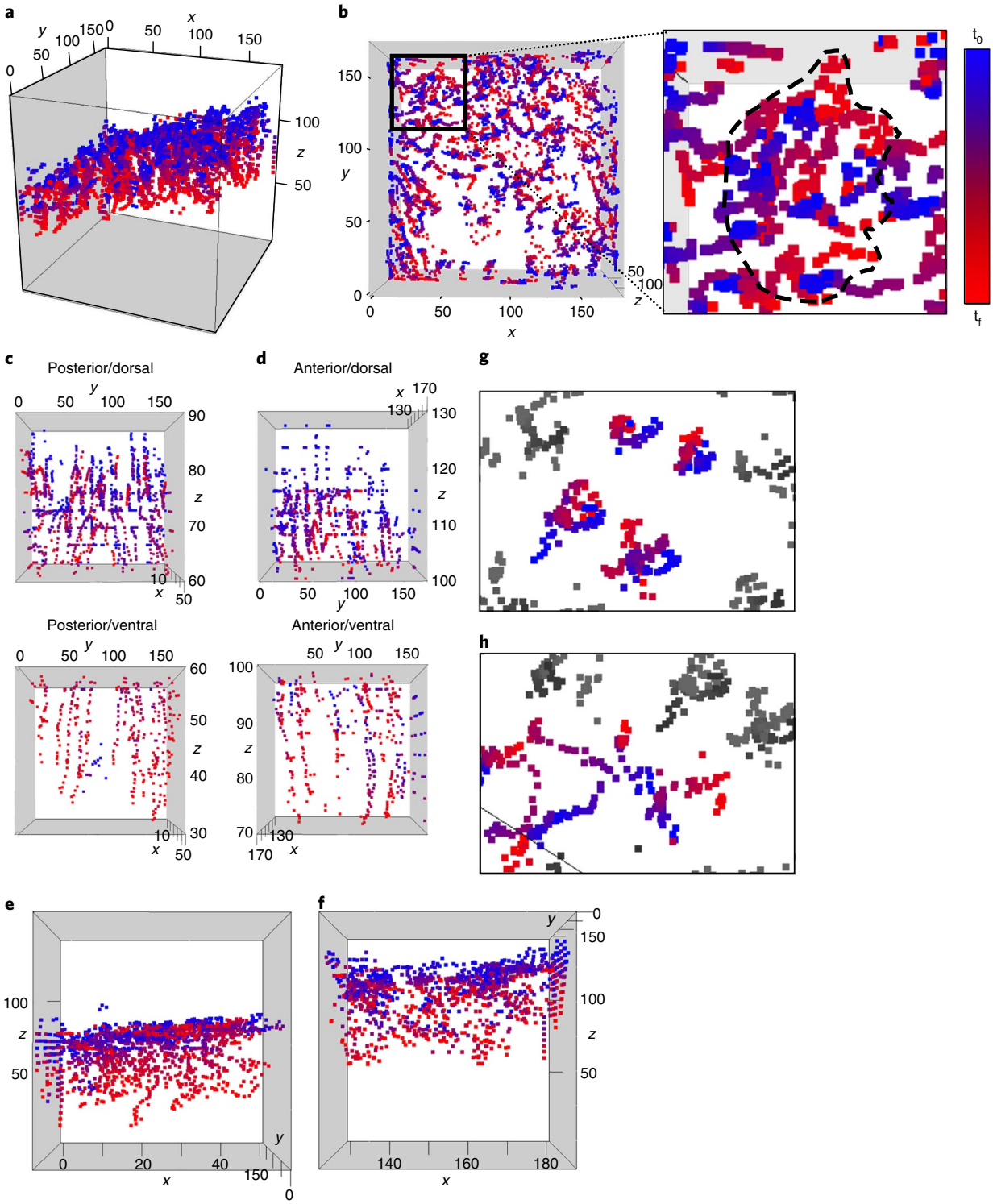

Figure 3 EPFs exhibit three migration behaviours in vivo. a, 4D scatter plot of individual tracks, the colour ramp indicates time (Blue = first; Red = last time point). **b**, Top X-Y view showing the reticular patterns of migration. Dashed lines in zoomed view (right panel) delimitate “converging” track points. **c**, **d**, Lateral Y-Z views of posterior (**c**) or anterior (**d**) tracks split in dorsal (up) and ventral (down) regions. **e, f**, Frontal X-Z views of posterior (**e**) or anterior (**f**) tracks. **g**, **h**, Amplified view of single tracks showing “localized” (**g**) or “diverging” (**h**) migrations. Colour ramps of tracks of no interest (**g**, **h**) were changed to grey-scale for clarity. Axes units = µm. The 144 cell tracks were derived from one representative video.

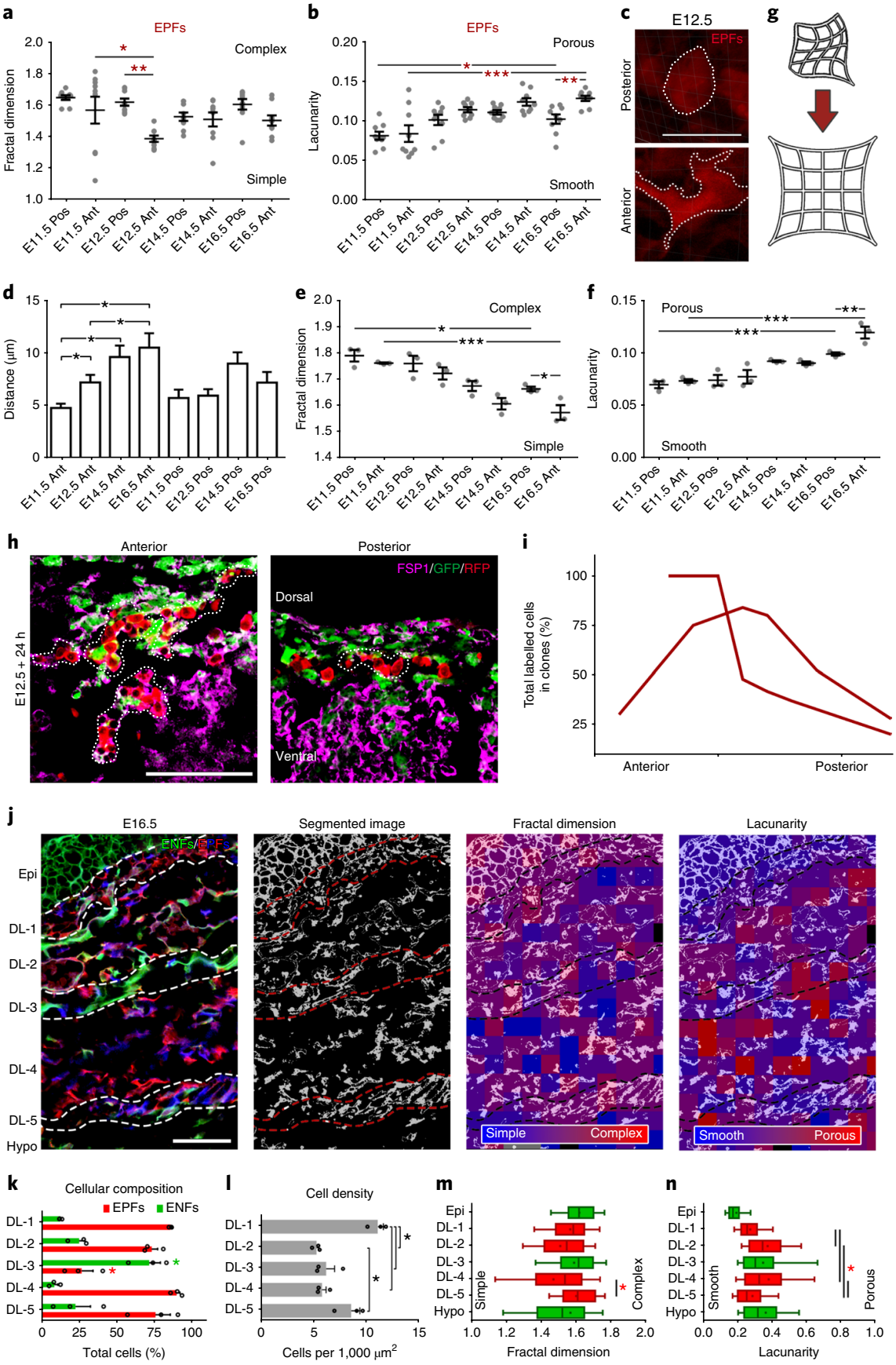

Figure 4 Dermal lattice is actively changing during development. **a**, **b**, Fractal dimension (**a**) and lacunarity (**b**) values derived from confocal images of EPFs from different regions and developmental stages. Mean ± SEM. RM ANOVA, Newman-Keuls test, n = 9 optical fields of anterior or posterior regions at E11.5, E12.5, E14.5, E16.5, respectively. *p<0.05, **p<0.01, ***p<0.001. **c**, 3D reconstructions of posterior (up) and anterior (down)

En1^{Cre};*R26*$^{VT2/GK3}$ EPFs. **d**, Distances in µm between fibronectin fibres calculated from linear profiles of three confocal images of fibronectin immuno-labelled sections (Supplementary figure 6, n = 184 (E11.5 ant), 138 (E11.5 pos), 135 (E12.5 ant), 155 (E12.5 pos), 98 (E14.5 ant), 105 (E14.5 pos), 91 (E16.5 ant), and 128 (E16.5 pos) measurements), Mean ± SEM. ANOVA, Holm-Sidak test, *p<0.05. **e**, **f**, Fractal dimension (**e**) and lacunarity (**f**) values derived from Fibronectin staining of confocal images from different regions and developmental stages. Mean ± SEM. RM ANOVA, Newman-Keuls test, n = 3 optical fields of anterior or posterior regions at E11.5, E12.5, E14.5, E16.5, respectively. *p<0.05, **p<0.01, ***p<0.001. **g**, Fibronectin matrix changes from a relaxed framework to a rigid matrix. **h**, Fsp1 expression in anterior (left) or posterior (right) regions of E12.5 *Actin*$^{Cre-ER}$;*R26*$^{VT2/GK3}$ embryos after 24 h of 1 nM 4-Hydroxytamoxifen exposure. Dotted lines delimitate single clones. **i**, Percentage of labelled cells in clones from two independent embryos. **j**, Local (subsampled) fractal analysis of E16.5 *En1*^{Cre};*R26*$^{VT2/GK3}$ dermis. Dashed lines delimitate dermal layers. **k**, Percentages ± SEM of EPFs/ENFs in each layer, n = 3 optical fields. Two-way ANOVA, *p<0.05, Tukey test. **l**, Mean ± SEM number of cells per 1000 µm^2 of each layer, n = 3 optical fields. One-way ANOVA, *p<0.05, Tukey test. **m**, **n**, Fractal dimension (**m**) and lacunarity (**n**) values derived from different dermal layers, n for FD and L respectively = 58 and 58 (Epidermis), 65 and 65 (DL-1), 198 and 199 (DL-2), 62 and 62 (DL-3), 274 and 281 (DL-4), 92 and 92 (DL-5), and 87 and 91 (Hypodermis) subsampled values pooled from three confocal images. Box and whiskers plots with minimum, lower quartile, median, upper quartile, and maximum. One-way ANOVA, *p<0.05, Tukey test. Scales: c = 20 µm, h = 200 µm, j = 50 µm. The exact p values are listed in Supplementary Table 1.

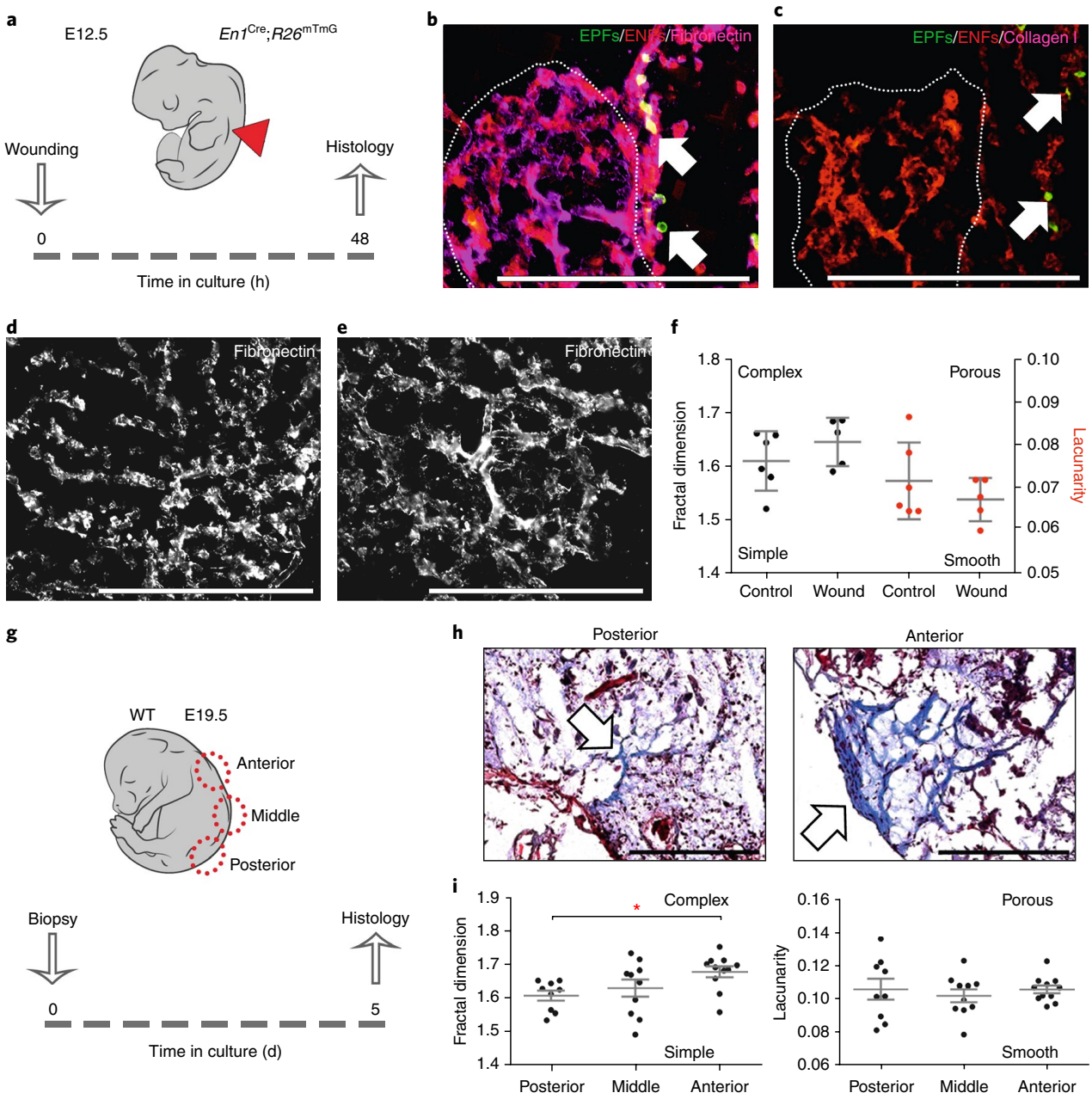

Figure 5 Regeneration-to-scar transition is coupled to EPFs development. a, E12.5 *En1*^{Cre};*R26*^{mTmG} embryos were collected, wounded on the back-skin, and kept in culture for 48 h. **b**, **c**, Immunofluorescence for Fibronectin (**b**) or Collagen I (**c**). Dotted lines delimitate lesion site. Arrows indicate EPFs. **d, e,** Representative immunofluorescence images of fibronectin staining at adjacent fetal skin (d) and wounded site (e) at 48 h post-wounding. **f,** Fractal dimension (left) and lacunarity (right) values derived from fibronectin staining at adjacent fetal skin (control) and wounded site at 24 h and 48 h after wounding. n = 6 optical fields of control skins, and n = 5 optical fields of wounds from two embryos. Mean ± SEM. Two-tailed unpaired Student's *t*-test. **g**, Skin biopsies were taken from anterior, middle, and posterior regions of E19.5 WT embryos and cultured for 5 days. **h**, Masson's trichrome stained sections of posterior (left) or anterior (right) biopsies. Arrows indicate the scar-like deposition of ECM. **i**, Fractal dimension (left) and lacunarity (right) values derived from the cyan channel of Masson's trichrome stained biopsies. Anterior n = 11, middle n = 10, and posterior n = 9. Mean ± SEM. One-way ANOVA, Tukey test, *p = 0.0436. Scales: 200 µm.

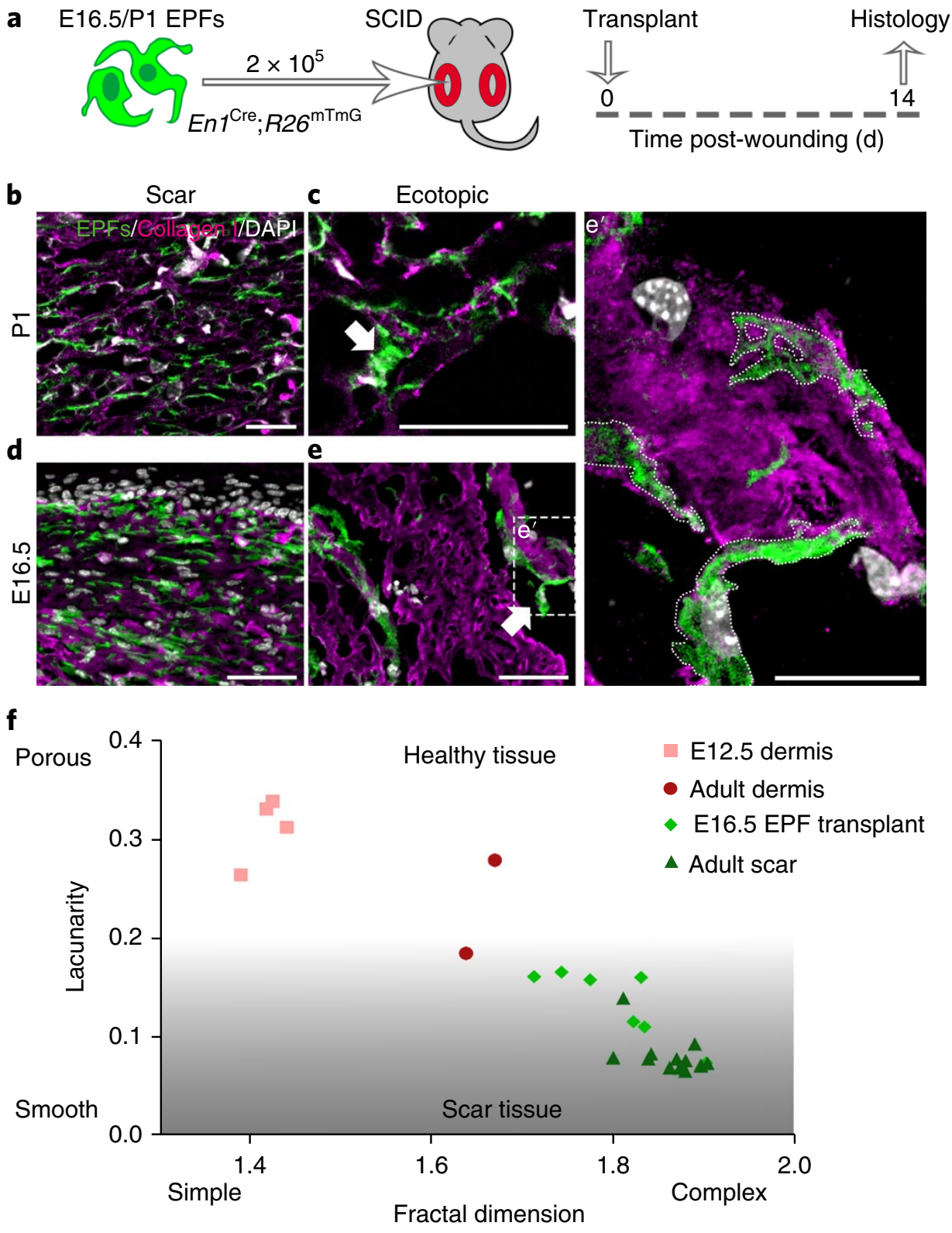

Figure 6 EPFs are a mature scar-matrix-depositing population. a, E16.5 or P1 *En1*^{Cre};*R26*^{mTmG} EPFs were sorted and transplanted (2x10^5) into fresh splinted wounds of adult Rag2$^{-/-}$ mice and the tissue was collected 14 days later. **b-e**, Immunofluorescence for Collagen I of scars (**b**, **d**) or ectopic un-injured sites (**c**, **e**) containing transplanted EPFs from P1 mice (**b-c**) or E16.5 embryos (**d-e**). **e'**, High magnification image of a Collagen I-attached EPF. Dotted line delimitates EPFs cell-body. **f**, Collagen I FD and L scatter plot of E12.5 (squares) and adult (circles) normal dermis, adult scars (triangles), and scars derived from

E16.5 EPFs transplants (diamonds). Scales: b-e = 50 µm, e' = 20 µm. Images represent 1 out of three experiments.

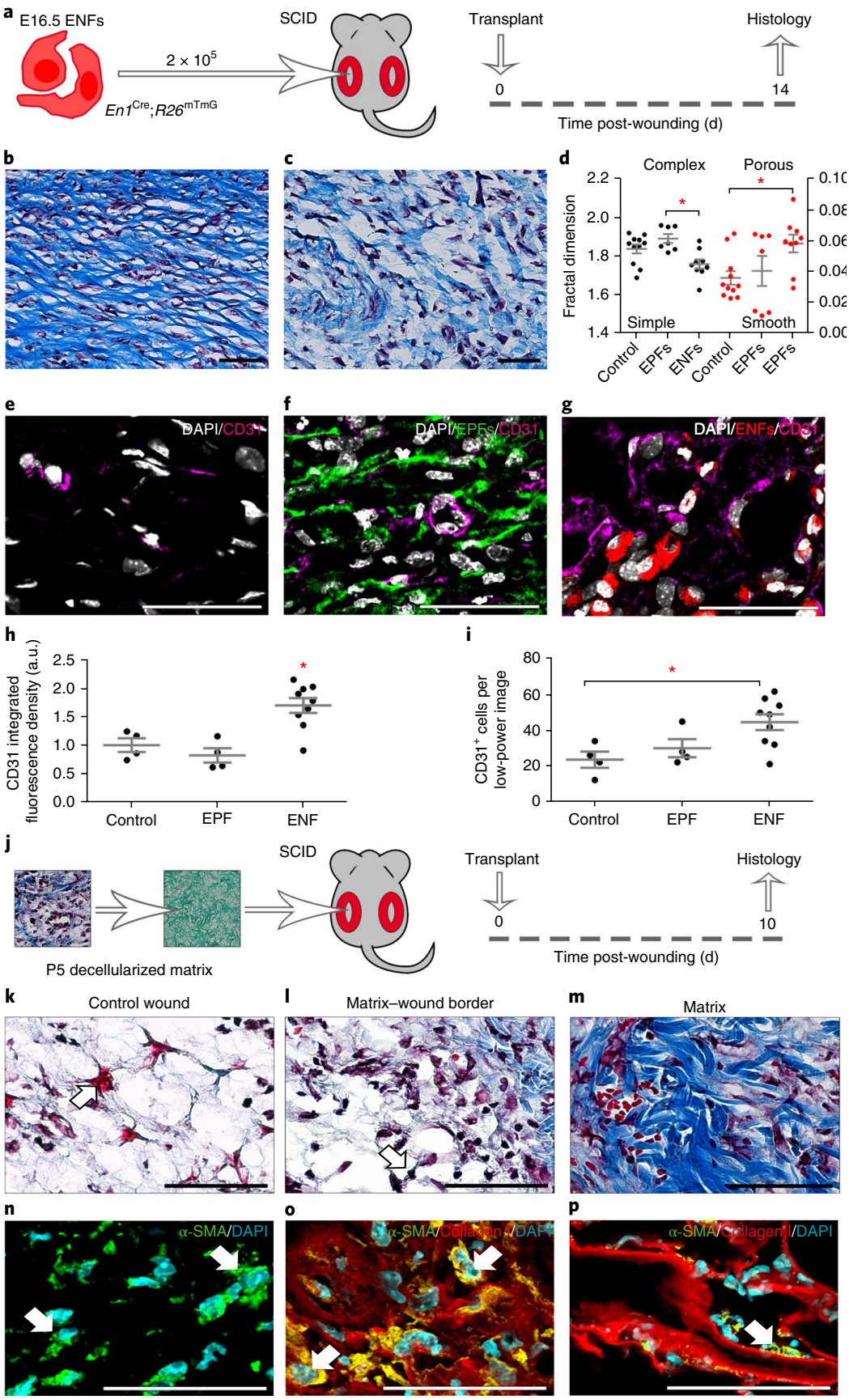

Figure 7 ENFs and ECM transplantations improve scar outcomes. a, E16.5 *En1*^{Cre};*R26*^{mTmG} EPFs were sorted and transplanted (2x10^5) into fresh splinted wounds of

adult Rag2$^{-/-}$ mice and the tissue was collected two weeks after. **b, c,** Masson's trichrome staining of EPFs-transplant scar (b) and ENF-transplant scar (c). **d**, Fractal dimension (left) and lacunarity (right) values derived from the cyan channel of Masson's trichrome stained sections. Mean ± SEM. n = 11 optical fields of control, n = 7 optical fields EPF-transplants, and n = 9 optical fields of ENF-transplants. One-way ANOVA, *p<0.05, Tukey test. . **e-g,** Representative immunofluorescence images of CD31 staining on mock-transplant scars (e), EPFs-transplant scars (f) or ENFs-transplant scars (g). **h-i,** Quantification of CD31 integrated fluorescence density (h) and CD31^{+} cells per low-power (20x) image (i) of mock-transplant, EPFs-transplant, and ENFs-transplant scars. Mean ± SEM. n = 4 optical fields of control, n = 4 optical fields EPF-transplant, and n = 9 optical fields of ENF-transplant, pooled from two independent experiments. One-way ANOVA, *p<0.05, Tukey test. AU, arbitrary unit. **j**, Decellularized matrix transplantation experiment. Back-skin explants from P5 WT mice were decellularized and transplanted into fresh splinted wounds of adult Rag2$^{-/-}$ mice and the tissue was collected 10 days after. **k-m,** Masson's trichrome (k-m) or αSMA and Collagen I (n-p) stained control wounds (**k, n**), border between the transplanted matrix and the wound (**l, o**), or within the transplanted matrix (**m, p**). Scales: 50 μm. Images in panels b,c, e-g and k-p represent 1 out of two experiments. The exact p values are listed in Supplementary Table 1.

Supplementary figures, tables, and videos are available online together with the publisher's version in: doi: 10.1038/s41556-018-0073-8.

Publication II

Correa-Gallegos D, Jiang D, Christ S, Ramesh P, Ye H, Wannemacher J, Gopal SK, Yu Q, Aichler M, Walch A, Mirastschijski U, Volz T, Rinkevich Y. Patch repair of deep wounds by mobilized fascia. Nature. 2019;576(7786):287-292.

Publisher's version is available online in: doi: 10.1038/s41586-019-1794-y.

In the presenting work my contribution included:

Experimental design, animal experiments, histological preparations, *ex vivo* cultures, image analysis, and manuscript and figure preparation.

In particular:

a) Fig.1, 2, extended data Fig.3, 4, and 6: Implementation of chimeric skin grafts to study the relative contributions of dermis and fascia compartments.
b) Extended data Fig 1: Complementary model to fate map fascia cells during wound healing.
c) Fig.3 f-j, Fig.4 j-k, extended data Fig.6, 7, and 10: Fascia ECM fate mapping to show the quick wound patch process mediated by fascia-derived EPFs.
   Fig.4 a-c, extended data Fig.8: Fascia blocking experiments showing the generation of chronic wounds-like phenotype in absence of the fascia influence.
d) Extended data Fig.9 a-c and f-g: *Ex vivo* cultures to prove the irrelevance of cell proliferation in the ECM mobilization process.
e) Fig.5 e-g: Expression analysis of the novel marker NOV in murine fascia and scars.
f) Fig.6: Preparation of summary scheme depicting the major findings of the research.

Patch repair of deep wounds by mobilized fascia
(Final manuscript)

Donovan Correa-Gallegos[1, ξ], Dongsheng Jiang[1, ξ], Simon Christ[1], Pushkar Ramesh[1], Haifeng Ye[1], Juliane Wannemacher[1], Shruthi Kalgudde Gopal[1], Qing Yu[1], Michaela Aichler[2], Axel Walch[2], Ursula Mirastschijski[4,5], Thomas Volz[6], Yuval Rinkevich[1,3*]

[1] Helmholtz Zentrum München, Institute of Lung Biology and Disease, Group Regenerative Biology and Medicine, Munich, Germany
[2] Helmholtz Zentrum München, Research Unit Analytical Pathology, Munich, Germany
[3] Member of the German Centre for Lung Research (DZL)
[4] Rotkreuzklinikum München, Munich, Germany
[5] Wound Repair Unit, CBIB, Faculty of Biology and Biochemistry, University of Bremen, Bremen, Germany
[6] Technical University of Munich, School of Medicine, Klinikum rechts der Isar, Department of Dermatology and Allergology, Munich, Germany

[ξ] These authors have contributed equally

* Correspondence should be addressed to:
Yuval Rinkevich
Phone: +49 (89) 3187 4685
Fax: +49 (89) 3187 4661
yuval.rinkevich@helmholtz-muenchen.de

Mammals form scars to quickly patch up wounds and ensure survival by an incompletely understood mechanism. Here, we discover that skin scars originate from prefabricated matrix in the subcutaneous fascia that homes into wounds. Fate

mapping and live imaging revealed that fascia fibroblasts rise to the skin surface after wounding, dragging their surrounding extracellular jelly-like matrix, including embedded blood vessels, macrophages, and peripheral nerves, to form the provisional matrix. Genetic ablation of fascia fibroblasts prevented matrix from homing into wounds and resulted in poor scars, whereas placing an impermeable film beneath the skin, to prevent fascia fibroblasts migrating upwards, led to chronic open wounds. Thus, fascia contains a specialised prefabricated kit of sentry fibroblasts, embedded within a movable sealant, that preassemble together diverse cell types and matrix components needed to heal wounds. Our findings suggest that chronic and excessive skin wounds may be attributed to the mobility of the fascia matrix.

Mammalian scarring occurs when specialized fibroblasts immigrate into wounds to deposit plugs of extracellular matrix[1]. Abnormal scarring results in either non-healing chronic wounds or aggravating fibrosis[2-4] which represent a tremendous burden for patients and to the global healthcare system. Just in the US, costs related to impaired scarring rise to tens of billions of dollars per year[5].

The origin of fibroblasts in wounds remains unclear and so is the mechanism by which they act[6]. Possible sources such as papillary (upper) and reticular (lower) dermal layers[7], pericytes[8], adipocytes[9-10], and bone-marrow derived monocytes[11] have been suggested. We previously demonstrated that all scars in the back-skin derive from a distinct fibroblast lineage expressing the Engrailed-1 gene during embryogenesis and we refer to these cells as En1-lineage positive fibroblasts (EPFs)[12-13]. This lineage is present not only in the skin but also in the strata underneath, called fascia.

The fascia is a gelatinous viscoelastic membranous sheet that creates a frictionless gliding interface between the skin and the body's rigid structure below. Murine back-skin fascia extends as a single sheet separated from the skin by the *Panniculus carnosus* (PC) muscle, whereas in humans there is no intervening muscle and the fascia consists of several thicker sheets that are continuous with the skin. In humans the facia layers incorporate fibroblasts, lymphatics, adipose tissue, neurovascular sheets and sensory neurons[14-15].

Here, we explored the fundamental mechanisms of scar formation by using matrix-tracing techniques, live-imaging, genetic lineage-tracing and anatomic fate-mapping models. We identified the fascia as a major source for wound-native cells including fibroblasts. Strikingly, we found that wound provisional matrix originates from prefabricated matrix in the fascia that homes into open wounds as a movable sealant dragging along vasculature, immune cells and nerves, upwards into the skin.

Wound cells rise from fascia

To trace the origins of cells in wounds, we developed a fate mapping technique by transplanting chimeric, skin and fascia, grafts into living animals (Fig. 1a and see 'Methods'). At 14 days post wounding (dpw), 80.04 ± 3.443% of the labeled cells in the wound were from fascia origin (Fig. 1b). Fascia-derived cells clogged up the entire wound bordering the regenerated epidermis and even the surrounding dermis, making up 35.46 ± 4.938% of the total labeled cells within a 0.2 mm radius (Fig. 1b-c). 81.63 ± 12.84 % of the αSMA^{+} myofibroblasts, and strikingly, nerve, endothelial, and macrophages within wounds were all predominantly of fascia origin (Fig. 1d-e). Independently, I*n vivo* labeling of the fascia showed same results (Extended Data Fig. 1a and 'Methods'). Labeled cells populated the wounds and surrounding dermis at 14 dpw, whereas in uninjured controls labeled cells remained in the fascia (Extended Data Fig. 1b). 56.71 ± 9.319 % of fascia-derived cells in wounds expressed classical fibroblast markers (Extended Data Fig. 1c). Labeled monocytes/macrophages, lymphatics, endothelium and nerves derived from fascia as well (Extended Data Fig. 1d). Collectively, our two independent fate mapping approaches demonstrate that fascia is a major reservoir of fibroblasts, endothelial, macrophages, and peripheral nerves that populate wounds upon injury.

Fascia fibroblasts dictate scar severity

We then analyzed the scar-forming EPFs across dermal and fascia compartments by using a TdTomato to GFP replacement reporter[12-13] ($En1^{Cre}$;$R26^{mTmG}$, see 'Methods'). Fibroblasts were the predominant fascia cell type (71.1%), while dermis had a significantly lower fraction of fibroblasts (56.4%, Extended Data Fig. 2a-b). Within this population, there were two-times more EPFs than En1-naïve fibroblasts (ENFs) in the fascia (61.2% and 31.8% respectively). Whereas in dermis, there was a six-fold excess of EPFs (83.13% EPFs vs 12.78% ENFs, Extended Data Fig. 2c-d). Fascia was also enriched in regenerative cell types such as endothelial cells and lymphatics, while macrophages and nerve cells compositions were similar in both compartments (Extended Data Fig. 2e). Thus, a higher fibroblast, endothelial, and lymphatic cell content and a lower EPF to ENF ratio distinguishes the fascia from dermis. Two-photon microscopy revealed that fascia EPFs arrange in monolayers of consecutive perpendicular sheets across the dorsal-ventral axis (Extended Data Fig. 2f and Extended Data Video 1). EPFs populate the entire back in topographic continuums extending from the fascia and traversing the PC (Extended Data Fig. 2g-h and Extended Data Video 2). Regions where PC ended or where nerve bundles and blood vessels traversed it showed also continuums of EPFs without clear boundaries (Extended Data Fig. 2i-j). To test if fascia EPFs could access dermal layers upon injury, we generated superficial excisional wounds. Aggregates of EPFs rising into open wounds from fissures in the PC were observed after only 3 dpw (Extended Data Fig. 2k and Extended Data Video 3). Collectively, our observation suggests that fascia EPFs easily traverse upwards into dermal layers during wounding and are unobstructed by the PC muscle.

The deeper an injury, the bigger the scar[16]. We therefore investigated if this correlation can be attributed to fascia by analyzing the extent of fibroblast contributions from the fascia and dermis in deep vs. superficial wounds. For this, we combined genetic lineage-tracing ($En1^{Cre}$;$R26^{mTmG}$) with our anatomic fate-mapping chimeric grafts and performed superficial or deep injuries (Fig. 2a and see 'Methods'). Fourteen days after, wound size of deep injuries were 1.7-times larger than superficial injuries (Fig. 2b-c). Fascia EPFs were 2-times more numerous in deep wounds, whereas dermal EPFs remained constant in both conditions (Fig. 2d). The abundance of fascia EPFs in the wound directly correlated with wound size and thus scar severity, whereas dermal EPFs showed no correlation (Fig. 2e-f). No crossing of EPFs between these compartments was observed in uninjured controls, indicating that the influx of fascia EPFs was triggered by injury (Extended Data Fig. 3a-b).

Long-term tracing of fascia EPFs in wounds showed that they recede at 10 weeks (Extended Data Fig. 3c). This desertion from mature scars occurred through an apoptosis-independent mechanism, indicated by a low rate of cell death (<5 %) across earlier time points (Extended Data Fig. 3d-e).

We then sought to place fascia EPFs in the framework of known lineage markers used to define different populations of wound fibroblasts such as CD24, CD34, DPP4, DLK1, and LY6A[7, 10, 12]. All markers were prominent in fascia EPFs and were surprisingly downregulated upon entering the wound in our graft experiments (Extended Data Fig. 4). Flow cytometry confirmed the higher DPP4, ITGB1, LY6A, and PDGFRα expression in fascia than dermal fibroblasts (Extended Data Fig. 5a-c). Sorted fascia EPFs also revealed low cellular heterogeneity, with the predominant population expressing LY6G^{+}PDGFR^{+} (87.0%) and DPP4^{+}ITGB1^{+} (72.8%, Extended Data Fig. 5d). This broad marker convergence highlights fascia EPFs as the major cell source of wound fibroblasts.

Provisional matrix emerges from fascia matrix

We then looked at the fascia matrix itself. Second harmonic generation (SHG) signal and scanning electro-micrographs (SEM) revealed profuse coiled collagen fibrils in the fascia, indicative of a relaxed and immature matrix (Fig. 3a-b). Fractal measurements[13] of the fiber alignments showed a more condensed matrix configuration in fascia than the stretched and woven dermal matrix (Fig. 3c).

The immaturity of the fascia matrix motivated us to check if it could work as a repository for scar tissue. For this, we developed an incubation chamber that enabled live imaging of fascia biopsies over days (see 'Methods'). Recording of SHG signal showed steering of the matrix at a rate of 11.4 μm/h (Fig. 3d-e and Extended Data Video 4). Assuming a similar rate *in vivo*, the fascia matrix could move ~2 mm in 7 days, accounting for the dynamics of provisional matrix deposition in mammals.

To test if fascia matrix steers into wounds *in vivo*, we developed a technique to trace the fascia matrix in our chimeric grafts using NHS esters. (Fig. 3f and see 'Methods'). Streams of traced matrix from the fascia already extended upwards and plugged the open wounds at 7 dpw (Fig. 3g and Extended Data Fig. 6a-b). Fascia-derived matrix covered 74.78 ± 12.94% of total collagen content in the wound (Extended Data Fig. 6c). Our data indicated that individual fascia matrix fibers are not being pulled but rather pliable matrix is extended upwards to mold the wound. Advanced wound stages showed a label decline in specific regions of the wound suggesting an active remodeling process of the fascia-derived matrix (Extended Data Fig. 6d-f, and Extended Data Video 5).

We then tested whether dermal matrix could be steered by double labeling our chimeric grafts. Only the fascia matrix plugged deep injury wounds (Extended Data Fig. 6g-j) while dermal matrix remained immobile in deep and superficial injuries, the later which healed via *de novo* matrix deposition (Extended Data Fig. 6k-l).

To further prove that fascia matrix is steered into open wounds, we labeled the fascia matrix *in situ* prior to injury (Fig. 3h-i and "Methods"). Label-carrying matrix made most of the wound provisional matrix (Fig. 3j), which underwent remodeling during the first two weeks (Extended Data Fig. 7 a-b). Fractal measurements showed fascia fiber interfaces expanded by 3 dpw, ,changing from a parallel sheet arrangement, into a highly porous plug. This expansion is followed by contraction into thicker and more complex mature scar matrix architecture (Extended Data Fig. 7c-e). Surprisingly, traced matrix was also present in the eschar. Activated platelets infiltrated and clustered within fascia fibers before eschar formation (Extended Data Fig. 7f), indicating that the coagulation cascade occurs in parallel with fascia matrix steering.

EPFs steer fascia matrix into wounds

To test if matrix steering from fascia is caused by EPFs, we blocked fascia by implanting an impermeable dual surface ePTFE membrane[17] between the fascia and the PC in wounds of $En1^{Cre};R26^{VT2/GK3}$ mice (Fig. 4a and 'Methods'). Surprisingly, wounds with implants remained completely open whereas sham controls closed within 21 days (Fig. 4b). After two months EPFs trailed from the wound margins and under the membrane without generating scars (Fig. 4c and Extended Data Fig. 8a). Implants produced a transient inflammation that resolved even when the wound remained open. Two-month-old wounds with implants showed normal leukocyte and pro- and anti-inflammatory interleukins levels (Extended Data Fig. 8b-i), consistent with the clinical use of ePTFE as immunologically inert membranes. The coagulation cascade also was unaltered at the border between the dermis and the membrane (Extended Data Fig. 8j-k). These results indicate that the lack of scarring with ePTFE membranes does not reflect chronic inflammation or poor clotting, but a fascia steering blockade that is mediated by the fascia fibroblasts. These findings further support the notion that scar tissue is mostly fascia-derived, since in the absence of fascia movements, dermal EPFs or dermal matrix are unable to repair wounds.

We then asked whether mechanical separation between dermis and fascia alone, without barrier implants, would affect matrix steering and scar formation. To address this question, we performed full excisional wounds in wild type mice and physically released the fascia below the PC around the wound (Fig. 4d). Wound closure from released-fascia wounds was significantly delayed, and wounds remained open early on similarly to those documented following membrane implantations (Fig. 4e-f).

To definitively link fascia EPFs to matrix steering, we genetically ablated fascia EPFs using two separate strategies. First, we used a transgenic line that expresses the diphtheria toxin receptor (DTR) in a Cre-dependent manner ($R26^{iDTR}$), allowing us to deplete cells expressing Cre recombinase upon diphtheria toxin (DT) exposure. We thus generated Cre-expressing adeno-associated viral particles (AAV6-Cre) and injected them into the fascia of $R26^{iDRT}$ pups underneath freshly made full excisional wounds (Fig. 4g). Scar size from AAV6-Cre transduced mice treated with DT were significantly smaller than controls (Fig. 4h-i).

Secondly, we used $En1^{Cre};R26^{iDTR}$ double transgenics in which DTR expression is restricted to EPFs, making them susceptible to DT-mediated ablation. We corroborated the ablation of fascia EPFs in cultured biopsies 6 days after acute exposure to DT for 1h. Effective dose of DT prevented the normal increase in collagen fiber density observed in control samples and decreased 2.5-times the cell density (Extended Data Fig. 9a-c). Live imaging showed absence of any matrix steering after DT exposure (Extended Data Fig. 9d-e and Extended Data Video 6), confirming that fascia EPFs are pivotal for matrix steering.

Next, we created chimeric grafts using dermis from wild-type mice and fascia from $En1^{Cre};R26^{iDTR}$ mice. We ablated fascia EPFs using DT as before and labeled the matrix before transplantation (Fig. 4j). Ablation of fascia EPFs prevented matrix steering into the wound (Fig. 4k-l) and Instead labeled matrix remained in the fascia layer below. Altogether, our data conclusively demonstrate that fascia resident EPFs actively steer matrix to seal open wounds.

To check if fibroblast proliferation preceded and was needed for matrix steering, we analyzed the proliferation rate in our matrix-tracing experiments. Expansion of the fascia gel beneath the wound occurred during the first days after injury, whereas cell proliferation peaked after a week (Extended Data Fig. 10a-c), indicating that proliferation is not required for matrix steering. Furthermore, treatment with a proliferation inhibitor had no effect on fascia matrix steering *in vitro* (Extended Data Fig. 9f-k and Extended Data Video 7). Our results prove that fascia matrix works as an expanding sealant that quickly clogs deep wounds independently of cell proliferation.

Fascia and keloid share marker signatures

Human keloids show features of early and unresolved wounds, such as itchiness, inflammation, and pain[18]. This motivated us to investigate the presence of fascia fibroblasts in keloid tissue. We screened for markers present in keloids and compared them with healthy dermis and the connective tissue in the subcutaneous space (Fascia) of human skin across multiple anatomic locations (Fig. 5a-b). FAP and DPP4 markers were highly expressed in both fascia and keloids with low expression in dermis. The fascia-restricted protein NOV was also prominently expressed in both human and mouse fascia, as well as in human keloids and mouse scars (Fig. 5c-g). This preservation of fascia markers across mouse and human fascia and keloid scars suggests a common fascia origin for human cutaneous scars.

Discussion

Current wound healing models propose that dermal fibroblasts migrate into wounds and locally deposit matrix *de novo* onto the granulation tissue provided by the coagulation cascade. This provisional matrix is then remodeled into a mature scar. Based on our findings, we propose a revised model (Fig. 6) where, in deep injuries, fascia fibroblasts pilot their local composite matrix into wounds that, in coordination with the coagulation cascade, form the provisional matrix. Thus, instead of *de novo* matrix deposition by dermal fibroblasts, a “scar primordium” is steered by the fascia fibroblasts. Thus, fascia serves as an *externum repono* for scar-forming provisional matrix, which represent a much efficient mechanism to quickly seal large open wounds. Previous studies have shown that the matrix undergoes motion during early development and organ morphogenesis[19-22]. To our knowledge, the extent and magnitude of matrix movements we document here have never been observed during injury or regenerative settings. Cultured dermal fibroblasts have been shown to pull and reorient individual collagen or fibronectin fibers locally in cultured plates as well as in 3D *in vitro* assays[23-24]. Whereas, our findings reveal an unprecedented dynamic and scale of motion for composite tissue matrix during injury that is mediated exclusively by specialized fibroblasts of the fascia.

Our findings on fascia contribution to large scars and its blockage leading to chronic open wounds, indicates that the spectrum of poor and excessive scarring in the skin, such as diabetic and ulcerative wounds, as well as hypertrophic and particularly keloid scars might all be attributed to fascia. Indeed, the subcutaneous fascia varies widely in different species, sex, age, and anatomic skin locations[25]. In some mammals, the superficial fascia is loose, whereas in scar-prone species like human, dog and horse, the superficial fascia is thicker. Human fascia further varies in thickness on different regions of the body[26]. For example, lower chest, back, thigh and arm have much thicker and multi-layered membranous sheets, and it is these anatomic sites that are prone to form large and keloid scars. Whereas other sites such as the foot have a much thinner or inexistent fascia[27]. Understanding the topographic anatomy of the fascia layer may help explain scar phenotypes and severities, including the occurrences of hypertrophic and keloid scars.

References

1. Marshall, C. D., Hu, M. S., Leavitt, T., Barnes, L. A., Lorenz, H. P. & Longaker, M. T. Cutaneous scarring: basic science, current treatments, and future directions. Advances in wound care **7** (2), 29-45 (2018).

2. Finnerty, C. C., Jeschke, M. G., Branski, L. K., Barret, J. P., Dziewwulski, P. & Herndon, D. N. Hypertrophic scarring: the greatest unmet challenge after burn injury. The Lancet **388**, 1437-1436 (2016).

3. Morton, L. M. & Phillips, T. J. Wound healing and treating wounds: differential diagnosis and evaluation of chronic wounds. J Am Acad Dermatol **74** (4), 589-605 (2016).

4. Do, N. N. & Eming, S. A. Skin fibrosis: models and mechanisms. Curr Res Transl Med **64** (4), 185-193 (2016).

5. Sen, C. K., Gordillo, G. M., Roy, S., Kirsner, R., Lambert, L., Hunt, T. K., Gottrup, F., Gurtner, G. C. & Longaker, M. T. Human skin wounds: a major and snowballing threat to public health and the economy. Wound Repair Regen **17** (6), 763-71 (2009).

6. Hinz, B. Myofibroblasts. Exp Eye Res **142**, 56-70 (2016).

7. Driskell, R. R., Lichtenberger, B. M., Hoste, E., Kretzschmar, K., Simons, B. D., Charalambous, M., Ferron, S. R., Herault, Y., Pavlovic, G., Ferguson-Smith, A. C., & Watt, F. M. Distinct fibroblast lineages determine dermal architecture in skin development and repair. Nature **504** (7479), 277-281 (2013).

8. Greenhalgh, S. N., Conroy, K. P., & Henderson, N., C. Healing scars: targeting pericytes to treat fibrosis. QJM **108** (1), 3-7 (2015).

9. Plikus, M. V., Guerrero-Juarez, C. F., Ito, M., Li, Y. R., Dedhia, P. H., Zheng, Y., Shao, M., Gay, D. L., Ramos, R., His, T. C., Oh, J. W., Wang, X., Ramirez, A., Konopelski, S. E., Elzein, A., Wang, A., Supapannachart, R. J., Lee, H. L., Lim, C. H., Nace, A., Guo, A., Treffeisen, E., Andl, T., Ramirez, R. N., Murad, R., Offermanns, S., Metzger, D., Chambon, P., Widgerow, A. D., Tuan, T. L., Mortazavi, A., Gupta, R. K., Hamilton, B. A., Millar, S. E., Seale, P., Pear, W. S., Lazar, M. A., & Cotsarelis, G. Regeneration of fat cells from myofibroblasts during wound healing. Science **355** (6326), 748-752 (2017).

10. Shook, B. A., Wasko, R. R., Rivera-Gonzalez, G. C., Salazar-Gatzimas, E., López-Giráldez, F., Dash, B. C., Muñoz-Rojas, A. R., Aultman, K. D., Zwick, R. K., Lei, V., Arbiser, J. L., Miller-Jensen, K., Clark, D. A., Hsia, H. C., & Horsley, V. Myofibroblast proliferation and heterogeneity are supported by macrophages during skin repair. Science **362** (6417), eaar2971 (2018).

11. Mori, L., Bellini, A., Stacey, M. A., Schmidt, M., & Mattoli, S. Fibrocytes contribute to the myofibroblast population in wounded skin and originate from the bone marrow. Exp Cell Res **304** (1), 81-90 (2005).

12. Rinkevich, Y., Walmsley, G. G., Hu, M. S., Maan, Z. N., Newman, A. M., Drukker, M., Januszyk, M., Krampitz, G. W., Gurtner, G. C., Lorenz, H. P., Weissman, I. L. & Longaker, M. T. Skin fibrosis. Identification and isolation of a dermal lineage with intrinsic fibrogenic potential. Science **348** (6232), aaa2151 (2015).

13. Jiang, D., Correa-Gallegos, D., Christ, S., Stefanska, A., Liu, J., Ramesh, P., Rajendran, V., De Santis, M. M., Wagner, D. E. & Rinkevich, Y. Two succeeding fibroblastic lineages drive dermal development and the transition from regeneration to scarring. Nat Cell Biol **20** (4), 422-431 (2018).

14. Adstrum, S., Hedley, G., Schleip, R., Stecco, C., Yucesoy, C. A. Defining the fascia system. J Bodyw Mov Ther **21** (1), 173-177 (2017).

15. Stecco, C. & Schleip, R. A fascia and the fascia system. J Bodyw Mov Ther **20** (1), 139-140 (2016).

16. Dunkin, C. S., Pleat, J. M., Gillespie, P. H., Tyler, M. P., Roberts, A. H. & McGrouther, D. A. Scarring occurs at a critical depth of skin injury: precise measurement in a graduated dermal scratch in human volunteers. Plast Reconstr Surg **119** (6), 1722-34 (2007).

17. Koehler, R., H., Begos, D., Berger, D., Carey, S., LeBlanc, K., Park, A., Ramshaw, B., Smoot, R., & Voeller, G. Minimal adhesions to ePTFE mesh after laparoscopic ventral incisional hernia repair: reoperative findings in 65 cases. JSLS **7** (4), 335-40 (2003).

18. Rippa, A., L., Kalabusheva, E., P., & Vorotelyak, E., A. Regeneration of dermis: scarring and cells involved. Cells **8** (6). 607 (2019).

19. Zamir, E. A., Rongish, B.J. & Little, C. D. The ECM moves during primitive streak formation--computation of ECM versus cellular motion. PLoS Biol **6** (10), e247 (2008).

20. Szabó, A., Rupp, P. A., Rongish, B. J., Little, C. D. & Czirók, A. Extracellular matrix fluctuations during early embryogenesis. Phys Biol **8** (4), 045006 (2011).

21. Aleksandrova, A., Czirók, A., Szabó, A., Filla, M. B., Hossain, M. J., Whelan. P. F., Lansford, R. & Rongish, B. J. Convective tissue movements play a major role in avian endocardial morphogenesis. Dev Biol **363** (2), 348-61 (2012).

22. Loganathan, R., Rongish, B. J., Smith, C. M., Filla, M. B., Czirok, A., Bénazéraf, B. & Little, C. D. Extracellular matrix motion and early morphogenesis. Development **143** (12), 2056-65 (2016).

23. Miron-Mendoza, M., Koppaka, V., Zhou, C. & Petroll, W. M. Techniques for assessing 3-D cell-matrix mechanical interactions in vitro and in vivo. Exp Cell Res **319** (16), 2470-80 (2013).

24. Sakar, M., S., Eyckmans, J., Pieters, R., Eberli, D., Nelson, B., J., & Chen, C., S., Cellular forces and matrix assembly coordinate fibrous tissue repair. Nat Commun **16** (7). 11036, (2016).

25. Abu-Hijleh, M., F., Roshier, A., L., Al-Shboul, Q., Dharap, A., S., & Harris, P., F. The membranous layer of superficial fascia: evidence for its widespread distribution in the body. Surg Radiol Anat **28** (6). 606-19 (2006).

26. Avelar, J. Regional distribution and behavior of the subcutaneous tissue concerning selection and indication for liposuction. Aesthetic Plast Surg **13** (3). 155-65 (1989).

27. Lockwood, T., E. Superficial fascia system (SFS) of the trunk and extremities: a new concept. Plast Reconstr Surg **87** (6). 1009-18 (1991).

Figures

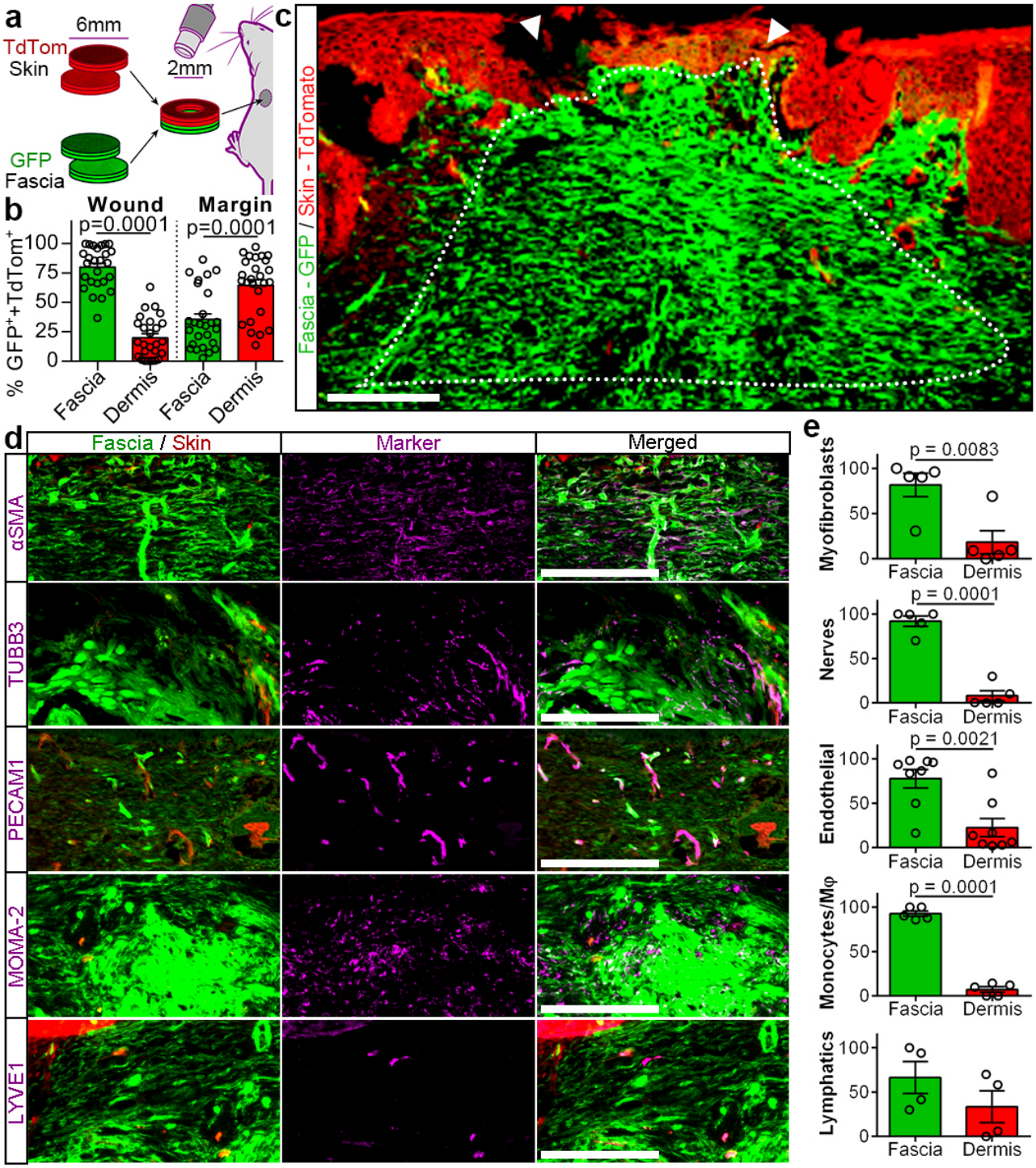

Fig. 1. Fascia is a major cellular source for wounds. **a**. Chimeric grafts to determine contributions of dermis and fascia. **b**. Percentages of TdTomato$^+$ or GFP$^+$ cells from total labeled cells in the wound and wound margin. Mean and SEM, n= 26 images from 4 biological replicates. One-way ANOVA, multiple comparison Tukey test, confidence interval = 95%. **c**. Wound showing skin- and fascia-derived cells at 14 dpw. **d-e.** Immunolabeling and contributions to myofibroblasts (αSMA), nerves (TUBB3), blood vessels (PECAM1), monocytes/macrophages (MOMA-2), and lymphatics (LYVE1). Mean and SEM, n= 4 (LYVE1), 5 (αSMA, TUBB3, and MOMA-2), or 8 (PECAM1) images from 4 biological replicates. Unpaired two-tailed T-test, confidence interval = 95%. Dotted lines delimitate the wound. Arrowheads indicate injury site. Scales = 200 microns.

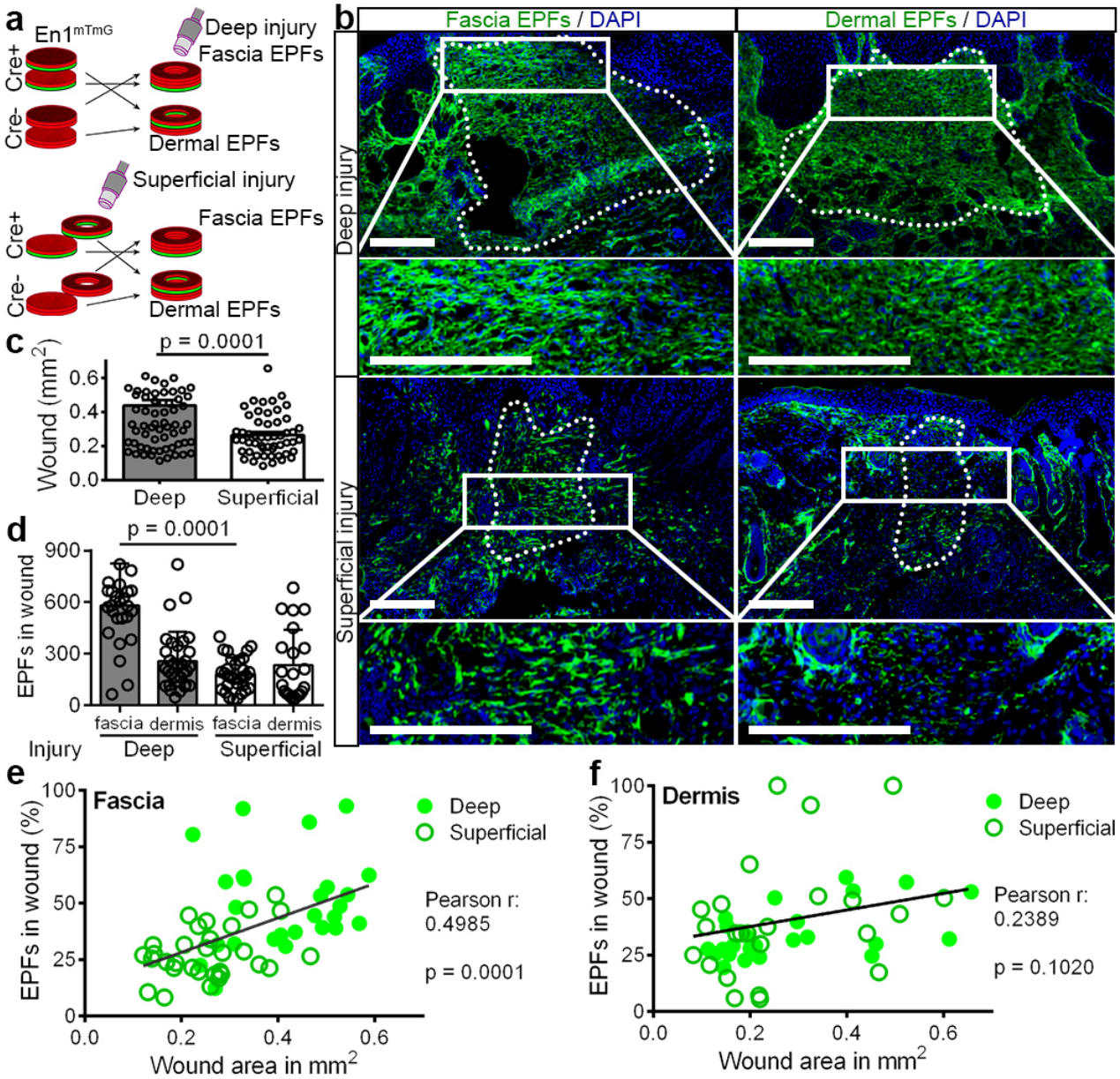

Fig. 2. Fascia EPFs dictate scar severity. **a**. Dermal vs fascia EPFs chimeric grafts. **b**. Images showing fascia EPFs (left) or dermal EPFs (right) in wounds after a deep (top) or superficial injury (bottom). **c**. Wound size. Mean with SEM, n= 70 (deep) and 53 (superficial) images analyzed from 5 biological replicates. Unpaired, two-tailed T-test, confidence interval = 95%. **d**. Fascia and dermal EPFs numbers. Mean with SEM, n= 27, 32, 27, and 22 images analyzed from 5 biological replicates. Unpaired, two-tailed T-test, confidence interval = 95%. **e-f**. XY plots of EPFs fractions and wound size from fascia (e) and dermal EPFs (f). n= 57 (e) and 48 (f) images analyzed from 5 biological replicates. Two-tailed R^2 Pearson correlation, confidence interval = 95%. Dotted lines delimitate wounds. Scale bars = 200 microns.

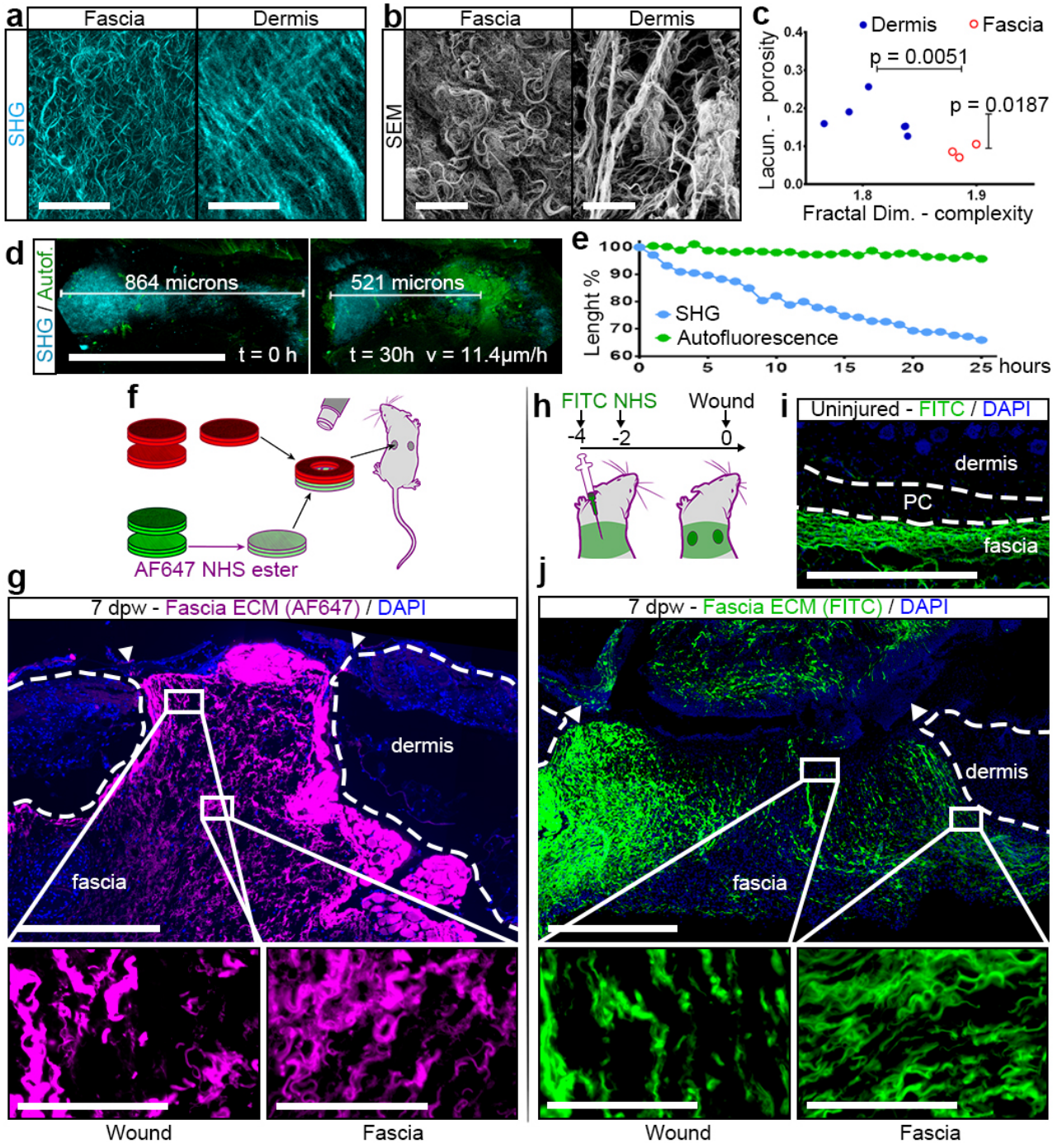

Fig. 3. Fascia matrix steers into wounds. **a**. SHG (a) and SEM images (b) of fascia (left) and dermis (right) showing matrix arrangements, representative images of 3 biological replicates. **c**. Fractal dimension and lacunarity values from SHG images. n = 5 and 3 images analyzed from 3 biological replicates. Unpaired two-tailed T-test, confidence interval = 95%. **d**. Time-lapse images of fascia in culture at time 0 (left), and 30 hours (right). Representative video from at least three independent experiments. **e**. Contraction rate from the SHG and autofluorescence. Data obtained from extended data video 4. **f**. Fascia matrix labeling with AF647 NHS ester in chimeric grafts. **g**. 7 dpw images showing fascia matrix covering the wound, representative image of at least three biological replicates. **h**. *In situ* fascia matrix tracing experiment using FITC NHS ester. **i**. Uninjured controls showing specificity of the labeling in fascia, representative sample of at least three biological replicates. **j**. 7 dpw images showing fascia matrix covering the wound area, representative samples of at least three biological replicates. Arrowheads indicate the original injury. Brocken lines delimitate dermis (g and j) or PC (i). Scale bars = 30 microns (a-b), 500 microns (d, g, and i-j), and 100 microns (g and j magnified areas).

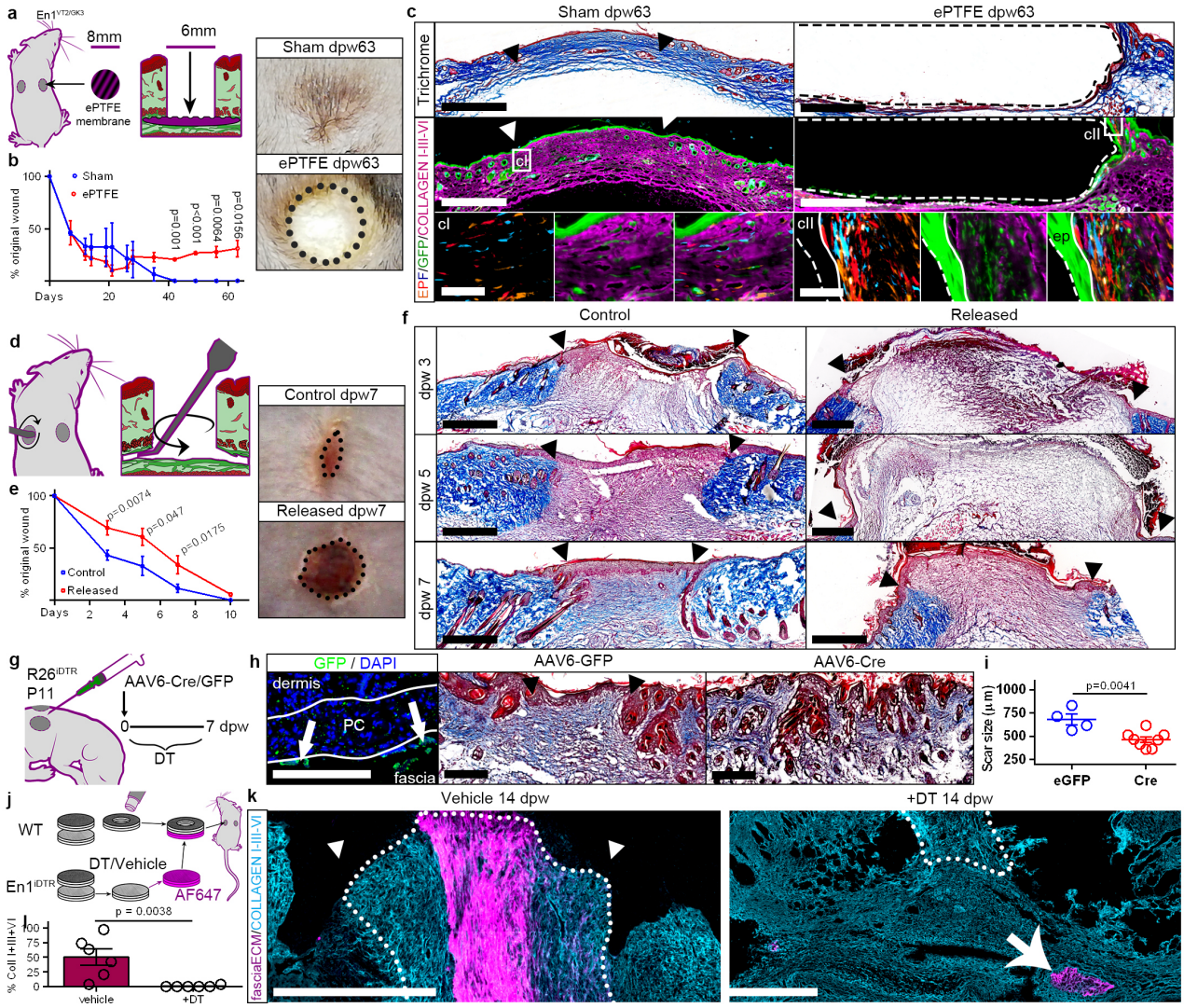

Fig. 4. Fascia EPFs steer scar primordium into wounds. **a**. ePTFE implants to block fascia steering. **b**. ePTFE-implanted or sham wound closure (left) determined from photographs (right) at specified time points. Mean with SEM, n = 3 biological replicates. Unpaired two-tailed T-test, confidence interval = 95%. **c**. Sham (left) or ePTFE-implanted (right) wounds at 63 dpw. Trichrome staining (top) and collagens immunolabeling (middle). Magnifications (**cI-II**, bottom) show multiclonal dermal EPFs. Representative images from 3 biological replicates. **d**. Fascia release experiment. **e**. Fascia-released or control wound closure (left) determined from photographs (right) at specified time points. Mean with SEM, n = 8 (0-3 dpw), 6 (5 dpw), 4 (7 dpw), and 2 (10 dpw) images from 8 biological replicates. Unpaired two-tailed T-test, confidence interval = 95%. **f**. Trichrome stained wounds at 3, 5, and 7 dpw (from top to bottom) from control (left) or fascia-released wounds (right). Representative images from 8 biological replicates. **g**. Fascia cell depletion in $R26^{iDTR}$ neonates. **h**. Trichrome stained wounds at 7 dpw in GFP- (left) or Cre-transduced (right). Arrows indicate GFP-positive cells. Representative images from 3 biological replicates. **i**. Scar-length measurements. Mean with SEM, n = 4 and 8 sections from 3 biological replicates. Unpaired two-tailed T-test, confidence interval = 95%. **j**. Fascia EPFs depletion in chimeric grafts with fascia matrix labeling. **k**. Immunolabeling for collagens, and fascia matrix in control (left) or DT-treated (right) grafts. Representative images from 3 biological replicates. **l**. Matrix labeling coverage. Mean with SEM, n = 6 sections from 3 biological replicates. Unpaired two-tailed T-test, confidence interval = 95%. Dashed lines delimit the implant. Dotted lines delimitate the wound. Arrowheads indicate original injury. Arrow indicates remaining labeled fascia matrix in DT-treated grafts. Scale bars = 50 microns (cI and cII), 200 microns (h), and 500 microns (c, f, h, and k).

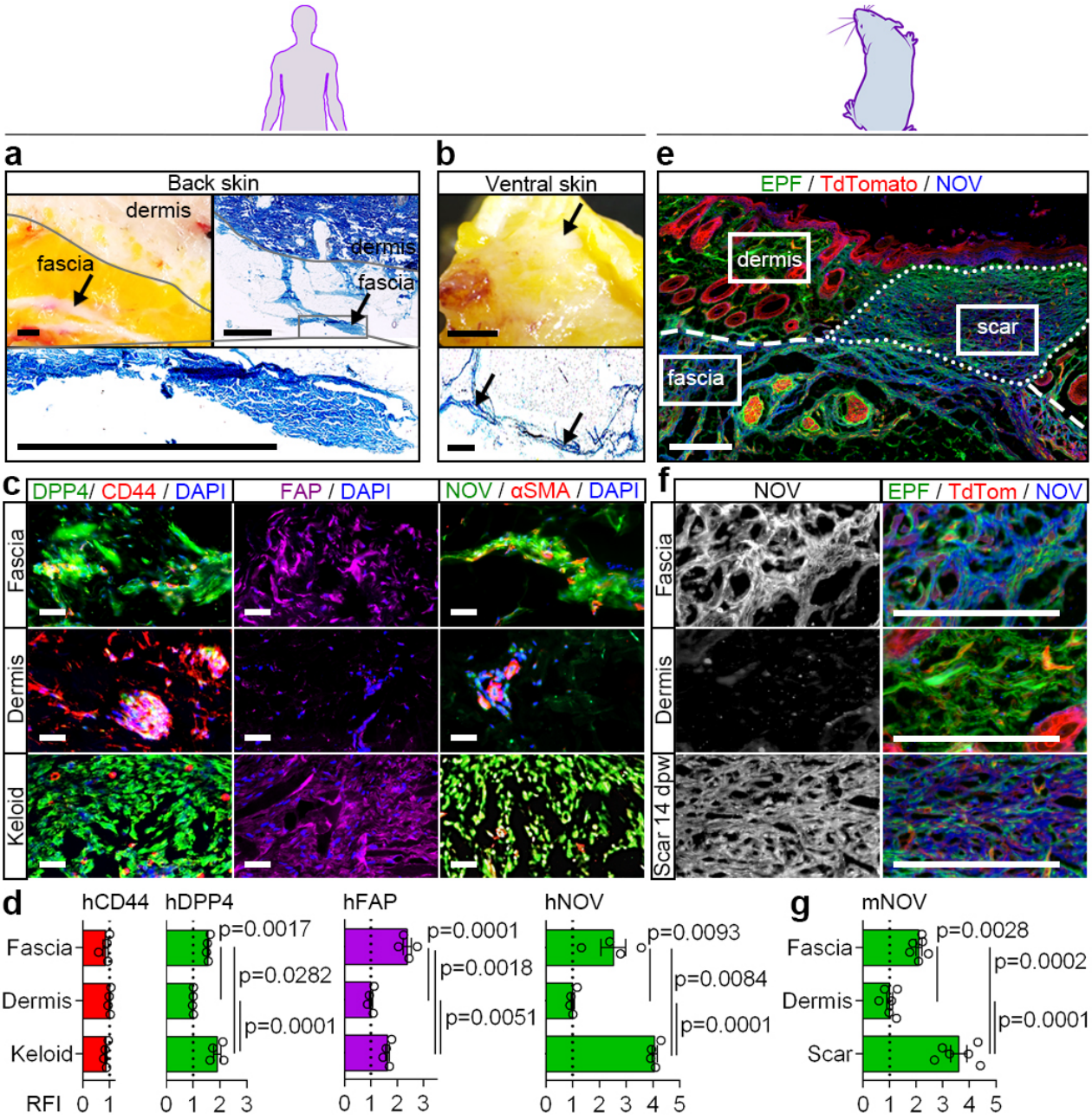

Fig. 5. Marker signature in keloids and fascia. **a-b**. macroscopic pictures and trichrome staining of human back and abdominal skin showing fascia layers embedded in subcutaneous tissue. Arrows indicate the fascia. Representative images from 4 independent samples **c**. Co-immunolabeling for DPP4-CD44, FAP, and NOV-αSMA on fascia, dermis, and keloids of human back skin. **d**. Relative fluorescence intensity (RFI) normalized to the dermis. Mean with SEM, n= 4 images analyzed from 4 biological replicates. One-way ANOVA with Tukey's test, 95% Confidence interval. **e-f**. Immunostaining for NOV on $En1^{Cre}$;$R26^{mTmG}$ 14 dpw scars. **g**. Relative fluorescence intensity normalized to the dermis. Mean with SEM, n = 6 images of 3 biological replicates. One-way ANOVA, Tukey's test, 95% Confidence interval. Dotted and broken lines delimitate scar and fascia respectively. Scale bars: 2 mm (a-b), 50 microns (c), and 200 microns (e-f).

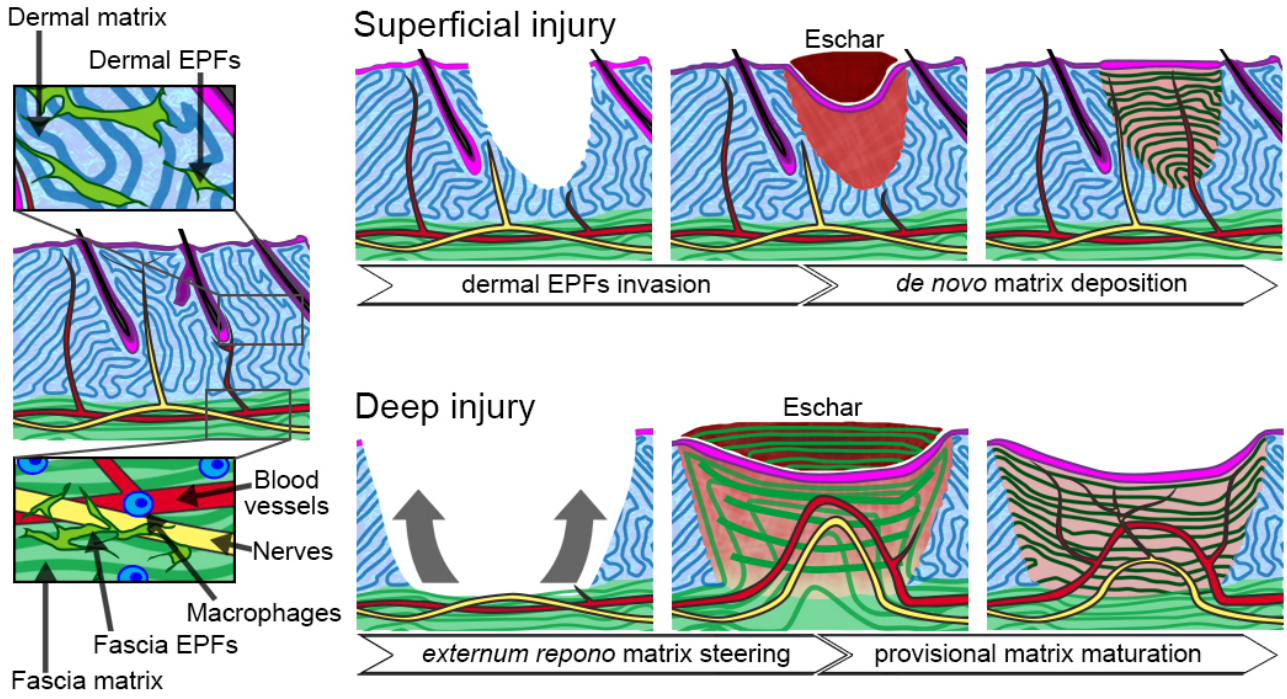

Fig. 6. Revised wound healing model. Superficial injuries heal by the classical fibroblast migration and *de novo* matrix deposition process. In response to a deep injury, fascia fibroblasts steer their surrounding tissue up into wounds. Fascia-derived macrophages, endothelial and peripheral nerves rapidly clog the open wound. In coordination with the platelet response, the fascia matrix serves as a provisional matrix that undergoes remodeling until curated into a mature scar.

Extended data figures

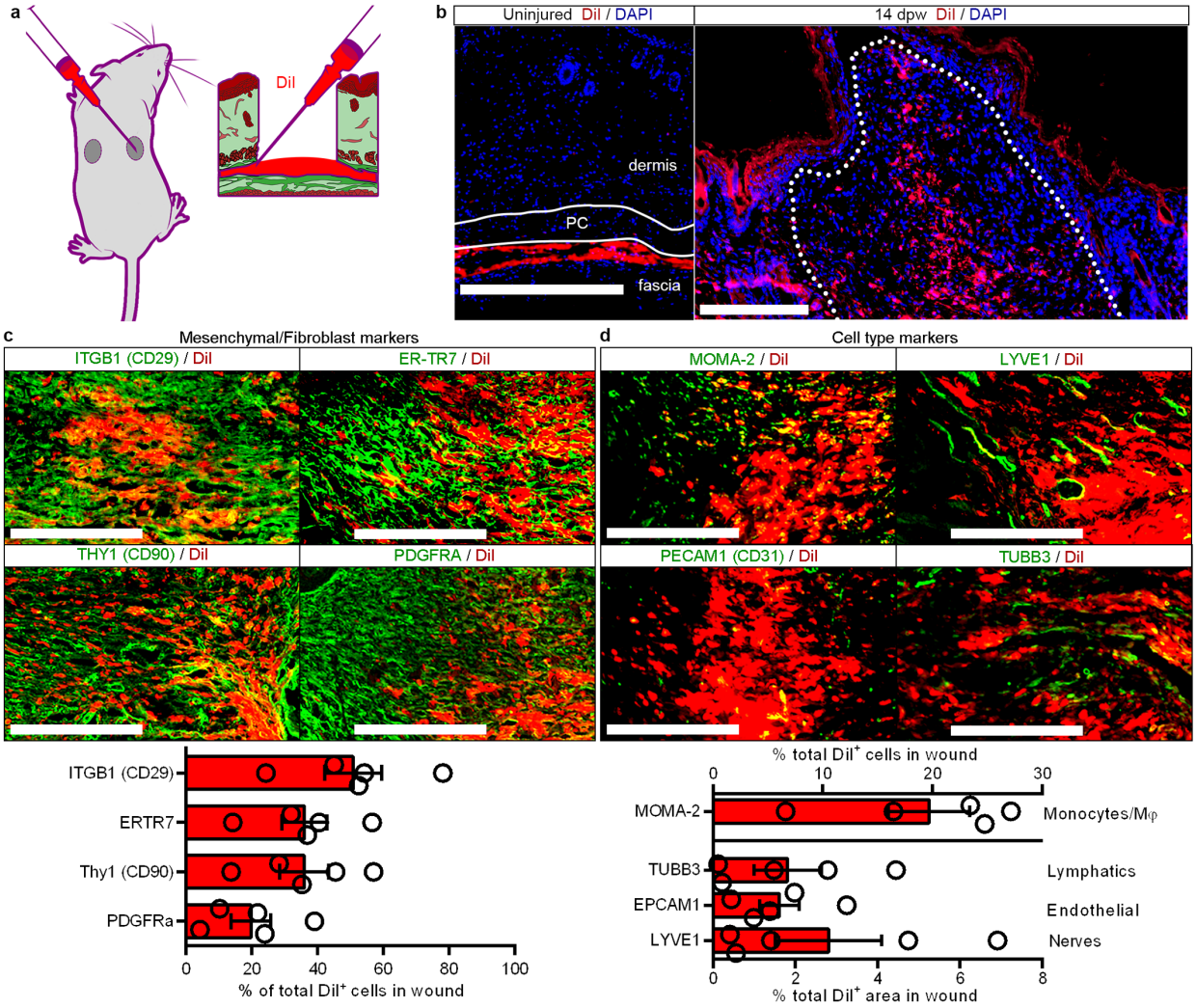

Extended Data Fig. 1. Fate mapping of fascia cells with DiI. **a**. DiI labeling of fascia cells. **b**. Histology showing DiI$^+$ cells in uninjured controls (left) and 14 dpw (right). Representative images of 5 biological replicates. **c**. Immunolabeling (top) and fractions (bottom) of DiI-positive cells expressing mesenchymal/fibroblast markers ITGB1 (CD29), ER-TR7, THY1 (CD90), and PDGFRA, **d**. Immunolabeling (top) and fractions of DiI-positive monocytes/macrophages (MOMA-2), lymphatics (LYVE1), endothelial (PECAM1), and nerves (TUBB3). Mean with SEM, n= 5 (4 in MOMA-2) images analyzed from 5 biological replicates. Lines delimitate PC. Dotted line delimitates the wound. Scale bars = 200 microns. PC = *Panniculus carnosus*.

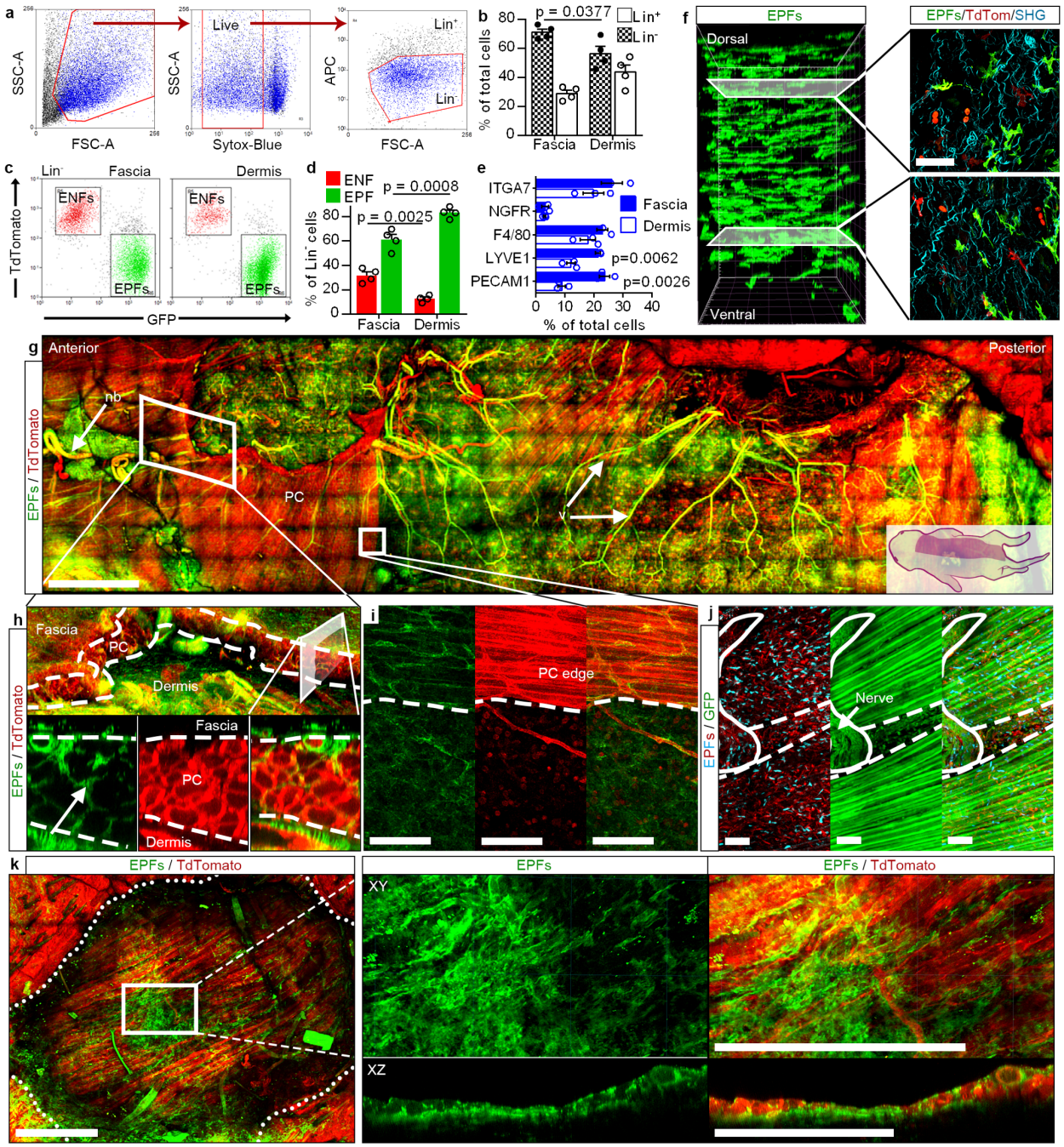

Extended Data Fig. 2. Fascia EPFs traverse PC. **a**. Gating strategy for fibroblasts analysis. **b**. Percentages of fibroblasts (Lin^-) and lineage-positive cells in fascia and dermis. Mean and SEM, n= 4 independent experiments. Unpaired two-tailed T-test, confidence interval = 95%. **c**. Scatter plots of EPFs (GFP^+, Lin^-) and ENFs ($TdTomato^+$, Lin^-) in fascia and dermis. Representative plots of three independent experiments. **d**. EPFs and ENFs fractions in fascia and dermis. Mean with SEM, n= 4 independent experiments. Two-way ANOVA, multiple comparison Tukey test, confidence interval = 95%. **e**. Endothelial ($PECAM1^+$), lymphatics ($LYVE1^+$), macrophages ($F4/80^+$), and nervous ($NGFR^+$) fractions in fascia and dermis. Mean with SEM, n= 3 biological replicates. Two-way ANOVA, multiple comparison Tukey test, confidence interval = 95%. **f-k**. Representative images of 3D rendered $En1^{Cre}$;$R26^{mTmG}$ or $En1^{Cre}$;$R26^{VT2/Gk3}$ back skin fascia from at least three biological replicates. **f**. Lateral view (left) and cross-sections (right) of adult fascia. **g**. Top view (ventral side up) of neonate back-skin. **h**. Top side view (top) and lateral cross-section (bottom) at the forelimb junction showing EPF traversing the PC. **i**. Top view at a muscle breach showing EPFs in both locations. **j**. Top view at a muscle opening where nerves pass through and polyclones

of EPFs reside. **k**. Top view (top, epidermis side up) and lateral cross-section (bottom) of an adult superficial wound (3 dpw). Brocken lines delimitate the PC muscle layer. Dotted lines delimitate the epidermis. Scale bars = 1500 microns (g), 100 microns (f, i-j), and 500 microns (k). PC = *Panniculus carnosus*, v = vessels, nb = nerve bundles.

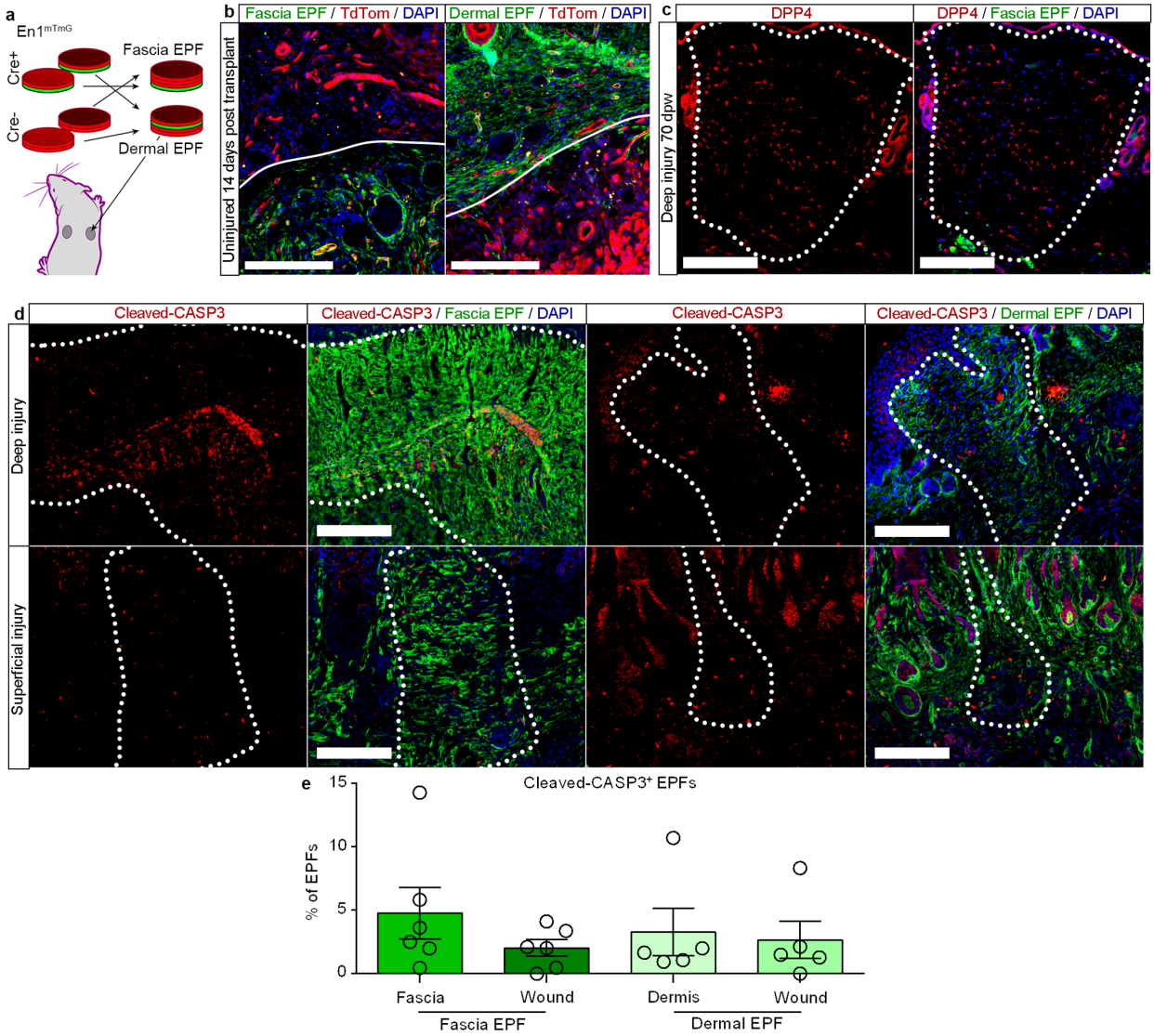

Extended Data Fig. 3. Fascia EPFs maintain position in steady conditions and recede from wounds over time. **a**. Dermal versus fascia EPFs chimeras in uninjured conditions. **b**. Fascia (left) or dermal (right) EPFs-traced chimeras. Representative images of 3 biological replicates. **c**. 70 dpw scars from deep injuries of fascia EPFs-traced chimeras immunolabeled for DPP4. Representative images of 3 biological replicates. **d**. Cleaved-CASP3 expression in wounds from fascia (left) or dermal (right) EPFs-traced chimeras from deep (top) or superficial (bottom) injuries at 14 dpw. **e**. Fractions of fascia or dermal EPFs in the wound, dermis, or fascia control regions positive for cleaved-CASP3. Mean with SEM, n= 6 and 5 (fascia and dermal EPF respectively) images analyzed from 5 biological replicates. Lines delimitate the border between fascia and dermis. Dotted lines delimitate the wound or scar. Scale bars = 200 microns.

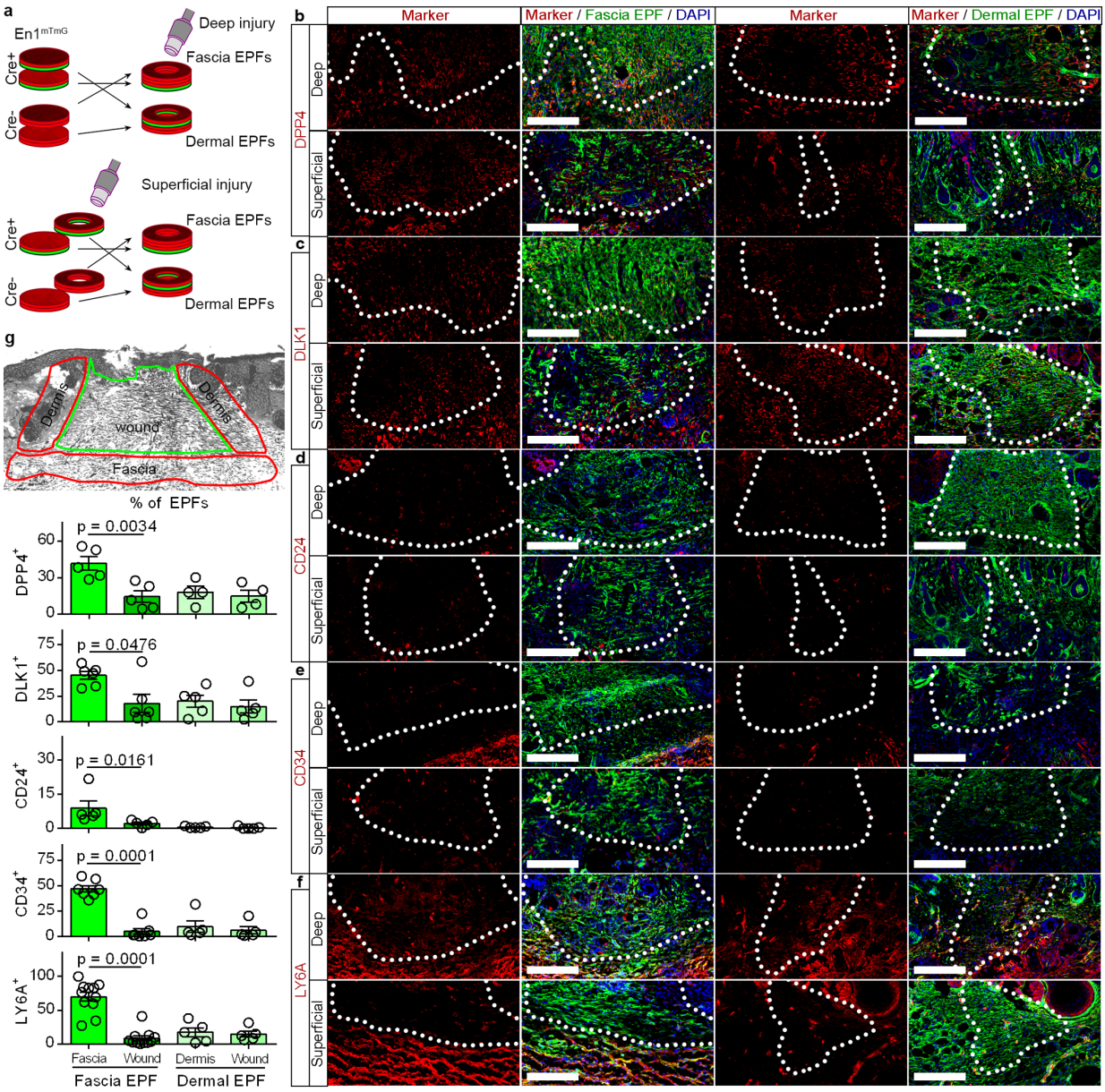

Extended Data Fig. 4. Fascia EPFs express wound fibroblast markers. **a**. Dermal versus fascia EPFs-traced chimeras with two injury conditions. **b-f**. Representative immunolabeling against the fibroblast markers DPP4 (b), DLK1 (c), CD24 (d), CD34 (e), and LY6A (f) from 4 biological replicates. **g**. Areas analyzed (top) for marker positive EPFs quantification (bottom). Mean with SEM, n= 5 images analyzed from 4 biological replicates. One-way ANOVA, multiple comparison Tukey test, confidence interval = 95%. Dotted lines delimitate the wound bed. Scale bars = 200 microns.

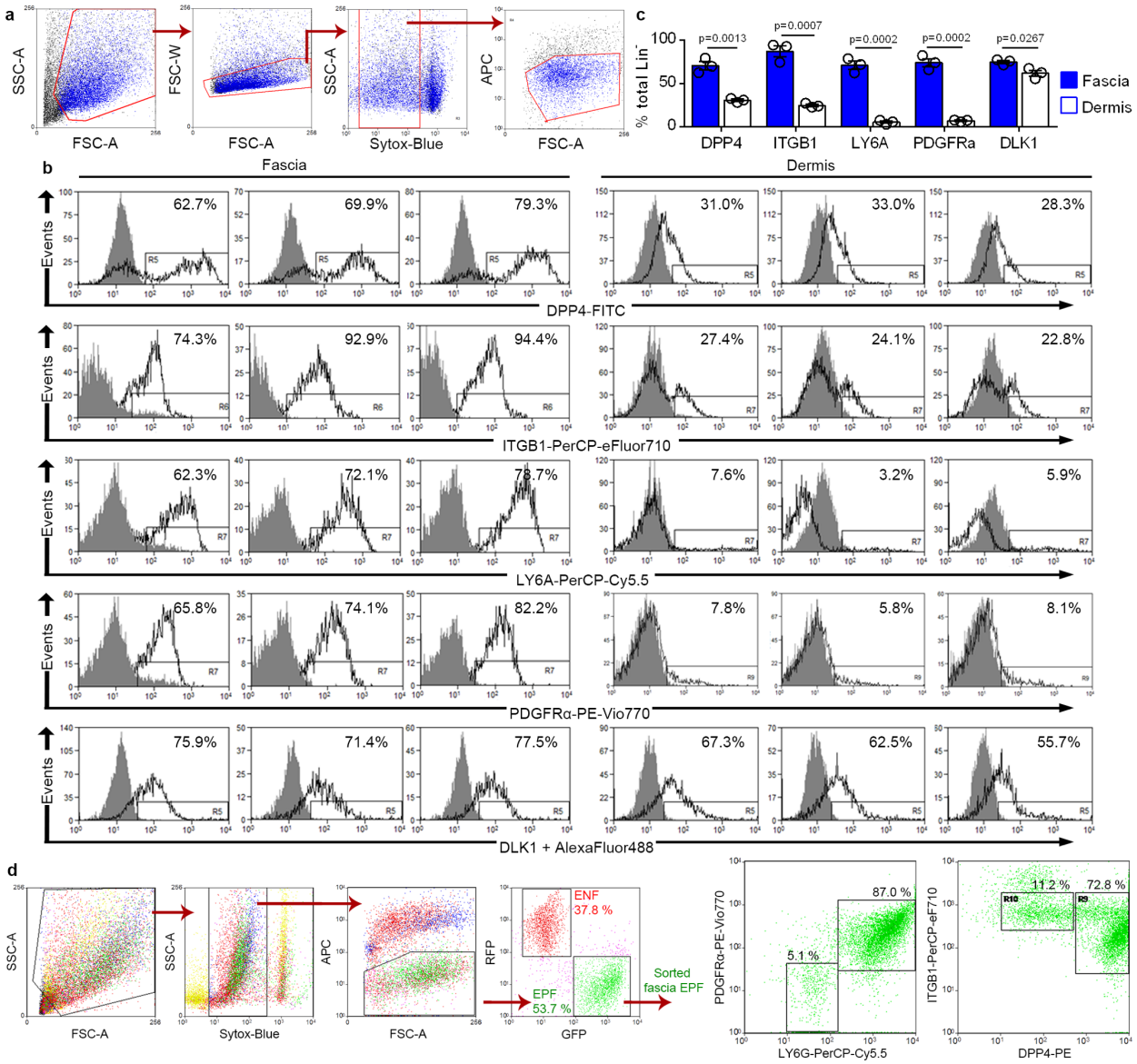

Extended Data Fig. 5. Differential expression of classical markers on fascia and dermal fibroblasts. **a**. Gating strategy for fibroblast (Lin^-) cytometry. **b**. Histo-plots of fibroblasts markers expression in fascia or dermis derived fibroblasts from three biological replicates. **c.** Fraction of marker positive cells from total fibroblast population. Mean with SEM, n= 3 biological replicates. Unpaired two-tailed T-test, confidence interval = 95%. **d**. Gating strategy for fascia EPF (Lin^-, GFP^+) sorting and expression detection of LY6A and PDGFR1, and DPP4 and ITGB1. Representative plots of three biological replicates.

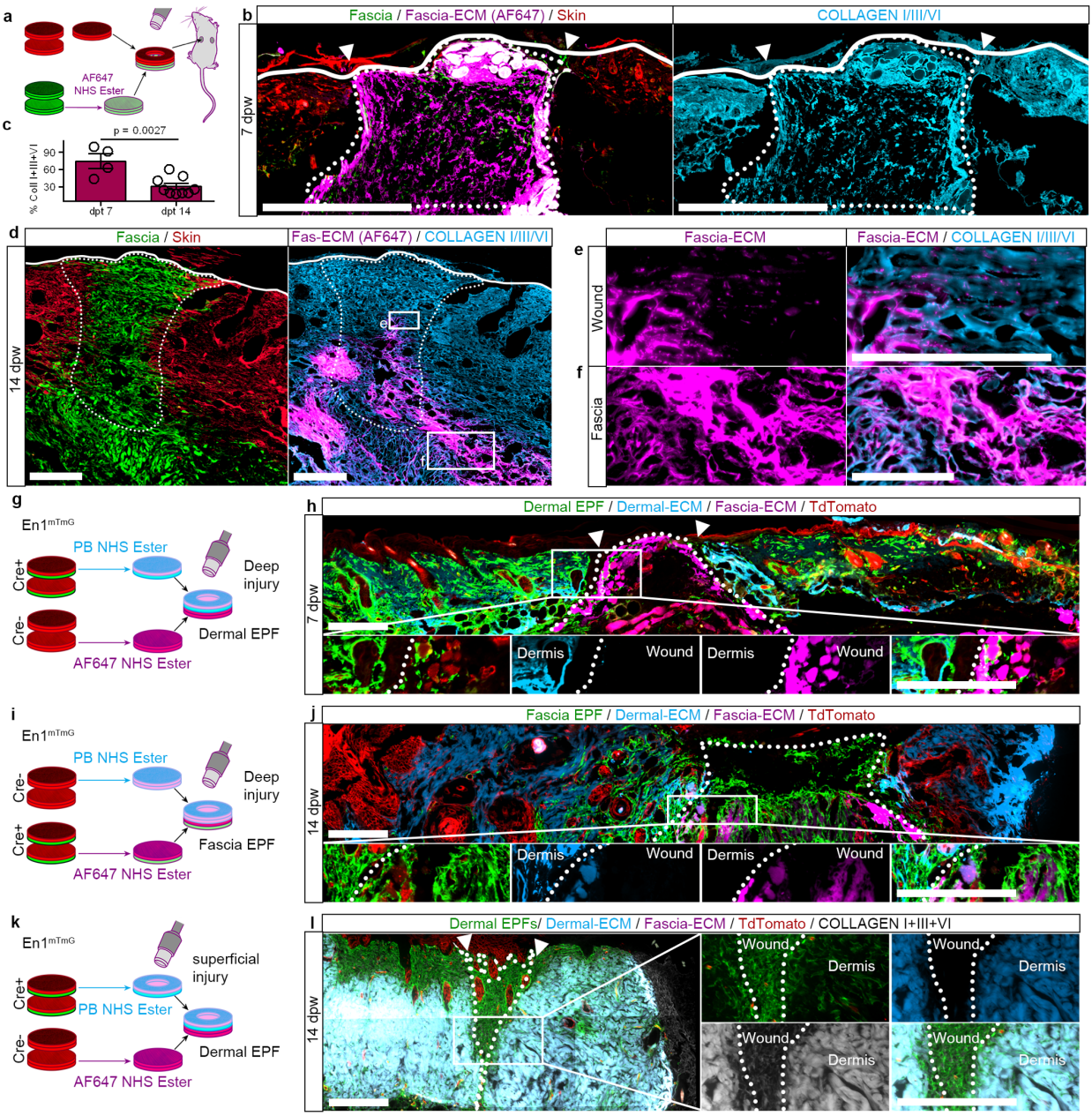

Extended Data Fig. 6. Fascia but not dermal matrix steers into wounds. **a**. Matrix tracing in chimeric grafts. **b**. Grafts at 7dpw immunolabeled against COLLAGEN I, III, and VI. Representative image of 3 biological replicates. **c**. Label coverage fraction from total collagens in the wound at defined time points. Mean with SEM, n= 4 and 9 sections analyzed from 3 biological replicates. Unpaired two-tailed T-test, confidence interval = 95%. **d**. Wounds at 14 dpw immunolabeled against collagens. Representative images of 3 biological replicates. **e-f**. High magnifications of inserts in "d". **g-h**. Double matrix tracing in deep-injured Dermal EPF-traced grafts at 7 dpw. Representative image of 3 biological replicates. **i-j**. Double matrix tracing in deep-injured Fascia EPF-traced grafts at 14 dpw. Representative image of 3 biological replicates. **k-l**. Double matrix labeling in superficial-injured Dermal EPF-traced grafts at 14 dpw immunolabeled against collagens. Representative image of 3 biological replicates. Dotted lines delimit the wound. Arrowheads mark the original injury. Continuous lines delimitate the epidermis dermis margin. Scale bars = 500 microns (b), 100 microns (d-f), and 200 microns (h, j, and l).

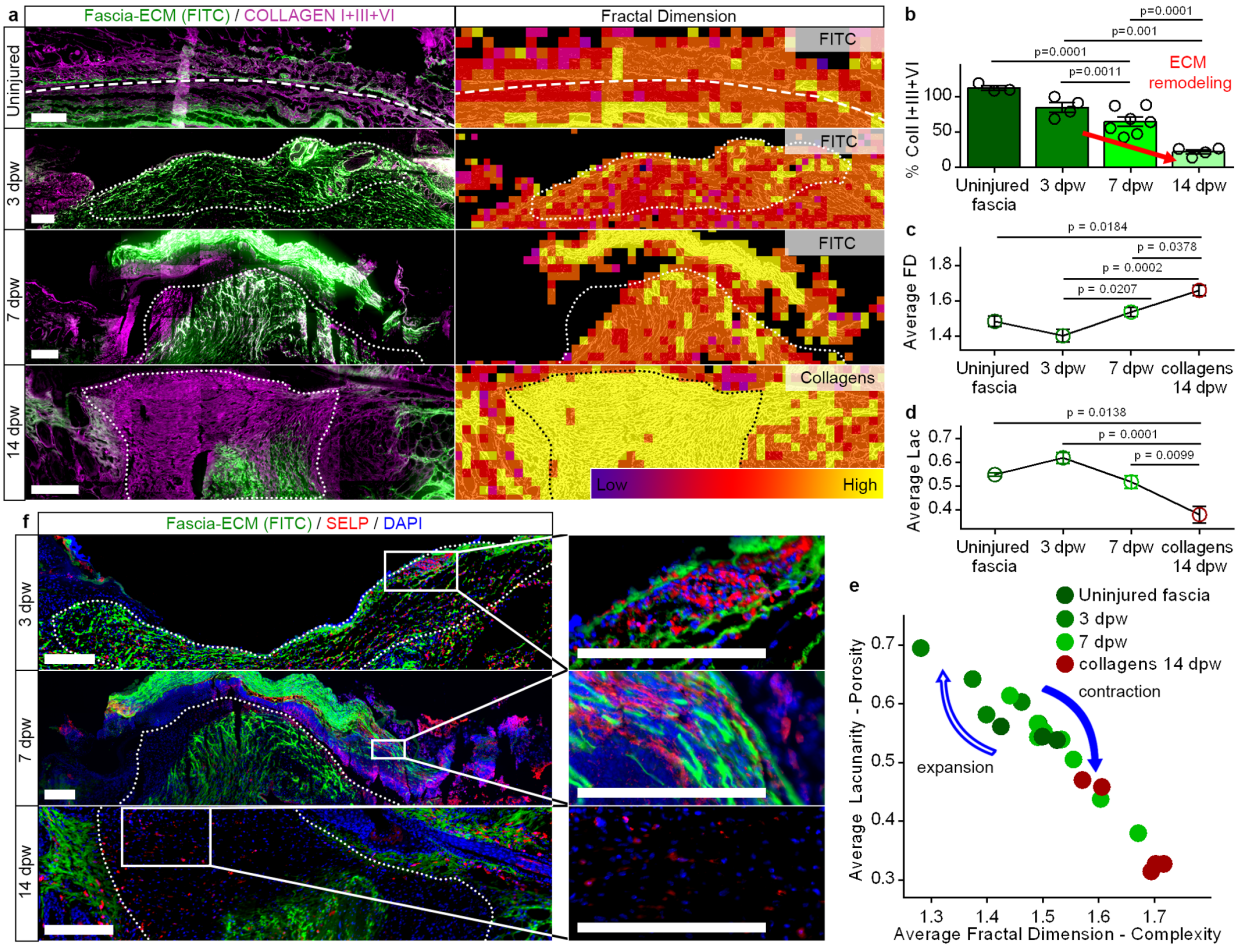

Extended Data Fig. 7. Fascia matrix forms the eschar and gets remodeled in the wound. **a**. Left: *In situ* matrix tracing and COLLAGENI+III+VI immunolabeling at defined time points after wounding. Representative images of 3 biological replicates. Right: Subsampled fractal dimension maps of the FITC signal at the uninjured, 3, and 7 dpw, and from collagens signal at 14 dpw. **b**. Matrix label coverage from total COLLAGEN I+III+VI signal in the wound. Mean with SEM, n= 3, 4, 7, and 4 sections analyzed from 3 biological replicates. One-way ANOVA, Tukey multiple comparisons. **c-d**. Average fractal dimension (c) and lacunarity (d) from subsampled maps. Mean with SEM, n= 5, 5, 8, and 3 images analyzed from 3 biological replicates. One-way ANOVA, Tukey test. Confidence interval = 95%. **e**. Scatter plot of average fractal dimension and lacunarity values. **f**. *In situ* matrix tracing and SELP immunolabeling at defined time points after wounding. Representative images of 3 biological replicates. Brocken line separates dermis from fascia. Dotted lines indicate the wound. Scale bars = 200 microns.

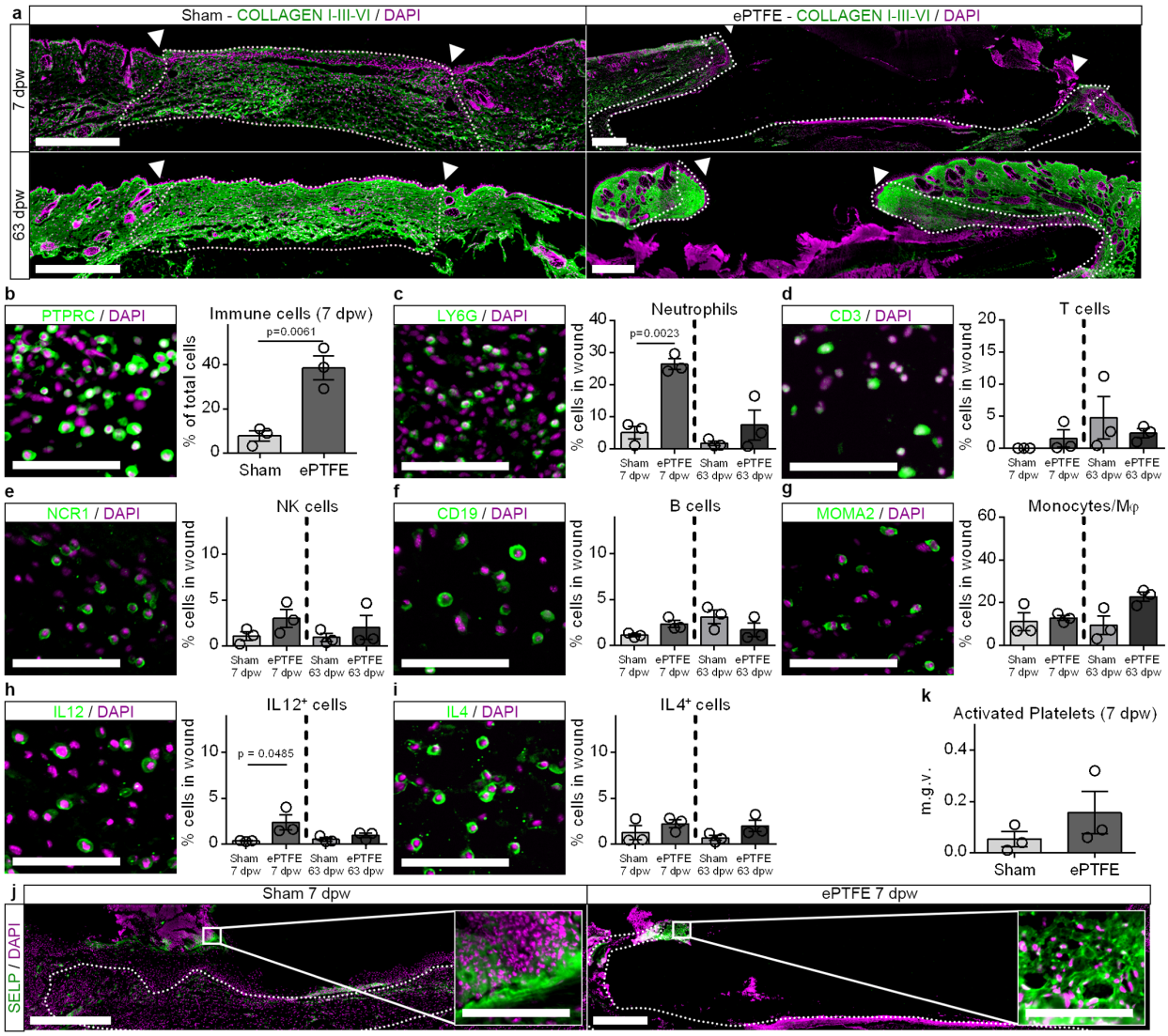

Extended Data Fig. 8. Inflammation resolution and coagulation stay unaffected during fascia blocking. **a**. Sham (left) or ePTFE-implanted (right) wounds at 7 (top) or 63 dpw (bottom) immunolabeled for COLLAGEN I-III-VI. Representative images of 3 biological replicates. **b-i**. Immunolabelings (left) and fractions (right) of immune cells (PTPRC$^+$, b), neutrophils (LY6G$^+$, c), T cells (CD3$^+$, d), NK cells (NCR1$^+$, e), B cells (CD19$^+$, f), macrophages and monocytes (MOMA2$^+$, g), and cells expressing the pro- and anti-inflammatory cytokines (IL12 and IL4 respectively, h-i). Mean with SEM, n= 3 images analyzed from 3 biological replicates. Unpaired two-tailed T-test, confidence interval = 95% (b). One-way ANOVA, Tukey test, confidence interval = 95% (c-i). **j**. Activated platelets (SELP) in 7 dpw sham and ePTFE-implanted wounds. Representative images of 3 biological replicates. **k**. Mean gray value of SELP signal. Mean with SEM, n = 3 images analyzed from 3 biological replicates. Two-tailed Student T-test, confidence interval = 95%. Dotted lines delimitate the wound area. Scale bars = 200 microns and 100 microns (inserts).

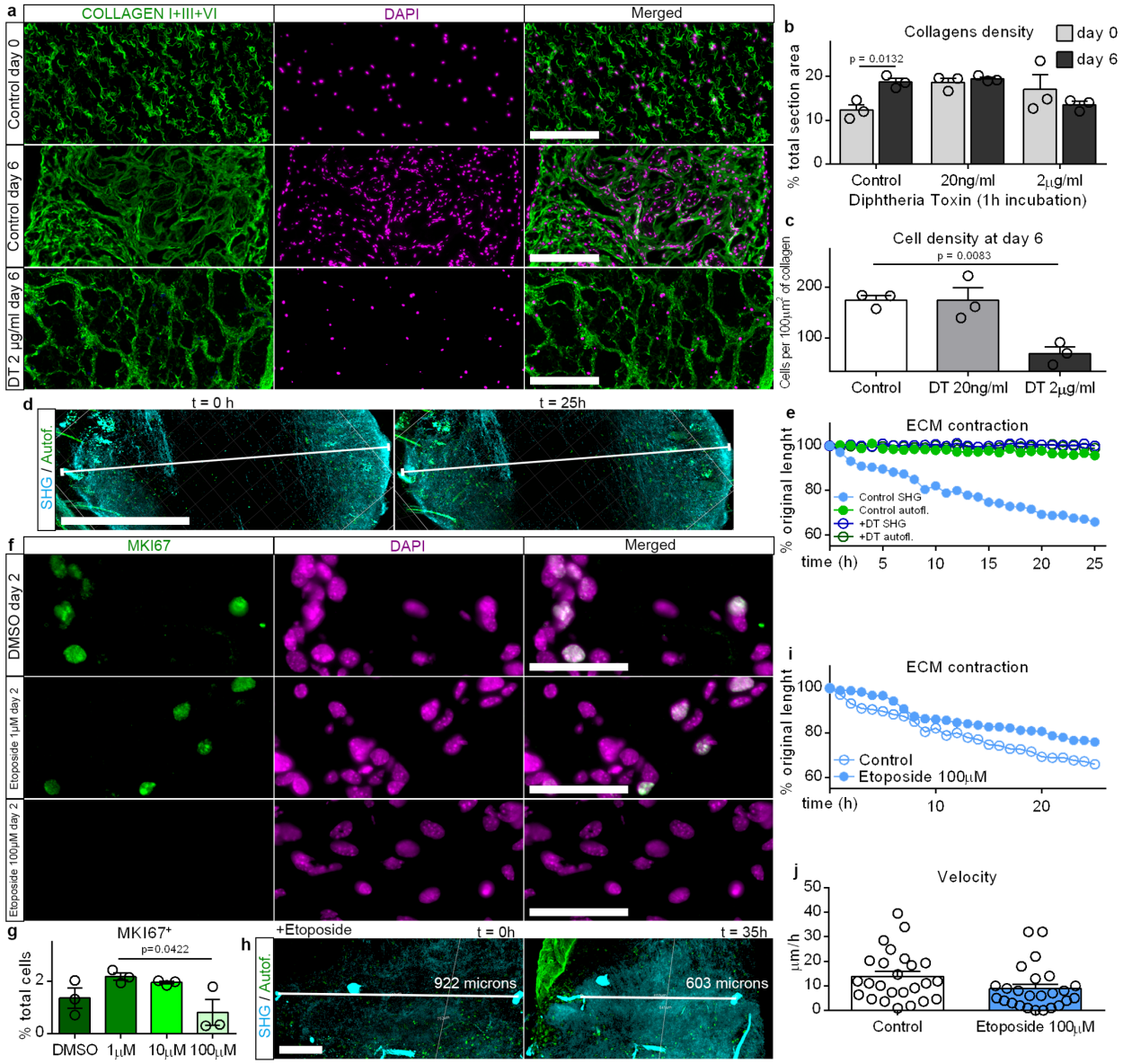

Extended Data Fig. 9. EPFs steer matrix in vitro independently of proliferation. **a**. En1^{Cre};R26^{iDTR} biopsies at day 0 and 6 after short treatment with DT or vehicle immunolabeled for COLLAGEN I, III, and VI. Representative images of 3 replicates. **b**. Collagens density. Mean with SEM, n= 3 images analyzed from 3 biological replicates. Two-way ANOVA, multiple comparison Tukey test, confidence interval = 95%. **c**. Cell density. Mean with SEM, n = 3 images analyzed from 3 biological replicates. One-way ANOVA, multiple comparison Tukey test, confidence interval = 95%. **d-e**. Time-lapse images (d) and contraction rate (e) of En1^{Cre};R26^{iDTR} neonate fascia biopsy in culture treated with DT for 1h. Representative samples from 3 replicates. Contraction values obtained from extended data video 4 and 6. **f**. Fascia biopsies treated with Etoposide and immunolabeled for MKI67. **g**. Fraction of MKI67^{+} cells. Mean with SEM, n= 3 images analyzed from 3 biological replicates. One-way ANOVA, Dunnett multiple comparisons, confidence interval = 95%. **h-i**. Time-lapse images (h) and contraction rate (i) of neonate fascia biopsy in culture treated with 100µM Etoposide. Representative samples from 3 replicates. Contraction values obtained from extended data video 4 and 7. **j**. Mean with SEM matrix contraction velocity during the first 25 h of imaging. n= 25 values from extended data video 7. Two-tailed Student T-test. Confident interval = 95%. Lines show the distance between two tracked points in the SHG channel. Scale bars = 50 microns (f), 200 microns (a and h), and 500 microns (d).

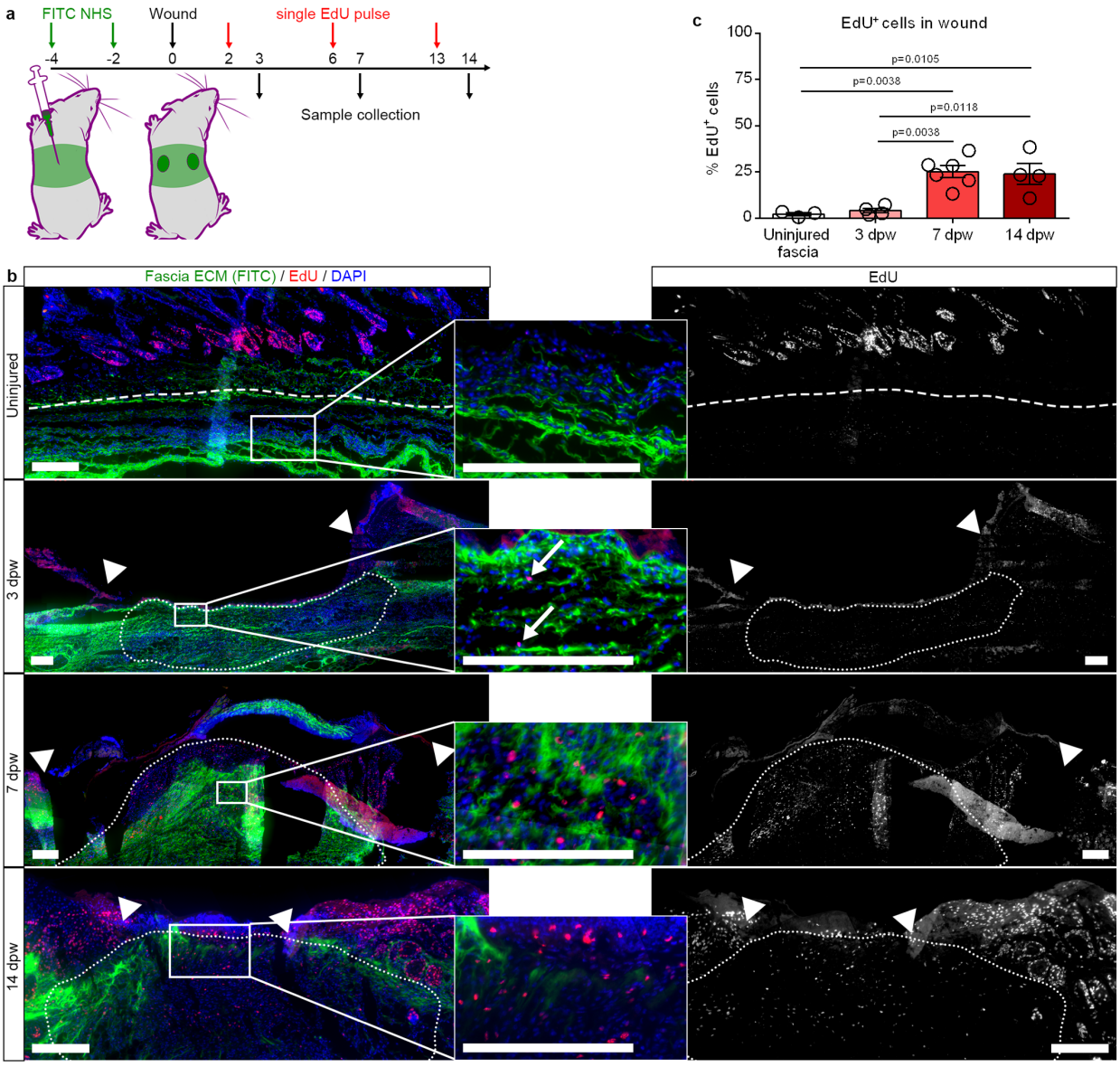

Extended Data Fig. 10. Fascia matrix steering precedes proliferation in vivo. **a**. *In situ* fascia matrix labeling and EdU pulses. **b**. EdU detection in sections at defined time points. **c**. Fraction of EdU$^+$ cells in the wound from total EdU$^+$ cells. Mean with SEM, n= 3, 4, 6, and 4 images analyzed from 3 biological replicates. One-way ANOVA, Tukey multiple comparisons. Arrows indicate EdU-positive nuclei. Arrowheads indicate the original injury site. Brocken and dotted lines delimitate fascia and wounds respectively. Scale bars = 200 microns.

All videos are available online together with the publisher's version of the manuscript

Extended data video 1. 3D reconstruction of adult $En1^{Cre};R26^{mTmG}$ fascia. EPFs in green and SHG in cyan.
Extended data video 2. 3D reconstruction of neonate $En1^{Cre};R26^{mTmG}$ back-skin and fascia. EPFs in green and TdTomato in red.
Extended data video 3. 3D reconstruction of adult $En1^{Cre};R26^{mTmG}$ back-skin wound bed 3 dpw. EPFs in green and TdTomato in red.
Extended data video 4. Time-lapse of 3D rendered P0 C57BL6/J fascia biopsy in culture. Second harmonic generation (SHG) in cyan and autofluorescence in green.
Extended data video 5. 3D reconstruction of day 14 wounds after transplantation of chimeric grafts with labeled matrix.
Extended data video 6. Time-lapse of 3D rendered P0 $En1^{Cre};R26^{iDTR}$ fascia biopsy in culture treated with an acute exposure of 2 µg/ml of diphtheria toxin. Second harmonic generation (SHG) in cyan and autofluorescence in green.
Extended data video 7. Time-lapse of 3D rendered P0 C57BL6/J fascia biopsy in culture treated with 100 µM etoposide. Second harmonic generation (SHG) in cyan and autofluorescence in green.

References

1. *The Cellular and Molecular Basis for Planarian Regeneration.* **Reddien, Peter W.** 2018, Cell, pp. 327-345.
2. *Whole-Body Regeneration in the Colonial Tunicate Botrylloides leachii.* **Blanchoud, Simon, Rinkevich, Buki and Wilson, Megan J.** 2018, Marine Organisms as Model Systems in Biology and Medicine, pp. 337-355.
3. *Towards Comparative Analyses of Salamander Limb Regeneration.* **Dwaraka, Varun D. and Voss, S. Randal.** 2019, J Exp Zool B Mol Dev Evol, p. doi: 10.1002/jez.b.22902.
4. *Comparative Analysis of the Mechanical Signals in Lung Development and Compensatory Growth.* **Hsia, Connie C W.** 2017, Cell Tissue Res, pp. 687-705.
5. *Cellular Mechanisms of Liver Regeneration and Cell-Based Therapies of Liver Diseases.* **Kholodenko, Irina V and Yarygin, Konstantin N.** 2017, Biomed Res Int, p. doi: 10.1155/2017/8910821.
6. *The Evolution of Regeneration - Where Does That Leave Mammals?* **Maden, Malcolm.** 2018, Int J Dev Biol, pp. 369-372.
7. *Learning From Regeneration Research Organisms: The Circuitous Road to Scar Free Wound Healing.* **Erickson, Jami R and Echeverri, Karen.** 2018, Dev Biol, pp. 144-154.
8. *Organ and Tissue Fibrosis: Molecular Signals, Cellular Mechanisms and Translational Implications.* **Weiskirchen, Ralf, Weiskirchen, Sabine and Tacke, Frank.** 2019, Mol Aspects Med, pp. 2-15.
9. *Recent Understandings of Biology, Prophylaxis and Treatment Strategies for Hypertrophic Scars and Keloids.* **Lee, Ho Jun and Jang, Yong Ju.** 2018, Int J Mol Sci, p. doi: 10.3390/ijms19030711.
10. *Inflammation in Chronic Wounds.* **Zhao, Ruilong, et al.** 2016, Int J Mol Sci, p. doi: 10.3390/ijms17122085.
11. *Human Wounds and Its Burden: An Updated Compendium of Estimates.* **Sen, Chandan K.** 2019, Adv Wound Care (New Rochelle), pp. 39-48.
12. *Wound Healing - A Literature Review.* **Gonzalez, Ana Cristina de Oliveira, et al.** 2016, An Bras Dermatol, pp. 614-620.
13. *The Myofibroblast, a Key Cell in Normal and Pathological Tissue Repair.* **Darby, Ian A, et al.** 2016, Cell Mol Life Sci, pp. 1145-1157.
14. *Reactions of Mammalian Fetal Tissues to Injury. II. Skin.* **Hess, A.** 1954, Anat Rec, pp. 435-447.
15. *Wound Healing in the New-Born Opossum (Didelphis Virginianam).* **Block, M.** 1960, Nature, pp. 340-341.
16. *Intra-uterine Healing of Fetal Rat Oral Mucosal, Skin and Cartilage Wounds.* **Goss, A N.** 1977, J Oral Pathol, pp. 35-43.
17. *Inflammation in the Foetal and Neonatal Rat: The Local Reactions to Skin Burns.* **Dixon, J B.** 1960, J Pathol Bacteriol, pp. 73-82.
18. *Intra-uterine Healing of Skin Wounds in Rabbit Foetuses.* **Somasundaram, K and Prathap, K.** 1970, J Pathol, pp. 81-86.
19. *Variation in Acute Phlogistic Reactions in the Skin of Rabbit Fetuses.* **Bracaglia, R, et al.** 1982, Ann Plast Surg, pp. 175-179.
20. *Wound Healing in the Fetal Lamb.* **Burrington, J D.** 1971, J Pediatr Surg, pp. 523-528.
21. *In Utero Lip Repair in the Rhesus Monkey: An Update.* **Hallock, G G, Rice, D C and McClure, H M.** 1987, Plast Reconstr Surg, pp. 855-858.
22. *Fetal Wound Healing. The Ontogeny of Scar Formation in the Non-Human Primate.* **Lorenz, H P, et al.** 1993, Ann Surg, pp. 391-396.
23. *Intrauterine Wound Healing in a 20 Week Human Fetus.* **Rowlatt, U.** 1979, Virchows Arch A Pathol Anat Histol, pp. 353-361.
24. *Scarless Wound Healing: From Development to Senescence.* **Pratsinis, Harris, Mavrogonatou, Eleni and Kletsas, Dimitris.** 2019, Adv Drug Deliv Rev, pp. 325-343.
25. *Scarless Wound Repair: A Human Fetal Skin Model.* **Lorenz, H P, et al.** 1992, Development, pp. 253-259.

26. *Adult Skin Wounds in the Fetal Environment Heal With Scar Formation.* **Longaker, M T, et al.** 1994, Ann Surg, pp. 65-72.
27. *Ontogenetic Transition of Wound Healing Pattern in Rat Skin Occurring at the Fetal Stage.* **Ihara, S, et al.** 1990, Development, pp. 671-680.
28. *A Mouse Fetal Skin Model of Scarless Wound Repair.* **Walmsley, Graham G, et al.** 2015, J Vis Exp, p. doi: 10.3791/52297.
29. *Studies in Fetal Wound Healing, VI. Second and Early Third Trimester Fetal Wounds Demonstrate Rapid Collagen Deposition Without Scar Formation.* **Longaker, M T, et al.** 1990, J Pediatr Surg, pp. 63-68.
30. *CICATRIZATION OF WOUNDS : III. THE RELATION BETWEEN THE AGE OF THE PATIENT, THE AREA OF THE WOUND, AND THE INDEX OF CICATRIZATION.* **Noüy, P L Du.** 1916, J Exp Med, pp. 461-470.
31. *Cutaneous Wound Healing in Aging Small Mammals: A Systematic Review.* **Kim, Dong Joo, Mustoe, Thomas and Clark, Richard A F.** 2015, Wound Repair Regen, pp. 318-339.
32. *Never Too Old to Regenerate? Wound Induced Hair Follicle Neogenesis After Secondary Intention Healing in a Geriatric Patient.* **Wong, Tak-Wah, Hughes, Michael and Wang, Szu-Han.** 2018, J Tissue Viability, pp. 114-116.
33. *Aging Suppresses Skin-Derived Circulating SDF1 to Promote Full-Thickness Tissue Regeneration.* **Nishiguchi, Mailyn A, et al.** 2018, Cell Rep, pp. 3383-3392.
34. *Heterogeneity in Old Fibroblasts Is Linked to Variability in Reprogramming and Wound Healing.* **Mahmoudi, Salah, et al.** 2019, Nature, pp. 553-558.
35. *Dysfunctional Wound Healing in Diabetic Foot Ulcers: New Crossroads.* **Davis, Frank M, et al.** 2018, Curr Diab Rep, pp. doi: 10.1007/s11892-018-0970-z.
36. *Regenerative Healing, Scar-Free Healing and Scar Formation Across the Species: Current Concepts and Future Perspectives.* **Ud-Din, Sara and Susan W Volk, Ardeshir Bayat.** 2014, Exp Dermatol, pp. 615-619.
37. *Equine Exuberant Granulation Tissue and Human Keloids: A Comparative Histopathologic Study.* **Theoret, Christine L, et al.** 2013, Vet Surg, pp. 783-789.
38. *A Novel Model for Cutaneous Wound Healing and Scarring in the Rat.* **Zhou, Sizheng, et al.** 2019, Plast Reconstr Surg, pp. 468-477.
39. *Hypertrophic Scarring in the Rabbit Ear: A Practical Model for Studying Dermal Fibrosis.* **Nabai, Layla and Ghahary, Aziz.** 2017, Methods Mol Biol, pp. 81-89.
40. *Hairless Descendants of Mexican Hairless Dogs: An Experimental Model for Studying Hypertrophic Scars.* **Kimura, Tohru.** 2011, J Cutan Med Surg, pp. 329-339.
41. *Preclinical Study of Novel Gene Silencer Pyrrole-Imidazole Polyamide Targeting Human TGF-β1 Promoter for Hypertrophic Scars in a Common Marmoset Primate Model.* **Igarashi, Jun, et al.** 2015, PLoS One, p. e0125295.
42. *Deer antler – A novel model for studying organ regeneration in mammals.* **Li, Chunyi, et al.** 2014, The International Journal of Biochemistry & Cell Biology, pp. 111-122.
43. *Deer Antlers as a Model of Mammalian Regeneration.* **Price, Joanna and Corrine Faucheux, Steve Allen.** 2005, Curr Top Dev Biol, pp. 1-48.
44. *Wound Healing During Hibernation by Black Bears (Ursus Americanus) in the Wild: Elicitation of Reduced Scar Formation.* **Iaizzo, Paul A, et al.** 2012, Integr Zool, pp. 48-60.
45. *Skin Shedding and Tissue Regeneration in African Spiny Mice (Acomys).* **Seifert, Ashley W, et al.** 2012, Nature, pp. 561-565.
46. *Insights Into the Regeneration of Skin From Acomys, the Spiny Mouse.* **Maden, Malcolm and Brant, Jason O.** 2019, Exp Dermatol, pp. 436-441.
47. *Optimal Skin Regeneration After Full Thickness Thermal Burn Injury in the Spiny Mouse, Acomys Cahirinus.* **Maden, Malcolm.** 2018, Burns, pp. 1509-1520.
48. *Regeneration-Competent and -Incompetent Murids Differ in Neutrophil Quantity and Function.* **Cyr, Jennifer L, et al.** 2019, Integr Comp Biol, pp. 1138-1149.

49. *Macrophages Are Necessary for Epimorphic Regeneration in African Spiny Mice.* **Simkin, Jennifer, et al.** 2017, Elife, p. e24623.
50. *Cellular Events During Scar-Free Skin Regeneration in the Spiny Mouse, Acomys.* **Brant, Jason O, et al.** 2016, Wound Repair Regen, pp. 75-88.
51. *A Comparative Analysis of Gene Expression Profiles During Skin Regeneration in Mus and Acomys.* **Brant, Jason Orr, et al.** 2015, PLoS One, p. e0142931.
52. *Comparative Transcriptomic Analysis of Dermal Wound Healing Reveals De Novo Skeletal Muscle Regeneration in Acomys Cahirinus.* **Brant, Jason O, et al.** 2019, PLoS One, p. e0216228.
53. *A Fine Structural Comparison of the Healing of Incisional Wounds of Mucosa and Skin.* **Sciubba, J J, Waterhouse, J P and Meyer, J.** 1978, J Oral Pathol, pp. 214-227.
54. *Exploring Scarless Healing of Oral Soft Tissues.* **Larjava, Hannu, et al.** 2011, J Can Dent Assoc, p. b18.
55. *Wnt-Responsive Stem Cell Fates in the Oral Mucosa.* **Yuan, Xue, et al.** 2019, iScience, pp. 84-94.
56. *Differential Injury Responses in Oral Mucosal and Cutaneous Wounds.* **Szpaderska, A M, Zuckerman, J D and DiPietro, L A.** 2003, J Dent Res, pp. 621-626.
57. *Positional Differences in the Wound Transcriptome of Skin and Oral Mucosa.* **Chen, Lin, et al.** 2010, BMC Genomics, pp. doi: 10.1186/1471-2164-11-471.
58. *Fibroblast Heterogeneity and Its Implications for Engineering Organotypic Skin Models in Vitro.* **Sriram, Gopu, Bigliardi, Paul Lorenz and Bigliardi-Qi, Mei.** 2015, Eur J Cell Biol, pp. 483-512.
59. *Corneal Injury: Clinical and Molecular Aspects.* **Barrientez, Brayden, et al.** 2019, Exp Eye Res, p. 107709.
60. *A Five-Year Retrospective Study of the Epidemiological Characteristics and Visual Outcomes of Pediatric Ocular Trauma.* **Puodžiuvienė, Edita, et al.** 2018, BMC Ophthalmol, pp. doi: 10.1186/s12886-018-0676-7.
61. *Vision-limiting Complications in Open-Globe Injuries.* **Thakker, Manoj M and Ray, Subhransu.** 2006, Can J Ophthalmol, pp. 86-92.
62. *Burn Injury: Challenges and Advances in Burn Wound Healing, Infection, Pain and Scarring.* **Wang, Yiwei, et al.** 2018, Adv Drug Deliv Rev, pp. 3-17.
63. *Outcome After Burns: An Observational Study on Burn Scar Maturation and Predictors for Severe Scarring.* **Wal, Martijn B A van der, et al.** 2012, Wound Repair Regen, pp. 676-687.
64. *Identification of Factors Predicting Scar Outcome After Burn in Adults: A Prospective Case-Control Study.* **Wallace, Hilary J, et al.** 2017, Burns, pp. 1271-1283.
65. *Patient-reported Scar Quality of Adults After Burn Injuries: A Five-Year Multicenter Follow-Up Study.* **Spronk, Inge, et al.** 2019, Wound Repair Regen, pp. 406-414.
66. *Biological Principles of Scar and Contracture.* **Kwan, Peter O and Tredget, Edward E.** 2017, Hand Clin, pp. 277-292.
67. *Prevalence of Scar Contractures After Burn: A Systematic Review.* **Oosterwijk, Anouk M, et al.** 2017, Burns, pp. 41-49.
68. *The Dynamic Anatomy and Patterning of Skin.* **Wong, Richard, et al.** 2016, Exp Dermatol, pp. 92-98.
69. *Regeneration of Dermis: Scarring and Cells Involved.* **Rippa, Alexandra L, Kalabusheva, Ekaterina P and Vorotelyak, Ekaterina A.** 2019, Cells, p. doi: 10.3390/cells8060607.
70. *Insight Into Reepithelialization: How Do Mesenchymal Stem Cells Perform?* **Chen, Deyun, et al.** 2016, Stem Cells Int, p. doi: 10.1155/2016/6120173.
71. *Scarring Occurs at a Critical Depth of Skin Injury: Precise Measurement in a Graduated Dermal Scratch in Human Volunteers.* **Dunkin, Christopher S J, et al.** 2007, Plast Reconstr Surg, pp. 1722-1732.
72. *Cutaneous Manifestations of Scleroderma and Scleroderma-Like Disorders: A Comprehensive Review.* **Ferreli, Caterina, et al.** 2017, Clin Rev Allergy Immunol, pp. 306-336.

73. *Dupuytren's Contracture: An Evidence Based Review.* **Mella, Juan Rodolfo, Guo, Lifei and Hung, Virginia.** 2018, Ann Plast Surg, pp. S97-S101.
74. *Presence of Modified Fibroblasts in Granulation Tissue and Their Possible Role in Wound Contraction.* **Gabbiani, G, Ryan, G B and Majne, G.** 1971, Experientia, pp. 549-550.
75. *Granulation Tissue as a Contractile Organ. A Study of Structure and Function.* **Gabbiani, G, et al.** 1972, J Exp Med, pp. 719-734.
76. *The Myofibroblast in Wound Healing and Fibrosis: Answered and Unanswered Questions.* **Bochaton-Piallat, Marie-Luce, Gabbiani, Giulio and Hinz, Boris.** 2016, F1000Res, p. doi: 10.12688/f1000research.8190.1.
77. *Bone Marrow-Derived Fibrocytes Participate in Pathogenesis of Liver Fibrosis.* **Kisseleva, Tatiana, et al.** 2006, J Hepatol, pp. 429-438.
78. *Mesothelial Cells Give Rise to Hepatic Stellate Cells and Myofibroblasts via Mesothelial-Mesenchymal Transition in Liver Injury.* **Li, Yuchang, Wang, Jiaohong and Asahina, Kinji.** 2013, Proc Natl Acad Sci U S A, pp. 2324-2329.
79. *Fibrocyte Migration, Differentiation and Apoptosis During the Corneal Wound Healing Response to Injury.* **Lassance, Luciana, et al.** 2018, Exp Eye Res, pp. 177-187.
80. *Fate Tracing Reveals the Pericyte and Not Epithelial Origin of Myofibroblasts in Kidney Fibrosis.* **Humphreys, Benjamin D, et al.** 2010, Am J Pathol, pp. 85-97.
81. *Perivascular Gli1+ Progenitors Are Key Contributors to Injury-Induced Organ Fibrosis.* **Kramann, Rafael, et al.** 2015, Cell Stem Cell, pp. 51-66.
82. *Evidence That Fibroblasts Derive From Epithelium During Tissue Fibrosis.* **Iwano, Masayuki, et al.** 2002, J Clin Invest, pp. 341-350.
83. *Myofibroblasts in Murine Cutaneous Fibrosis Originate From Adiponectin-Positive Intradermal Progenitors.* **Marangoni, Roberta Goncalves, et al.** 2015, Arthritis Rheumatol, pp. 1062-1073.
84. *Lineage Tracing and Genetic Ablation of ADAM12(+) Perivascular Cells Identify a Major Source of Profibrotic Cells During Acute Tissue Injury.* **Dulauroy, Sophie, et al.** 2012, Nat Med, pp. 1262-1270.
85. *Fate Tracing Reveals Hepatic Stellate Cells as Dominant Contributors to Liver Fibrosis Independent of Its Aetiology.* **Mederacke, Ingmar, et al.** 2013, Nat Commun, p. doi: 10.1038/ncomms3823.
86. *Dysfunction of Fibroblasts of Extrarenal Origin Underlies Renal Fibrosis and Renal Anemia in Mice.* **Asada, Nariaki, et al.** 2011, J Clin Invest, pp. 3981-3990.
87. *Resident Fibroblast Lineages Mediate Pressure Overload-Induced Cardiac Fibrosis.* **Moore-Morris, Thomas, et al.** 2014, J Clin Invest, pp. 2921-2934.
88. *Infarct Fibroblasts Do Not Derive From Bone Marrow Lineages.* **Moore-Morris, Thomas, et al.** 2018, Circ Res, pp. 583-590.
89. *Genetic Lineage Tracing Defines Myofibroblast Origin and Function in the Injured Heart.* **Kanisicak, Onur, et al.** 2016, Nat Commun, p. doi: 10.1038/ncomms12260.
90. *Distinct Fibroblast Lineages Determine Dermal Architecture in Skin Development and Repair.* **Driskell, Ryan R, et al.** 2013, Nature, pp. 277-281.
91. *Skin Fibrosis. Identification and Isolation of a Dermal Lineage With Intrinsic Fibrogenic Potential.* **Rinkevich, Yuval, et al.** 2015, Science, p. doi: 10.1126/science.aaa2151.
92. *Two-Way Conversion Between Lipogenic and Myogenic Fibroblastic Phenotypes Marks the Progression and Resolution of Lung Fibrosis.* **Agha, Elie El, et al.** 2017, Cell Stem Cell, pp. 261-273.
93. *What's in a Name? On Fibroblast Phenotype and Nomenclature.* **Nagalingam, Raghu S, Al-Hattab, Danah S and Czubryt, Michael P.** 2019, Can J Physiol Pharmacol, pp. 493-497.
94. *Differential Expression and Regulation of Extracellular Matrix-Associated Genes in Fetal and Neonatal Fibroblasts.* **Gosiewska, A, et al.** 2001, Wound Repair Regen, pp. 213-222.
95. *Increased Expression of Transforming Growth factor-beta1, Acidic Fibroblast Growth Factor, and Basic Fibroblast Growth Factor in Fetal Versus Adult Fibroblast Cell Lines.* **Lee, N J, et al.** 2000, Laryngoscope, pp. 616-619.

96. *Differential Gene Expression in Response to Transforming Growth factor-beta1 by Fetal and Postnatal Dermal Fibroblasts.* **Rolfe, Kerstin J, et al.** 2007, Wound Repair Regen, pp. 897-906.
97. *Transforming Growth Factor Beta (TGF-β) Isoforms in Wound Healing and Fibrosis.* **Lichtman, Michael K, Otero-Vinas, Marta and Falanga, Vincent.** 2016, Wound Repair Regen, pp. 215-222.
98. *Differential Proliferative Response of Fetal and Adult Human Skin Fibroblasts to Transforming Growth Factor-Beta.* **Pratsinis, Harris, et al.** 2004, Wound Repair Regen, pp. 374-383.
99. *The Effects of Ageing on Wound Healing: Immunolocalisation of Growth Factors and Their Receptors in a Murine Incisional Model.* **Ashcroft, G S, Horan, M A and Ferguson, M W.** 1997, J Anat, pp. 351-365.
100. *Reduced Expression of Connective Tissue Growth Factor (CTGF/CCN2) Mediates Collagen Loss in Chronologically Aged Human Skin.* **Quan, TaiHao, et al.** 2010, J Invest Dermatol, pp. 415-424.
101. *The Hallmarks of Fibroblast Ageing.* **Tigges, Julia, et al.** 2014, Mech Ageing Dev, pp. 26-44.
102. *Cellular Senescence in Aging Primates.* **Herbig, Utz, et al.** 2006, Science, p. 1257.
103. *p16INK4A Is a Robust in Vivo Biomarker of Cellular Aging in Human Skin.* **Ressler, Sigrun, et al.** 2006, Aging Cell, pp. 379-389.
104. *Accumulation of Senescent Cells in Mitotic Tissue of Aging Primates.* **Jeyapalan, Jessie C, et al.** 2007, Mech Ageing Dev, pp. 36-44.
105. *Local and Transient Inhibition of p21 Expression Ameliorates Age-Related Delayed Wound Healing.* **Jiang, Dongsheng, et al.** 2020, Wound Repair Regen, pp. 49-60.
106. *Type I and Type III Collagen Content of Healing Wounds in Fetal and Adult Rats.* **Merkel, J R, et al.** 1988, Proc Soc Exp Biol Med, pp. 493-497.
107. *Differential Expression of Procollagen Genes Between Mid- And Late-Gestational Fetal Fibroblasts.* **Carter, Richard, et al.** 2009, J Surg Res, pp. 90-94.
108. *Identity Noise and Adipogenic Traits Characterize Dermal Fibroblast Aging.* **Salzer, Marion Claudia, et al.** 2018, Cell, pp. 1575-1590.
109. *Single-cell Transcriptomes of the Human Skin Reveal Age-Related Loss of Fibroblast Priming.* **Solé-Boldo, Llorenç, et al.** 2020, Commun Biol, pp. doi: 10.1038/s42003-020-0922-4.
110. *Fetal Dermal Fibroblasts Retain a Hyperactive Migratory and Contractile Phenotype Under 2-and 3-dimensional Constraints Compared to Normal Adult Fibroblasts.* **Sandulache, Vlad C, et al.** 2007, Tissue Eng, pp. 2791-2801.
111. *Adult, Foetal and Transformed Fibroblasts Display Different Migratory Phenotypes on Collagen Gels: Evidence for an Isoformic Transition During Foetal Development.* **Schor, S L, et al.** 1985, J Cell Sci, pp. 221-234.
112. *Effect of Age and Hypoxia on TGFbeta1 Receptor Expression and Signal Transduction in Human Dermal Fibroblasts: Impact on Cell Migration.* **Mogford, Jon E, et al.** 2002, J Cell Physiol, pp. 259-265.
113. *Impaired Migration, Integrin Function, and Actin Cytoskeletal Organization in Dermal Fibroblasts From a Subset of Aged Human Donors.* **Reed, M J, Ferara, N S and Vernon, R B.** 2001, Mech Ageing Dev, pp. 1203-1220.
114. *Contractility, Transforming Growth Factor-Beta, and Plasmin in Fetal Skin Fibroblasts: Role in Scarless Wound Healing.* **Coleman, C, et al.** 1998, Pediatr Res, pp. 403-409.
115. *Fetal Fibroblast Contraction of Collagen Matrices in Vitro: The Effects of Epidermal Growth Factor and Transforming Growth Factor-Beta.* **Piscatelli, S J, et al.** 1994, Ann Plast Surg, pp. 38-45.
116. *Prostaglandin E2 Differentially Regulates Contraction and Structural Reorganization of Anchored Collagen Gels by Human Adult and Fetal Dermal Fibroblasts.* **Parekh, Aron, et al.** 2009, Wound Repair Regen, pp. 88-98.
117. *The Altered Mechanical Phenotype of Fetal Fibroblasts Hinders Myofibroblast Differentiation.* **Jerrell, Rachel J, Leih, Mitchell J and Parekh, Aron.** 2019, Wound Repair Regen, pp. 29-38.

118. *Loss of Contraction Force in Dermal Fibroblasts With Aging Due to Decreases in Myosin Light Chain Phosphorylation Enzymes.* **Fujimura, Tsutomu, et al.** 2011, Arch Pharm Res, pp. 1015-1022.
119. *TGF-beta 1 Induces the Expression of Type I Collagen and SPARC, and Enhances Contraction of Collagen Gels, by Fibroblasts From Young and Aged Donors.* **Reed, M J, et al.** 1994, J Cell Physiol, pp. 169-179.
120. *Two Succeeding Fibroblastic Lineages Drive Dermal Development and the Transition From Regeneration to Scarring.* **Jiang, Dongsheng, et al.** 2018, Nat Cell Biol, pp. 422-431.
121. *Myofibroblast Proliferation and Heterogeneity Are Supported by Macrophages During Skin Repair.* **Shook, Brett A, et al.** 2018, Science, p. doi: 10.1126/science.aar2971.
122. *Connective Tissue Fibroblasts From Highly Regenerative Mammals Are Refractory to ROS-induced Cellular Senescence.* **Saxena, Sandeep, et al.** 2019, Nat Commun, pp. doi: 10.1038/s41467-019-12398-w.
123. *The Presence of Oxygen in Wound Healing.* **Kimmel, Howard M, Grant, Anthony and Ditata, James.** 2016, Wounds, pp. 264-270.
124. *Targeting Oxidative Stress and Mitochondrial Dysfunction in the Treatment of Impaired Wound Healing: A Systematic Review.* **Sanchez, Mariola Cano, et al.** 2018, Antioxidants (Basel), p. doi: 10.3390/antiox7080098.
125. *Redox Signaling as a Therapeutic Target to Inhibit Myofibroblast Activation in Degenerative Fibrotic Disease.* **Sampson, Natalie, Berger, Peter and Zenzmaier, Christoph.** 2014, Biomed Res Int, p. doi: 10.1155/2014/131737.
126. *Unique Behavior of Dermal Cells From Regenerative Mammal, the African Spiny Mouse, in Response to Substrate Stiffness.* **Stewart, Daniel C, et al.** 2018, J Biomech, pp. 149-154.
127. *Gingivae Contain Neural-Crest- And Mesoderm-Derived Mesenchymal Stem Cells.* **Xu, X, et al.** 2013, J Dent Res, pp. 825-832.
128. *Involvement of Neural Crest and Paraxial Mesoderm in Oral Mucosal Development and Healing.* **Isaac, Juliane, et al.** 2018, Biomaterials, pp. 41-53.
129. *Gingival Fibroblasts Resist Apoptosis in Response to Oxidative Stress in a Model of Periodontal Diseases.* **Cheng, R, et al.** 2015, Cell Death Discov, p. doi: 10.1038/cddiscovery.2015.46.
130. *Gingival and Dermal Fibroblasts: Their Similarities and Differences Revealed From Gene Expression.* **Ebisawa, Katsumi, et al.** 2011, J Biosci Bioeng, pp. 255-258.
131. *Antioxidants and NOX1/NOX4 Inhibition Blocks TGFβ1-induced CCN2 and α-SMA Expression in Dermal and Gingival Fibroblasts.* **Murphy-Marshman, Hannah, et al.** 2017, PLoS One, p. doi: 10.1371/journal.pone.0186740.
132. *Human Dermal and Gingival Fibroblasts in a Three-Dimensional Culture: A Comparative Study on Matrix Remodeling.* **Miller, C Chaussain, et al.** 2002, Clin Oral Investig, pp. 39-50.
133. *Mechanisms of Lung Fibrosis Resolution.* **Glasser, Stephan W, et al.** 2016, Am J Pathol, pp. 1066-1077.
134. *Deep Dermal Fibroblasts Refractory to Migration and Decorin-Induced Apoptosis Contribute to Hypertrophic Scarring.* **Honardoust, Dariush, et al.** 2012, J Burn Care Res, pp. 668-677.
135. *Human Skin Fibroblasts Derived From Papillary and Reticular Dermis: Differences in Growth Potential in Vitro.* **Harper, R A and Grove, G.** 1979, Science, pp. 526-527.
136. *Heterogeneity of the Kinetics of Proliferation Within Human Skin Fibroblastic Cell Populations.* **Azzarone, B and Macieira-Coelho, A.** 1982, J Cell Sci, pp. 177-187.
137. *Differential Responses of Human Papillary and Reticular Fibroblasts to Growth Factors.* **Feldman, S R, et al.** 1993, Am J Med Sci, pp. 203-207.
138. *The Interaction of Human Papillary and Reticular Fibroblasts and Human Keratinocytes in the Contraction of Three-Dimensional Floating Collagen Lattices.* **Schafer, I A, et al.** 1989, Exp Cell Res, pp. 112-125.
139. *Clonal Characterization of Fibroblasts in the Superficial Layer of the Adult Human Dermis.* **Sorrell, J Michael, Baber, Marilyn A and Caplan, Arnold I.** 2007, Cell Tissue Res, pp. 499-510.

140. *Features of Wound Healing Shown by Fibroblasts Obtained From the Superficial and Deep Dermis.* **Kaminishi-Tanikawa, Akiko, et al.** 2011, J Plast Surg Hand Surg, pp. 219-225.
141. *Superficial Dermal Fibroblasts Enhance Basement Membrane and Epidermal Barrier Formation in Tissue-Engineered Skin: Implications for Treatment of Skin Basement Membrane Disorders.* **Varkey, Mathew, Ding, Jie and Tredget, Edward E.** 2014, Tissue Eng Part A, pp. 540-552.
142. *Differential collagen–glycosaminoglycan matrix remodeling by superficial and deep dermal fibroblasts: Potential therapeutic targets for hypertrophic scar.* **Varkey, Mathew, Ding, Jie and Tredget, Edward E.** 2011, Biomaterials, pp. 7581-7591.
143. *Site-matched Papillary and Reticular Human Dermal Fibroblasts Differ in Their Release of Specific Growth Factors/Cytokines and in Their Interaction With Keratinocytes.* **Sorrell, J Michael, Baber, M A and Caplan, A I.** 2004, J Cell Physiol, pp. 134-145.
144. *Subpopulations of Dermal Skin Fibroblasts Secrete Distinct Extracellular Matrix: Implications for Using Skin Substitutes in the Clinic.* **Ghetti, M, et al.** 2018, Br J Dermatol, pp. 381-393.
145. *Comparative Observation of Fibroblasts Derived From the Papillary and Reticular Dermis of Infants and Adults: Growth Kinetics, Packing Density at Confluence and Surface Morphology.* **Schafer, I A, et al.** 1985, Mech Ageing Dev, pp. 275-293.
146. *Aging Alters Functionally Human Dermal Papillary Fibroblasts but Not Reticular Fibroblasts: A New View of Skin Morphogenesis and Aging.* **Mine, Solène, et al.** 2008, PLoS One, p. doi: 10.1371/journal.pone.0004066.
147. *Papillary Fibroblasts Differentiate Into Reticular Fibroblasts After Prolonged in Vitro Culture.* **Janson, David, et al.** 2013, Exp Dermatol, pp. 48-53.
148. *Deep Dermal Fibroblasts Contribute to Hypertrophic Scarring.* **Wang, JianFei, et al.** 2008, Lab Invest, pp. 1278-1290.
149. *Reduced Decorin, Fibromodulin, and Transforming Growth factor-β3 in Deep Dermis Leads to Hypertrophic Scarring.* **Honardoust, Dariush, et al.** 2012, J Burn Care Res, pp. 218-227.
150. *Dermal Fibroblasts From Different Layers of Pig Skin Exhibit Different Profibrotic and Morphological Characteristics.* **Zuo, Yanhai, Yu, Xiaoping and Lu, Shuliang.** 2016, Anat Rec (Hoboken), pp. 1585-1599.
151. *Dermis, Acellular Dermal Matrix, and Fibroblasts From Different Layers of Pig Skin Exhibit Different Profibrotic Characteristics: Evidence From in Vivo Study.* **Zuo, Yanhai and Lu, Shuliang.** 2017, Oncotarget, pp. 23613-23627.
152. *Fibroblasts From the Human Skin Dermo-Hypodermal Junction Are Distinct From Dermal Papillary and Reticular Fibroblasts and From Mesenchymal Stem Cells and Exhibit a Specific Molecular Profile Related to Extracellular Matrix Organization and Modeling.* **Haydont, Valérie, et al.** 2020, Cells, p. doi: 10.3390/cells9020368.
153. *Different Gene Expression Patterns in Human Papillary and Reticular Fibroblasts.* **Janson, David G, et al.** 2012, J Invest Dermatol, pp. 2565-2572.
154. *Genome-wide Profiling of Adult Human Papillary and Reticular Fibroblasts Identifies ACAN, Col XI α1, and PSG1 as General Biomarkers of Dermis Ageing, and KANK4 as an Exemplary Effector of Papillary Fibroblast Ageing, Related to Contractility.* **Haydont, Valérie, et al.** 2019, Mech Ageing Dev, pp. 157-181.
155. *Lineage Identity and Location Within the Dermis Determine the Function of Papillary and Reticular Fibroblasts in Human Skin.* **Korosec, Ana, et al.** 2019, J Invest Dermatol, pp. 342-351.
156. *SFRP2/DPP4 and FMO1/LSP1 Define Major Fibroblast Populations in Human Skin.* **Tabib, Tracy, et al.** 2018, J Invest Dermatol, pp. 802-810.
157. *Transcriptome Landscape of Myeloid Cells in Human Skin Reveals Diversity, Rare Populations and Putative DC Progenitors.* **Xue, Dan, et al.** 2020, J Dermatol Sci, pp. 41-49.
158. *Single-cell Transcriptome Analysis of Human Skin Identifies Novel Fibroblast Subpopulation and Enrichment of Immune Subsets in Atopic Dermatitis.* **He, Helen, et al.** 2020, J Allergy Clin Immunol, p. doi: 10.1016/j.jaci.2020.01.042.

159. *Deciphering the Functional Heterogeneity of Skin Fibroblasts Using Single-Cell RNA Sequencing.* **Vorstandlechner, Vera, et al.** 2020, FASEB J, pp. 3677-3692.
160. *Dynamic Regulation of Retinoic Acid-Binding Proteins in Developing, Adult and Neoplastic Skin Reveals Roles for Beta-Catenin and Notch Signalling.* **Collins, Charlotte A and Watt, Fiona M.** 2008, Dev Biol, pp. 55-67.
161. *Dysfunction of Hair Follicle Mesenchymal Progenitors Contributes to Age-Associated Hair Loss.* **Shin, Wisoo, et al.** 2020, Dev Cell, pp. 185-198.
162. *Fibrocytes, Wound Healing, and Corneal Fibrosis.* **Oliveira, Rodrigo Carlos de and Wilson, Steven E.** 2020, Invest Ophthalmol Vis Sci, p. doi: 10.1167/iovs.61.2.28.
163. *Reduced WIF-1 Expression Stimulates Skin Hyperpigmentation in Patients With Melasma.* **Kim, Ji-Young, Lee, Tae-Ryong and Lee, Ai-Young.** 2013, J Invest Dermatol, pp. 191-200.
164. *Upregulation of CD26 Expression in Epithelial Cells and Stromal Cells During Wound-Induced Skin Tumour Formation.* **Arwert, E N, et al.** 2012, Oncogene, pp. 992-1000.
165. *SFRP2 and Slug Contribute to Cellular Resistance to Apoptosis in Hypertrophic Scars.* **Chen, Liang, et al.** 2012, PLoS One, p. doi: 10.1371/journal.pone.0050229.
166. *Wnt/β-catenin Signaling Is Hyperactivated in Systemic Sclerosis and Induces Smad-dependent Fibrotic Responses in Mesenchymal Cells.* **Wei, Jun, et al.** 2012, Arthritis Rheum, pp. 2734-2745.
167. *Oxidative DNA Damage Induces the ATM-mediated Transcriptional Suppression of the Wnt Inhibitor WIF-1 in Systemic Sclerosis and Fibrosis.* **Svegliati, Silvia, et al.** 2014, Sci Signal, p. doi: 10.1126/scisignal.2004592.
168. *Elevated CD26 Expression by Skin Fibroblasts Distinguishes a Profibrotic Phenotype Involved in Scar Formation Compared to Gingival Fibroblasts.* **Mah, Wesley, et al.** 2017, Am J Pathol, pp. 1717-1735.
169. *Expansion of CD26 Positive Fibroblast Population Promotes Keloid Progression.* **Xin, Yu, et al.** 2017, Exp Cell Res, pp. 104-113.
170. *Dipeptidylpeptidase 4 as a Marker of Activated Fibroblasts and a Potential Target for the Treatment of Fibrosis in Systemic Sclerosis.* **Soare, Alina, et al.** 2020, Arthritis Rheumatol, pp. 137-149.
171. *The Molecular Anatomy of Mouse Skin During Hair Growth and Rest.* **Joost, Simon, et al.** 2020, Cell Stem Cell, pp. 441-457.
172. *Single-cell Analysis Reveals Fibroblast Heterogeneity and Myeloid-Derived Adipocyte Progenitors in Murine Skin Wounds.* **Guerrero-Juarez, Christian F, et al.** 2019, Nat Commun, pp. doi: 10.1038/s41467-018-08247-x.
173. *Phagocytosis of Wnt Inhibitor SFRP4 by Late Wound Macrophages Drives Chronic Wnt Activity for Fibrotic Skin Healing.* **Gay, Denise, et al.** 2020, Sci Adv, p. doi: 10.1126/sciadv.aay3704.
174. *The Pericyte Antigen RGS5 in Perivascular Soft Tissue Tumors.* **Shen, Jia, et al.** 2016, Hum Pathol, pp. 121-131.
175. *Patch Repair of Deep Wounds by Mobilized Fascia.* **Correa-Gallegos, Donovan, et al.** 2019, Nature, pp. 287-292.

Acknowledgements

I appreciate the support from the German Academic Exchange Service (DAAD) in collaboration with the Mexican National Council of Science and Technology (CONACyT) for granting me a scholarship for my PhD studies. This research was funded by the Human Frontier Science Program Career Development Award (CDA00017/2016), the German Research Foundation (RI 2787/1-1 AOBJ: 628819), the Fritz – Thyssen – Stiftung (2016-01277) and the European Research Council Consolidator Grant (ERC-CoG 819933).

My thankfulness to the Comprehensive Pneumology Center (CPC) and Institute of Lung Biology and Disease (ILBD) and all the supportive institutes and dependencies under the Helmholtz Center Munich umbrella. My appreciation as well to the coordinators and professors at the Lung Research School.

I extend my gratitude to my thesis committee, Prof. Dr. Jürgen Behr as my principal advisor, Prof. Dr. Silke Meiners as my university supervisor, Dr. Alexander Wolf for his support as external expert, and particular to my direct supervisor Dr. Yuval Rinkevich for all his guidance and teachings.

I would like to acknowledge the invaluable contribution of our collaborators; whose work enriched the research presented in this dissertation. Thanks to our previous colleagues from the CPC, Martina De Santis and Dr. Darcy Wagner. To the members of the Analytical Pathology unit Prof. Dr. med. Axel Walch and Dr. Michaela Aichler. To our collaborators Prof. Dr. Ursula Mirastschijski and Dr. med. Thomas Volz. I thank the members of the SMAP team and Unit34 for their priceless support in the animal facility.

I thank to the entire past and present members of the regenerative medicine group, Dr. Dongsheng Jiang, Simon Christ, Dr. Tim Koopmans, Shruthi Kalgudde Gopal, Dr. Anna Stefanska, Juan Liu, Dr. Adrian Fisher, Haifeng Ye, Dr. Juliane Wannemacher, Qing Yu, Aydan Sardogan, Wan Li, Dr. Martin Mück Häusl, Pushkar Ramesh, Vijayanand Rajendran, Shaohua Zhu, Ruoxuan Dai, Dr. Mahesh Gouda, Dr. Tankut Guney, Dr. Young Hwa Kim, Andy Qarri, and Jiakuan Zhao, thanks for the assistance and insights throughout these years. A special recognition to Sandra Schiener, whose support and advice has always gone beyond her duty, for what I am and will be forever grateful.

My gratefulness to the friends I have made during this journey that softened the loads and fears of being far away from my first home. Thanks to Aimee, Hans, Perla, Ernesto, Luis, Monica, Manuel, and Norma for the bountiful moments and laughs.

My thankfulness from afar to all my family, Brenda, Javier, Daniela, Sara, and my “abue” Martha, whose support and warm surpass frontiers all the way to the other side of the globe.

My most sincere gratitude to my beloved wife. Thanks for joining me, or better said for allowing me to join you in this journey. Thanks for believing in me, even when at times I lose hope in myself. Thanks for all your teachings and patience when I feel overwhelmed and anxious. Thanks for your love and understanding when times are hard and when they are not too. I dedicate this work to you Valeria as, without you, this work would not exist.